HARVARD METEOROLOGICAL STUDIES
No. 6

HEAT TRANSFER BY INFRARED RADIATION IN THE ATMOSPHERE

By WALTER M. ELSASSER
BLUE HILL METEOROLOGICAL OBSERVATORY, HARVARD UNIVERSITY

With a copy of the Atmospheric Radiation Chart, second edition

HARVARD UNIVERSITY
BLUE HILL METEOROLOGICAL OBSERVATORY
MILTON, MASSACHUSETTS
1942

First Printing, June, 1942
Second Printing, August, 1942

PRINTED AT THE HARVARD UNIVERSITY PRINTING OFFICE
CAMBRIDGE, MASSACHUSETTS, U.S.A.

PREFACE

THE PRESENT MONOGRAPH has three parts. Part I deals with the general theory of radiative heat transfer in the atmosphere, without regard to the particular structure of the far infrared spectrum. Part II analyzes this spectrum and shows the connection between its structural elements, which are the primary data of spectroscopy, and the integral effects observed as radiative flow of heat. Part III deals with the direct measurement of radiative heat flow in the atmosphere, or in the laboratory under conditions simulating those of the atmosphere, and with empirical relationships derived from such measurements. An attempt has been made to keep the three parts as nearly independent of each other as feasible, although this could not be done rigorously; but it is hoped that each part is understandable with a not-too-thorough perusal of the others. The subject presented is at the borderline between dynamic meteorology and infrared spectroscopy and we hope to show that out of the interplay of these two branches of science new problems may arise whose solution is of interest to both of them.

The author wishes to use this opportunity to express his appreciation of the cooperation which he has had during the years at the California Institute of Technology while working on the subject of these pages. His thanks go to Professor John Strong, whose advice and coöperation have been most valuable, to Dr. J. Anderson for the use of the facilities of the Astrophysics Department for the infrared measurements, and to Mr. Charles E. Miller, who has been of great assistance in the design and construction of the calculating machine and in several other stages of the work. Professor H. G. Houghton of the Massachusetts Institute of Technology has kindly read the proofs of this paper and has contributed a number of valuable suggestions.

The author's investigations would not have been possible without the support of the United States Government with funds appropriated under the Bankhead-Jones act. In the publication of this monograph and in the editing of the atmospheric radiation chart in particular, he has been greatly assisted by a grant from the United States Weather Bureau.

CONTENTS

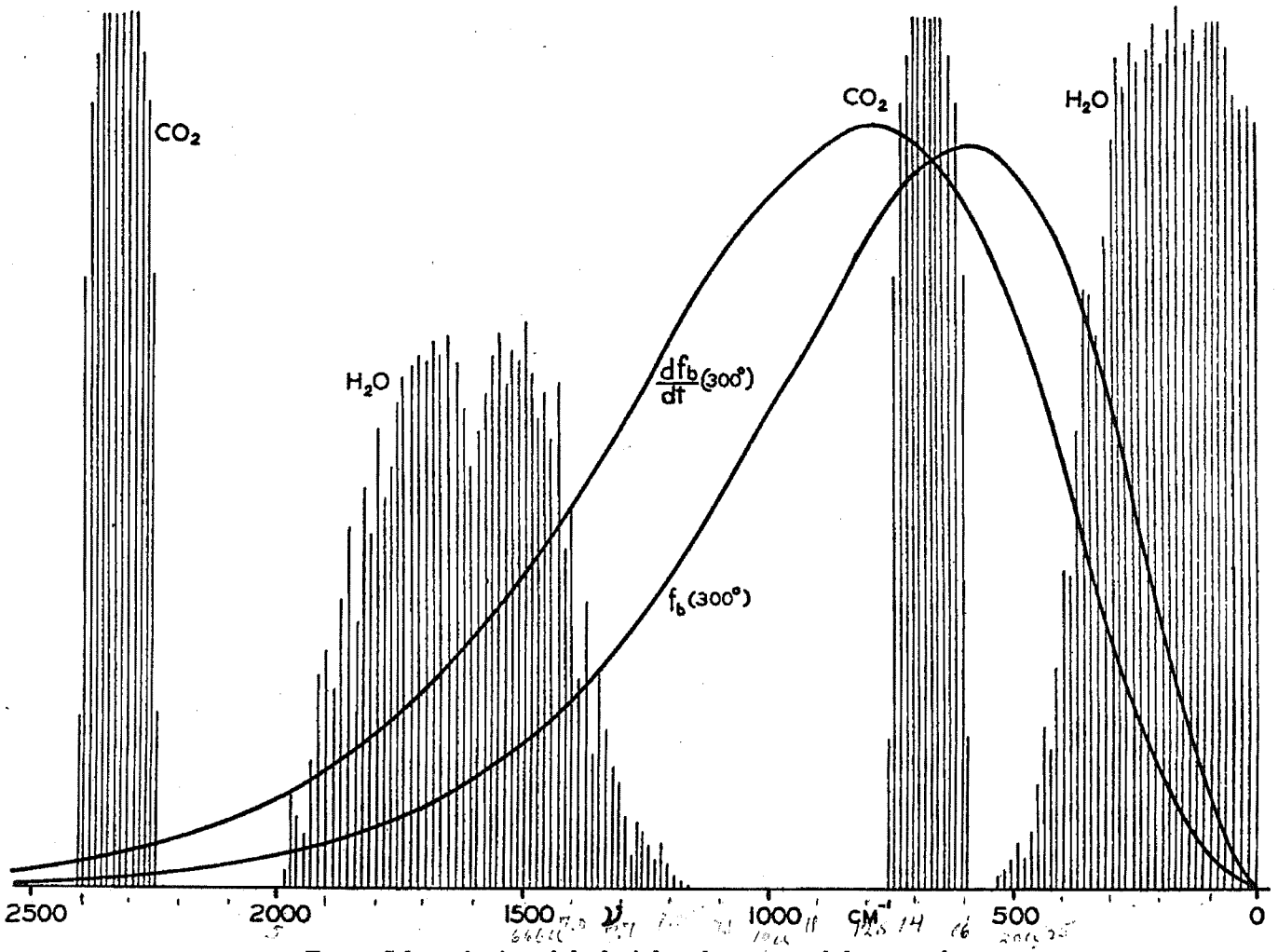

FIG. 1. Schematic view of the far infrared spectrum of the atmosphere.

HEAT TRANSFER BY INFRARED RADIATION IN THE ATMOSPHERE

PART I. PRINCIPLES OF RADIATIVE TRANSFER

1. Kirchhoff's Law; The Equation of Transfer; Planck's Law

Some Definitions: For any wave the wave length λ and the frequency ν' are connected by the formula:

$$\lambda\nu' = c \tag{1.1}$$

where c is the velocity of propagation of the wave. In the atmosphere this velocity is practically equal to the velocity of light in a vacuum, $c = 3 \cdot 10^{10}$ cm/sec. We shall usually characterize the radiation by its frequency or, what amounts to the same thing, the reciprocal wave length:

$$\nu = 1/\lambda = \nu'/c \tag{1.2}$$

This quantity is called the *wave number*, its dimension being cm^{-1}. Since wave number and frequency differ only by a constant factor, we will often use these two terms interchangeably; this is not likely to lead to confusion.

It seems reasonable to start out with a brief sketch of *Kirchhoff's law*. Kirchhoff investigates the *thermodynamic equilibrium between matter and radiation*. To illustrate this concept, let us consider an enclosure surrounded on all sides by thick walls. The walls may be absorbing for a certain frequency and so thick that a beam of radiation of this frequency falling upon a wall does not penetrate to the other side. Such a wall will be called *perfectly opaque* for this frequency. A wall which is perfectly opaque for *all* frequencies is called *black*. The walls will emit a certain amount of temperature radiation into the enclosure. If all the walls have the same temperature, and if the temperature remains constant, an equilibrium will be reached in which there must be, inside the enclosure, a certain amount of radiation flowing in all directions. This state is called the thermodynamic equilibrium between radiation and matter at this temperature. We can show that the emission of a perfectly opaque wall does not depend on the chemical constitution of the wall. Indeed, assume that two opposite sides of our enclosure are made of different materials but have the same temperature. The radiation going from the first to the second wall must be exactly equal to the radiation going in the opposite direction,

since otherwise there would be a net flow of heat from one body to another body of the same temperature, which is in contradiction to the second law of thermodynamics. Therefore, the emission of the first wall must equal the emission of the second wall. Since this must be true for any pair of substances, the emission of all walls in thermodynamic equilibrium must be the same. Now the emission of a wall does not depend upon the existence of equilibrium radiation in an adjacent enclosure; indeed, it does not depend at all upon the conditions outside the wall. Therefore, the emission of a *perfectly opaque* wall is generally independent of the optical properties of the wall. The intensity of this emission is called the *black body intensity* at the respective wave length and temperature. To avoid misunderstanding it must be remembered that a black body is defined as a body which is perfectly opaque at *all* wave lengths. A wall, however, may be perfectly opaque for radiation of one wave length, while it is partly or completely transparent for radiations of other wave lengths. The wall will then emit the black body intensity at those particular wave lengths for which it is completely opaque; for these wave lengths a thermodynamic equilibrium between the radiation and matter will be established inside the enclosure.

We consider now a slab of material of finite thickness which absorbs a part and transmits another part of the radiation at a given wave length. Let us suppose first that this slab is inside our enclosure, and let us consider a beam of radiation crossing the slab under any angle. We call I_b the intensity of this beam which, in thermodynamic equilibrium, is just the black body intensity.[1] Let A be the *fractional absorption* of the slab; i.e., let the amount of intensity of the beam absorbed inside the slab be AI_b. The amount transmitted through the slab is $(1 - A)I_b$. Further, let E designate the intensity of radiation *emitted* by the slab in the direction of the beam. Now in thermodynamic equilibrium the total intensity of the beam after passing through the slab must be the same as the intensity of the beam before it strikes the slab. Indeed, if this were not the case, the slab would gain or lose energy at the expense of the wall towards which the beam is directed, and we would have a steady flow of energy between two bodies of the same temperature, which is again in contradiction to the second law of thermodynamics. We have, therefore, in thermodynamic equilibrium:

$$I_b = (1 - A)I_b + E$$

which gives

$$E/A = I_b \tag{1.3}$$

[1] The intensity of a beam of radiation is generally defined as the amount of energy which per unit time flows through a cross section of unit area perpendicular to the direction of the beam.

and this is Kirchhoff's law: The ratio of emission and fractional absorption in any direction of a slab of any thickness in thermodynamic equilibrium equals the black body intensity. This result remains unchanged if reflection at the slab's boundaries is taken into account. The primary beam loses part of its intensity by reflection on entering the slab; purely geometrical considerations show then that the intensity of the beam is augmented by exactly the same amount when leaving the slab; the additional intensity is produced by reflection out of the beam which travels in the opposite direction. For infrared thermal radiation, with which we are dealing here, reflection is mostly negligible.

As we saw, I_b is a universal function of frequency and temperature and is independent of the material. Since the function is universal, Kirchhoff's law (1.3) represents a *universal relationship between the emission and the fractional absorption* of a radiating body at any given wave length, which may be stated without reference to the concept of a thermodynamic equilibrium. We may apply (1.3) to the case of an infinitely thin sheet of absorbing material. Let dm be the mass per cm^2 of the sheet and k the absorption coefficient of the substance. Then $A = k\,dm$, and this will be the definition of the absorption coefficient k. According to (1.3) the emission of the sheet perpendicular to its boundary is:

$$dE = kI_b dm$$

We next consider radiation which is *not* in thermodynamic equilibrium with matter. Take again an infinitesimal sheet of absorbing matter and a beam of radiation perpendicular to it. The change in intensity which takes place if the beam passes through the sheet is equal to the amount emitted minus the amount absorbed by the sheet. If I is the intensity of the beam, then the amount absorbed is $k\,I\,dm$, while the amount emitted is given by (1.3). We have, therefore:

$$dI = -k(I - I_b)\,dm \tag{1.4}$$

This is the fundamental equation of radiative transfer, often called Schwarzschild's equation. The first part of this paper is mainly devoted to the integration of this equation under the particular conditions which prevail in the earth's atmosphere. In the atmosphere there are beams of radiation traveling in all directions. Let ds be a line element in a given direction; we can then divide the atmosphere into infinitesimal sheets which are perpendicular to this direction. The mass per unit surface of a sheet may be written $dm = \rho ds$ where ρ is the density of the absorbing material. Then

$$\frac{dI}{ds} = -k\rho(I - I_b) \tag{1.5}$$

and this must be true for any point of the atmosphere and for *any* direction ds. In this form we will use the equation of transfer further on.

* * *

The mathematical expression of the black body intensity as a function of the wave number is derived in atomic physics. This function is known as *Planck's law.* Originally introduced by Planck as a semi-empirical formula which fitted the observations, this law can also be deduced from the principles of quantum theory. Thus it is well founded, both empirically and theoretically. Planck's law reads:

$$I_b = \frac{p\nu^3/\pi}{e^{q\nu/T} - 1} \tag{1.6}$$

where p and q are universal constants. We must notice that a finite flux of energy is obtained only if one integrates over an interval of the spectrum. Therefore $I_b d\nu$ has the dimension of an energy per unit time per unit surface. The constants in (1.6) have the numerical values [1]

$$p = (3.732 \pm 0.006)\cdot 10^{-5}\ \frac{\text{erg}\cdot\text{cm}^2}{\text{sec}} = 9.63\cdot 10^{-9}\frac{\text{cal}\cdot\text{cm}^2}{3\ \text{hours}}$$

$$q = (1.436 \pm 0.001)\ \text{cm}\cdot\text{degree}$$

and the absolute temperature T is connected with the temperature t in the centigrade scale by

$$T = t + 273.16$$

The total radiation of a black body is obtained by integrating (1.6) over all wave-numbers. We have with $x = q\nu/T$

$$\int_0^\infty I_b\, d\nu = \frac{pT^4}{\pi q^4}\int_0^\infty \frac{x^3 dx}{e^x - 1}$$

The evaluation of this integral is somewhat intricate,[2] and only the result may be indicated. The integral has the value $\pi^4/15$ and we obtain, using a current notation:

$$\int_0^\infty I_b\, d\nu = \frac{\sigma}{\pi}\, T^4 \tag{1.7}$$

where σ is a constant:

$$\sigma = \pi^4 p/15q^4 = 5.70\cdot 10^{-5}\ \frac{\text{erg}}{\text{sec}\cdot\text{cm}^2\cdot\ \text{deg.}^4} = 1.470\cdot 10^{-8}\ \frac{\text{cal}}{3\ \text{hours}\cdot\ \text{cm}^2\cdot\ \text{deg.}^4}$$

[1] H. T. Wensel, Bur. of Stand. Journ. of Res. 22: 375. 1939.

[2] If we develop $(e^x - 1)^{-1} = e^{-x} + e^{-2x} + e^{-3x} + \ldots$, we can integrate term by term and we obtain for our integral the series $6\,(1 + 2^{-4} + 3^{-4} + 4^{-4} + \ldots)$, the summation of which is carried out in the theory of Riemann's zeta function (see Whittaker-Watson, *Modern Analysis*, ch. 13).

In practice we are usually not so much interested in the radiation of a straight beam as in the total emission of a black surface into the hemisphere. We designate the latter emission by f_b and, as will be demonstrated in the next chapter, we have the simple relation $f_b = \pi I_b$. We write $F_b = \int_0^\infty f_b d\nu$ and have

$$F_b = \sigma T^4 \tag{1.8}$$

Formula (1.8) is known as *Stefan's law.*

Numerical values of the black body function may be obtained from Table 1.

TABLE 1. INTEGRATION OF RADIATION INTENSITY BY WAVE NUMBER, $\int_0^\nu f_b d\nu = RT^4\phi(x)$, AND OF CHANGE OF INTENSITY WITH TEMPERATURE, $\int_0^\nu (df_b/dT)\, d\nu = RT^3\phi'(x)$, WHERE $x = q\nu/T$, $q = 1.436$ cm · degree, $R = 2.264 \cdot 10^{-9}$ cal / (3 hours · cm^2 · degree^4), $\phi(x) = \int_0^x x^3 (e^x - 1)^{-1} dx$ and $\phi'(x) = \int_0^x x^4 e^x (e^x - 1)^{-2} dx$.

x	$\frac{100\phi(x)}{\phi(\infty)}$	$\phi(x)$	$\phi'(x)$	x	$\frac{100\phi(x)}{\phi(\infty)}$	$\phi(x)$	$\phi'(x)$	x	$\frac{100\phi(x)}{\phi(\infty)}$	$\phi(x)$	$\phi'(x)$
0.1	0.004	0.0003	0.000	3.5	49.937	3.2429	8.299	6.9	91.945	5.9709	21.597
0.2	0.038	0.0024	0.003	3.6	51.974	3.3752	8.783	7.0	92.443	6.0032	21.821
0.3	0.123	0.0080	0.009	3.7	53.973	3.5050	9.269	7.1	92.911	6.0336	22.036
0.4	0.281	0.0183	0.021	3.8	55.928	3.6319	9.756	7.2	93.354	6.0624	22.242
0.5	0.529	0.0343	0.041	3.9	57.839	3.7561	10.245	7.3	93.770	6.0894	22.438
0.6	0.880	0.0571	0.071	4.0	59.703	3.8771	10.732	7.4	94.164	6.1150	22.626
0.7	1.342	0.0871	0.112	4.1	61.516	3.9948	11.218	7.5	94.534	6.1390	22.805
0.8	1.923	0.1249	0.166	4.2	63.279	4.1094	11.701	7.6	94.883	6.1617	22.976
0.9	2.629	0.1707	0.233	4.3	64.989	4.2204	12.179	7.7	95.210	6.1830	23.140
1.0	3.462	0.2248	0.317	4.4	66.647	4.3281	12.653	7.8	95.521	6.2031	23.295
1.1	4.421	0.2871	0.418	4.5	68.250	4.4322	13.123	7.9	95.810	6.2219	23.443
1.2	5.507	0.3576	0.536	4.6	69.799	4.5328	13.585	8.0	96.084	6.2397	23.584
1.3	6.714	0.4360	0.674	4.7	71.293	4.6298	14.040	8.2	96.581	6.2720	23.845
1.4	8.040	0.5221	0.831	4.8	72.734	4.7233	14.488	8.4	97.020	6.3005	24.082
1.5	9.478	0.6155	1.008	4.9	74.121	4.8134	14.929	8.6	97.405	6.3254	24.294
1.6	11.022	0.7158	1.206	5.0	75.452	4.8999	15.360	8.8	97.744	6.3475	24.485
1.7	12.667	0.8226	1.424	5.1	76.732	4.9830	15.782	9.0	98.039	6.3667	24.657
1.8	14.402	0.9353	1.662	5.2	77.960	5.0627	16.195	9.2	98.299	6.3835	24.810
1.9	16.221	1.0534	1.922	5.3	79.135	5.1390	16.598	9.4	98.526	6.3983	24.946
2.0	18.115	1.1764	2.201	5.4	80.259	5.2120	16.990	9.6	98.723	6.4111	25.069
2.1	20.074	1.3036	2.500	5.5	81.335	5.2819	17.373	9.8	98.896	6.4223	25.177
2.2	22.091	1.4346	2.820	5.6	82.362	5.3486	17.744	10.0	99.045	6.4320	25.274
2.3	24.158	1.5688	3.157	5.7	83.343	5.4123	18.106	10.4	99.290	6.4479	25.435
2.4	26.265	1.7056	3.512	5.8	84.278	5.4730	18.456	10.8	99.472	6.4597	25.561
2.5	28.402	1.8444	3.885	5.9	85.168	5.5308	18.795	11.2	99.609	6.4686	25.659
2.6	30.564	1.9849	4.273	6.0	86.015	5.5858	19.123	11.6	99.712	6.4753	25.735
2.7	32.743	2.1263	4.676	6.1	86.821	5.6382	19.440	12.0	99.787	6.4802	25.793
2.8	34.929	2.2683	5.094	6.2	87.588	5.6879	19.747	12.4	99.843	6.4838	25.838
2.9	37.118	2.4104	5.523	6.3	88.315	5.7352	20.042	12.8	99.885	6.4866	25.872
3.0	39.301	2.5522	5.965	6.4	89.005	5.7800	20.328	13.2	99.916	6.4885	25.898
3.1	41.472	2.6932	6.416	6.5	89.659	5.8224	20.602	13.6	99.939	6.4900	25.918
3.2	43.627	2.8332	6.877	6.6	90.279	5.8627	20.866	14.0	99.955	6.4911	25.933
3.3	45.759	2.9716	7.345	6.7	90.866	5.9008	21.120	15.0	99.980	6.4927	25.955
3.4	47.865	3.1083	7.820	6.8	91.422	5.9370	21.364	∞	100.000	6.4940	25.976

Since we commonly use the integrated intensity $\int f_b d\nu$ over a given interval of the spectrum rather than the intensity f_b itself, the integral between the limits 0 and x has been calculated. The integral over the temperature derivative df_b/dT which will be used later is also given. The quantity R appearing at the head of Table 1 is readily seen from (1.6) to have the value

$$R = p/q^4 = 8.78 \cdot 10^{-4} \frac{\text{erg}}{\text{sec} \cdot \text{cm}^2 \cdot \text{deg.}^4} = 2.264 \cdot 10^{-9} \frac{\text{cal}}{3 \text{ hours} \cdot \text{cm}^2 \cdot \text{deg.}^4}$$

2. Transfer of Monochromatic Radiation

We shall now treat the simplest problem of transfer, namely, the absorption of radiation by a slab of finite thickness which does not radiate itself. From Kirchhoff's law we know that the emission is not independent of the absorption, and we cannot, in principle, equate the emission to zero. For low temperatures, however, the emission becomes small. As a first approximation we may treat the case of zero emission; the equation of transfer (1.5) reduces then to:

$$\frac{dI}{ds} = -k\rho I \tag{2.1}$$

Here ds is a line element in an arbitrary direction in the absorbing medium whose density is ρ. The absorption coefficient k is, in general, a function of the frequency. In this chapter we consider the case that k is a constant, independent of frequency, or else we confine ourselves to a frequency interval so small that k is appreciably constant within it (monochromatic radiation). We assume throughout that the absorbing material is bounded by two parallel planes of infinite extension. We speak then of an absorbing *slab*. If the slab is infinitely thin, we shall call it an absorbing *sheet*. The z-coördinate is always taken perpendicular to the bounding planes (i.e., vertical in the atmosphere), the x- and y-coördinates are parallel to these planes.

Equation (2.1) can be put in a somewhat more convenient form. If, instead of s in (2.1), we use the height z, we have (Fig. 2): $dz = ds \cos\theta$. Furthermore, it is convenient to introduce the new variable

$$u = \int_{z_0}^{z} \rho \, dz \tag{2.2}$$

We have then $du = \rho \, dz$ and therefore

$$\rho \, ds = du \sec\theta$$

where as usual $\sec\theta = 1/\cos\theta$. The quantity u measures the total amount of absorbing material above the reference level z_0. Equation (2.1) becomes now:

$$\frac{dI}{du} = -kI \sec\theta$$

If the incident beam has the intensity I_0, we obtain by integration:

$$I = I_0 e^{-ku \sec\theta} \tag{2.3}$$

The next simple case is that of *isotropic* radiation of intensity I_0 falling upon one face of the slab. By isotropic radiation we designate a diffuse radiation which has the same intensity in all directions. It is useful to introduce the *flux* f which per unit time crosses a unit surface perpendicular to the z-direction. This flux is obtained by integrating I over a hemisphere. Now if a beam with intensity I per unit cross section perpendicular to itself falls upon a surface under the angle θ,

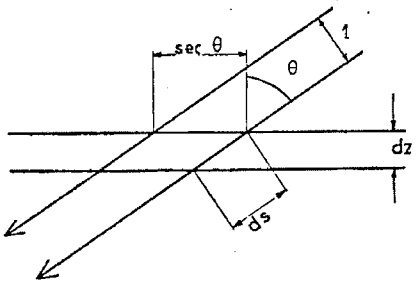

FIG. 2.

a unit area on the surface will receive the intensity $I \cos\theta$. Therefore, we have for the flux:

$$f = \int_0^{2\pi} d\phi \int_0^{\pi/2} I \cos\theta \sin\theta \, d\theta \tag{2.4}$$

with the integration extending over the hemisphere. We consider first an isotropic flux $I = I_0$ independent of the angles. We obtain then

$$f_0 = \pi I_0 \tag{2.5}$$

For isotropic radiation the flux is π times the intensity of a straight beam, a result of great usefulness. A word might be said about the physical significance of this relation. Strictly speaking, a parallel beam carries a vanishing amount of energy while a beam of the small solid angle of divergence $d\omega$ carries an amount $I_0 \, d\omega$. Hence, to be physically correct such formulae as (2.1) should be multiplied on both sides by $d\omega$, but little confusion is created by omitting this factor. Since $d\omega$ is a pure number, f and I have the same dimension. We have made use of (2.5) at the end of Section 1, applying it to black body radiation.

Formula (2.5) gives the flux incident on one side of our slab; the flux emerging at the other side is by (2.4):

$$f = \int_0^{2\pi} d\phi \int_0^{\pi/2} I_0 \, e^{-ku \sec\theta} \cos\theta \sin\theta \, d\theta \tag{2.6}$$

The emerging radiation is, in general, no longer isotropic. To simplify the last integral we put $\eta = \sec\theta$, and we obtain:

$$f = 2\pi I_0 \int_1^\infty e^{-ku\eta} \frac{d\eta}{\eta^3}$$

We may here introduce the incident flux f_0 from (2.5), and we write the result in the abbreviated form:

$$f = 2f_0\, Ei_3(ku) \tag{2.7}$$

The function introduced here is one of a set of functions which play a great role in the transfer problems. We define

$$Ei_n(x) = \int_1^\infty e^{-x\eta} \frac{d\eta}{\eta^n} \tag{2.8}$$

The function defined in this way is called the *n-th exponential integral.* Changing the integration variable to $y = x\eta$, we may also write:

$$Ei_n(x) = x^{n-1} \int_x^\infty e^{-y} \frac{dy}{y^n}$$

Through an integration by parts we obtain from this the recursion formula:

$$Ei_n(x) = \frac{e^{-x}}{n-1} - \frac{x}{n-1} Ei_{n-1}(x) \tag{2.9}$$

By differentiating (2.8) we obtain further:

$$\frac{dEi_n(x)}{dx} = -Ei_{n-1}(x) \tag{2.10}$$

We might remark that a notation introduced by Gold (74) is sometimes found in meteorological papers. Gold writes H_2 and H_3 for Ei_2 and Ei_3, respectively. Some mathematical writers use $-Ei(-x)$ instead of $Ei_1(x)$. The notation employed here is that of E. A. Milne in his work on thermodynamics of the stars (10) which contains a most comprehensive treatise on radiative transfer. Numerical values of Ei_2 and Ei_3 are given in Table 4, Section 7.

We shall now proceed to a more general problem, taking into account emission. If we substitute the variable u of (2.2) in the general transfer equation (1.5), the latter reads:

$$\frac{dI}{du} = -k \sec\theta\, (I - I_b) \tag{2.11}$$

where I_b is the black body intensity. The following special case is of importance and will be used frequently later on: An infinitesimal emitting sheet is adjacent to one

face of an absorbing slab (Fig. 3). The slab itself does not radiate but absorbs part of the radiation emitted by the sheet. The (infinitesimal) intensity of emission in a direction which makes an angle θ with the z-axis is obviously proportional to the thickness of the sheet in this direction; i.e., is proportional to sec θ. Indeed, from (2.11) we have for the emission of the sheet:

$$dI = k \sec\theta \, I_b \, du$$

We obtain now the infinitesimal flux which emerges at the other side of the slab by substituting dI instead of I_0 in formula (2.6). This gives

$$df = k \, du \int_0^{2\pi} d\phi \int_0^{\pi/2} I_b \, e^{-ku \sec\theta} \sin\theta \, d\theta \tag{2.12}$$

Proceeding as above after (2.6) and carrying out the integration over θ we may write this

$$df = 2\pi \, k \, I_b \, Ei_2 \, (ku) \, du \tag{2.13}$$

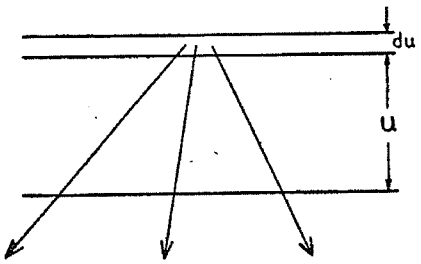

FIG. 3.

From this expression we can readily obtain the formula for the radiation emitted by a slab or an atmosphere of arbitrary structure. By this we mean a stratified medium in which the temperature is a given arbitrary function of the thickness u. We make the assumption, fundamental for all subsequent calculations, *that the absorption coefficient k does not depend on the temperature.* This is only approximately true in the atmosphere; the corrections caused by deviations from this rule in the actual atmosphere will be discussed in Section 8. In fact, the assumption of constant k was already implied in the integral (2.3) of the differential equation of transfer. Now the black body intensity I_b is a function of the temperature T. In any actual slab or atmosphere there is a definite relation between the temperature and the density of the absorber. Hence T is a definite function of u, consequently I_b is a definite function of u, the functional relationship depending of course upon the structure of the particular atmosphere. If u_0 and u_1 designate the boundaries of the slab or atmosphere, we obtain from (2.13) for the total flux arriving at u_0

$$f(u_0) = 2\pi k \int_{u_0}^{u_1} I_b \, Ei_2 \, (k(u - u_0)) \, du \tag{2.14}$$

Using (2.10) and introducing the black flux f_b which is connected with I_b by (2.5), this may also be written

$$f(u_0) = -\int_{u_0}^{u_1} f_b \frac{2d\, Ei_3(k(u-u_0))}{du}\, du \tag{2.15}$$

This formula expresses the flux emerging from an arbitrary atmosphere.

3. Transfer of Non-Monochromatic Radiation

The actual radiation emitted by the atmosphere is a mixture of radiations of various frequencies. The resultant total flux is obtained by integrating (2.15) over all frequencies:

$$F(u_0) = -\int_0^\infty d\nu \int_{u_0}^{u_1} f_b \frac{2d\, Ei_3(k(u-u_0))}{du}\, du \tag{3.1}$$

It must here be considered that both the black flux f_b and the absorption coefficient k are functions of ν. Now (3.1) is the general solution of our transfer problem and our next step is a discussion of the integrals appearing in this formula.

The evaluation of these integrals is complicated by the fact that the actual absorption coefficients are not simple functions of the frequency. The spectra of atmospheric gases in the infrared are *line spectra*; they consist of a large number of relatively narrow strips of intense absorption (or emission, as the case may be). Each such strip is called a *spectral line*. The water vapor spectrum alone contains several hundred lines (see Fig. 16). This means that the absorption coefficient k oscillates very rapidly in function of ν. A direct evaluation of the integral (3.1) would therefore be quite impossible in practice. In order to simplify the procedure we perform it in two steps, introducing as a first step an operation of *smoothing* over the rapid oscillations of the absorption coefficient. For this purpose we divide the whole interval of integration into a number of smaller intervals. We choose the latter intervals so that the black body flux may be considered as approximately constant within each interval, but on account of the large number of spectral lines each interval will still contain several lines. In each interval we average over the rapid fluctuations of the absorption coefficient k.

Let us first consider this averaging operation for the case of the absorption of a straight beam,

$$I = I_0 e^{-ku}$$

Assuming that I_0 is constant in the small interval of the spectrum over which the average extends we may write

$$[I]_{av} = I_0 [e^{-ku}]_{av} \tag{3.2}$$

Now the result of the averaging process may depend on the particular way in which the absorption coefficient k fluctuates within the interval. One might therefore get different types of functions in different intervals. This again would greatly complicate the theory. Fortunately it is possible in practice to get along with only a few types of such functions. The latter will be called *transmission functions*. If the absorption coefficient is constant in the interval, the transmission function reduces to e^{-ku} itself. In the more general case of a variable k we introduce the abbreviation τ_I for the transmission function:

$$\tau_I = [e^{-ku}]_{av} \tag{3.3}$$

The case of interest for us is that there is a considerable number of spectral lines in the interval considered. This case is mathematically treated in Section 7, and analytical expressions for the transmission functions are given. It is found that the transmission due to a group of spectral lines can be represented by the function

$$\tau_I = 1 - \phi\left(\sqrt{\frac{lu}{2}}\right) \tag{3.4}$$

where ϕ is the so called probability integral. The quantity l will be called the generalized absorption coefficient. The function (3.4) no longer contains the rapid fluctuations of the absorption coefficient caused by the presence of many spectral lines. The quantity l may be considered as constant in any of the intervals introduced above; if the intervals are sufficiently numerous, we might look at the variation of l from interval to interval as a continuous variation with wave length; this variation might in practice be taken to be of the same order as the variation of the black body intensity with wave length.

From (3.2) and (3.3) we see that

$$\tau_I = [I]_{av}/I_0 \tag{3.5}$$

This formula may readily be generalized to the case of an absorbing *slab*. The transition from the intensity I of a beam to a two-dimensional flux is given by (2.4) or (2.6); we may write (2.4) in the form:

$$f = \pi \int_0^1 I(u \sec\theta)\, d(\sin^2\theta) \tag{3.6}$$

Averaging over a spectral interval we can write in analogy to (3.5) for the transmission of the flux

$$\tau_f = [f]_{av}/f_0 \tag{3.7}$$

If now we average on both sides of (3.6) and use (3.5) and (2.5) on the right hand side, we have

$$\tau_f = \int_0^1 \tau_I\, (u \sec\theta)\, d(\sin^2\theta) \tag{3.8}$$

a formula which is convenient for numerical computations. It must be remembered however that this derivation of (3.8) is based upon the assumption that the incident intensity I_0 is independent of the direction θ, i.e., isotropic, while the intensity I of the radiation leaving the slab might be a function of θ.

In the particular case where the absorption of a beam is exponential we have by (2.7)

$$\tau_f = 2Ei_3 \tag{3.9}$$

Formulae for the more general case of transmission by a group of spectral lines will be given later on, in Section 7.

It is obvious that the two operations just performed, namely, the averaging of the absorption over a spectral interval and the integration over all angles of incidence θ, both being linear, are interchangeable. Hence we can as well carry out the integration over the angles first and then average over the fluctuations of the absorption coefficient. From (3.7), on substituting the value (2.7) for f we have indeed

$$\tau_f = [2Ei_3(ku)]_{av} \tag{3.10}$$

The averaging extends again over the rapid fluctuations of k in a small spectral interval, and the resultant transmission function τ_f is a function of the thickness u and of a generalized absorption coefficient l whose variation with frequency is much slower than that of the original coefficient k.

4. The General Transfer Problem

We shall now go back to our general expression (3.1) for the flux emitted by an atmosphere of arbitrary constitution. We may carry out under the integral of (3.1) the process just described of averaging over the rapid oscillations of k and have by (3.10) for the flux arriving at $u = u_0$

$$F = -\int_0^\infty dv \int_{u_0}^{u_1} f_b \frac{d}{du} \tau_f (l(u - u_0))\, du \tag{4.1}$$

This is the fundamental formula which solves the radiative transfer problem. We cannot, however, reduce the solution any further, since (4.1) involves the relation between u and T which is not given analytically but is a purely empirical relation. Indeed, τ_f is a function of the thickness of the absorbing matter u while f_b is a function of the temperature T at each point of the atmosphere. The functional relationship between T and u is different in each atmosphere. It is therefore convenient to solve (4.1) by *graphical* integration, a method introduced by Mügge and Möller (83). We shall present this method in the form developed by the writer (69).

By means of an integration by parts we obtain from (4.1)

$$F = -\left| \int_0^\infty f_b \tau_f \, d\nu \right|_{u_0}^{u_1} + \int_{u_0}^{u_1} du \int_0^\infty \frac{df_b}{dT} \tau_f \, d\nu \tag{4.2}$$

In place of u we introduce the temperature T as independent variable and have

$$\int du \int_0^\infty \frac{df_b}{dT} \tau_f \, d\nu = \int dT \int_0^\infty \frac{du}{dT} \frac{df_b}{du} \tau_f \, d\nu = \int dT \int_0^\infty \frac{df_b}{dT} \tau_f \, d\nu$$

We introduce the abbreviation

$$\int_0^\infty \frac{df_b(T)}{dT} \tau_f(lu) \, d\nu = Q(u, T) \tag{4.3}$$

Furthermore, as a special case of this

$$\left| \int_0^\infty f_b \tau_f \, d\nu \right|_{T_0(u_0)} = \int_0^{T_0} Q(u_0, T) \, dT \tag{4.4}$$

A similar expression is valid at the upper boundary T_1 (u_1). Substituting these expressions in (4.2) and putting $u_0 = 0$ we get

$$F = \int_0^{T_0} Q(0, T) \, dT + \int_{T_0}^{T_1} Q(u(T), T) \, dT + \int_{T_1}^{0} Q(u_1(T_1), T) \, dT \tag{4.5}$$

It is seen that the three integrals together give a closed path in the $Q - T$ plane. The area enclosed by this path is equal to the flux F.

The quantity Q is a function of the two variables u and T, and, as seen from (4.3), it can be computed once and for all if the transmission function τ_f is known. Q and T are essentially the variables of a diagram which is used to carry out graphically the integration in (4.5). Such a diagram will be called a radiation chart. The abscissae and ordinates of the chart are, respectively,

$$x = aT^2 \quad \text{and} \quad y = Q/2aT \tag{4.6}$$

where a is a constant. We have then

$$ydx = QdT$$

so that an area on this chart is equal to a flux F as defined by (4.5). The details of the construction of the chart, that is the numerical computation of the integrals (4.3), will be given in Part II of this paper.

We note a few specializations of the above formulae. For $u = 0$, we have $\tau_f = 1$, and therefore by (1.8).

$$Q(0, T) = \frac{d}{dT}\int_0^\infty f_b \, d\nu = \frac{dF_b}{dT} = 4\sigma T^3 \tag{4.7}$$

where σ is Stefan's constant of black body radiation as defined before. From (4.6) we see now that for $u = 0$ we have $y = 2\sigma x/a^2$ so that $u = 0$ is represented by a straight line on our chart. Furthermore, since τ_f decreases as u increases we see from (4.3) that $u = 0$ corresponds to the maximum value of Q for a given temperature T. The straight line $u = 0$ forms therefore the upper edge of our chart. For $u = \infty$ we have $\tau_f = 0$, and by (4.3) this gives $Q = 0$ so that the x-axis of our chart represents a layer of infinite thickness.

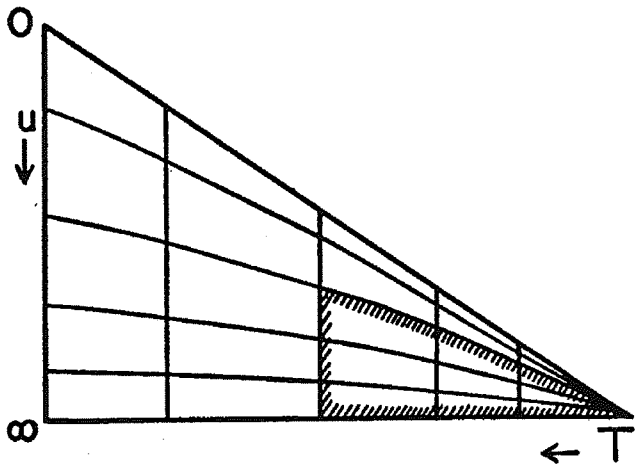

FIG. 4.

Unless τ_f is identically zero in some part of the spectrum (which is not the case in practice), a slab of *infinite* thickness u must absorb all radiation falling upon it. If the slab is moreover *isothermal*, it follows from Kirchhoff's law of Section 1 that the slab must itself radiate as a black body of its own temperature. This relationship is very useful, as it permits us to replace black surfaces, such as the ground or clouds which frequently occur in computations of atmospheric transfer, by isothermal slabs of infinite thickness. In the practical use of the radiation chart this method is constantly applied.

Fig. 4 shows a schematic view of the radiation chart. The abscissae increase from right to left and the ordinates are proportional to Q by (4.6). The vertical lines in the drawing are consequently isotherms, T = const., while the slanting curves are curves of constant thickness, u = const., which we shall call *isopleths*.

It is seen from (4.4) and (4.5) that an area such as indicated by the dashed triangular boundary at the lower right of Fig. 4 represents the absorption of an isothermal slab for black body radiation of its own temperature, while the strip above the dashed wedge and limited by the upper edge of the chart would represent the emission of the isothermal slab, the temperature of the slab and of the radiation being that of the isotherm which bounds the triangles on the left.

The point at the right of the chart to which all the isopleths converge represents the absolute zero of the temperature; it follows from (4.5) that our integrations extend always to $T = 0$. It is not necessary, however, to have the actual chart extend to the absolute zero, since we shall see that for sufficiently low temperatures the path of integration on the chart always follows closely one of the isopleths $u = \text{const}$. Consequently part of the area to be evaluated has always the form of the wedge-shaped area of Fig. 4. Areas of this type for various values of T and u have been calculated once and for all and are given in an auxiliary table printed on the chart. The actual chart extends only over a range of temperatures that occurs in the atmosphere, from $+40°$ C to $-80°$ C.

5. Atmospheric Radiation Chart

Thus far we have not specified the nature of the absorbing medium. In the atmosphere there are two radiating substances, water vapor and carbon dioxide. Ozone has also absorption bands in the infrared region, but its influence upon infrared radiative transfer in the lower atmosphere is negligible, while it may become of some importance in the stratosphere. In the present monograph we deal mainly with heat transfer in the lower atmosphere and we may disregard ozone as a radiator. The relationship between water and carbon dioxide radiation is rather complicated, partly because the relative ratio of water vapor and carbon dioxide in the atmosphere varies between wide limits. In the radiation chart this difficulty has been overcome by an approximative method. It is found that the absorption of carbon dioxide is concentrated chiefly in one rather narrow region of the spectrum where it is very intense. Hence the atmosphere, even in relatively thin layers, is practically opaque with respect to this particular radiation. Let us now consider the fundamental formula (4.1) for the flux

$$F = -\int d\nu \int_{u_0}^{u_1} f_b \frac{d\tau_f}{du}\, du$$

Now in the spectral interval occupied by the carbon dioxide band the absorption of carbon dioxide is very intense while outside of this band it is practically zero. The

integration over ν will in this case only extend over the width of the band. Within the band τ_f will decrease very rapidly with increasing u, so rapidly indeed that we may put f_b = const. in an interval of u in which τ_f decreases from unity to zero. Now

$$\int_0^\infty \frac{d\tau_f}{du}\,du = \Big|\,\tau_f\,\Big|_0^\infty = -1$$

so that we may write approximately

$$F_{CO_2} = \int_{CO_2} f_b\,d\nu \tag{5.1}$$

the integration extending over the width of the band. Hence at each level of the atmosphere the flux created by the carbon dioxide band is equal to that fraction of the black body radiation contributed by the carbon dioxide interval which corresponds to the temperature of that particular level. We may express this in our chart by drawing a carbon dioxide isopleth on top of all the other isopleths. The wedge-shaped area above this isopleth represents the fraction of the black body radiation originating in the carbon dioxide band. The isopleths below this top isopleth represent then only variations in water vapor thickness, the amount of water vapor increasing as we go downwards on the chart. Now according to definition the thickness u is the total amount of absorbing matter contained in a given slab, the thickness being measured in a direction normal to the slab, i.e., vertically in the real atmosphere. Hence, if ρ is the density of water vapor, we have by (2.2):

$$u = \int_{z_0}^{z} \rho\,dz = \frac{1}{g}\int_{p}^{p_0} w\,dp \tag{5.2}$$

where w is the ratio of water vapor to air density and g the acceleration of gravity and where z_0 and z represent the boundaries of the slab and p_0 and p the pressures at these boundaries.

It has been found that the absorption of water vapor, more accurately the absorption coefficients, depends upon the air pressure. This dependence of the absorption upon the pressure is rather complex; it is discussed in detail in Section 8, below. It will be shown there that an increase or decrease in air pressure by a factor a, say, has very nearly the same effect as a change in optical thickness by the factor $\sqrt{a}$. It follows that the pressure effect may be taken into account by introducing a "reduced specific moisture" $w\sqrt{p/p_s}$, (where p_s is a standard pressure, 1000 mb, say). We have then

$$u = \frac{1}{g}\int_{p}^{p_0} w\sqrt{p/p_s}\,dp \tag{5.3}$$

For most practical purposes we may put $g = 1000$. The formula remains unchanged if we express w in units of grams of water per kilogram of air as is customary, and at the same time change the unit of pressure from the c.g.s. unit to a millibar. Formula (5.3) will then give the moisture thickness in grams of precipitable water per cm^2.

Before proceeding to show the actual use of the chart, we shall briefly indicate how radiative cooling or heating in the atmosphere is computed from the flux F obtained by means of the chart. In the first place it seems useful to notice that the actual flux at any given level is the difference between a flux component directed upwards and originating in the layers below that particular level and a flux component directed downwards and originating in the layers above that level:

$$F = F_{\text{up}} - F_{\text{down}} \tag{5.4}$$

It may be noted that since the flux in the carbon dioxide band is equal, at any level, to a definite fraction of the black body radiation corresponding to the temperature of that level both in upward and downward direction, the *resultant* flux of carbon dioxide radiation vanishes in the approximation of the chart. This is a fair approximation to the truth in the lower atmosphere (for the upper atmosphere see Section 12). The upward and downward fluxes may be recognized as distinct areas on the chart (see Fig. 5). If F is the resultant flux at any level, it follows from the first law of thermodynamics that the divergence of this flux, dF/du, must be equal to the loss of heat energy of the layer of thickness du. In practice it is rather inconvenient to calculate this derivative, instead we may compute fluxes at a number of successive levels; then $F_1 - F_2$ will represent the loss of heat of the layer between the levels (1) and (2), etc. If we assume that this amount is distributed in the layer so as to cool or heat it uniformly, the mean cooling ΔT (i.e. averaged over the height of the layer) per unit time will be given by the formula

$$c_p \Delta T (p_1 - p_2)/g = F_1 - F_2 \tag{5.5}$$

the factor on the left being the heat capacity of the layer per cm^2 cross section. If the pressures are given in millibars we obtain from (5.5) the following numerical formula for the cooling

$$\Delta T = 4.1 \frac{F_1 - F_2}{p_1 - p_2} \tag{5.6}$$

Formula (5.5) presupposes evidently that the flux is expressed in calories per unit time; (5.6) gives the fall of temperature per unit time. In our radiation chart the flux is expressed in calories per three hours, hence the cooling obtained from (5.6) will refer to a period of three hours.

We shall now discuss some actual applications of the graphical method of obtaining the flux. Consider the path of integration given by formula (4.5). Assume that we want to obtain the total radiation received from the sky at the ground. The first integral in (4.5) goes from the absolute zero of temperature to the temperature T_0 of the ground along the upper edge, $u = 0$, of the chart. The second integral goes from there along the actual $u(T)$ relationship in our atmosphere to the temperature T_1 at the top of the atmosphere or rather at a point so high that all moisture is practically below it (usually one need not go extremely high for this purpose). This path is obtained on the chart by plotting the actual values of T and u, where T is the temperature at a variable level and u the total moisture below

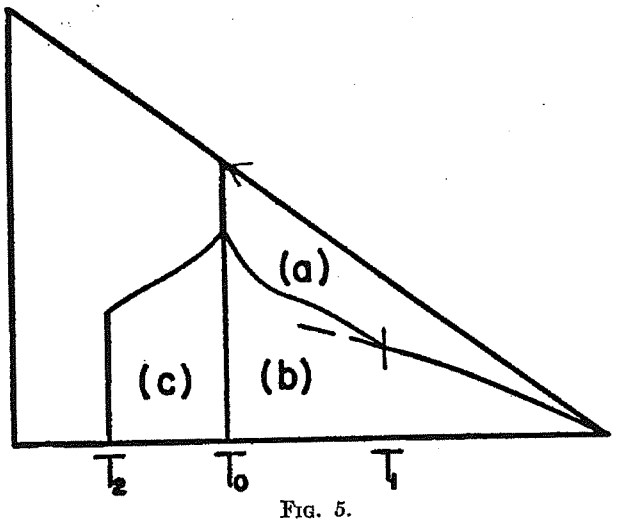

FIG. 5.

this level as computed from (5.3). The last integral in (4.5) goes from the point u_1 (T_1) representing the top of our atmosphere to the absolute zero of temperature along the isopleth $u = u_1$. Our total downward flux is now represented by an area such as designated by (a) in Fig. 5.

Applying a similar procedure to the flux coming from an isothermal layer of infinite thickness, we see that this flux is given by the area of the triangle to the right of the isotherm giving the temperature of the layer. The triangle represents therefore the black body flux, a fact that has already been derived in the previous section. In Fig. 5 this black body flux of temperature T_0, which might be taken as the emission of the ground, is given by the triangular area (a) + (b). The net flux (which is the net loss of heat at the ground) is equal to the difference of the upward and downward flux and is represented by the area (b).

In order to determine this area we may use the auxiliary table on the chart

which gives us the wedge-shaped area to the right of T_1. The remainder of the area may be measured by means of a planimeter. If no planimeter is at hand, we might approximate the moisture curve by a succession of straight lines and thus divide the area into a number of triangular and trapezoidal sections each of which can be evaluated without difficulty. Usually a small number of such subdivisions, three or four, say, will give a reasonable degree of accuracy. We might also proceed by taking from the auxiliary chart the wedge-shaped area to the right of T_0 and below the isopleth $u = u_1$; there remains then only a small area above $u = u_1$ to be evaluated by means of a planimeter or by the method just indicated.

Assume now that we want to compute the flux at a higher level in the atmosphere. Let T_0 in Fig. 5 represent the temperature at that level. The *downward* flux coming from the atmosphere above our level is again found in the same way as before, the thickness u being now counted upwards from our level as zero. The downward flux is therefore again given by an area of the type (a). The *upward* flux originates partly in the atmosphere below our level and partly at the ground itself. We plot again the $u(T)$ relationship on the chart, now counting u downwards with our fixed level as starting point $u = 0$; we continue in this way until we arrive at the ground, whose temperature may be T_2. The radiation of the ground itself is now replaced by that of an infinitely thick isothermal layer of temperature T_2. This means that on our chart we have to go all the way down along the isotherm T_2. The upward flux at our reference level T_0 appears now on the chart as the area (a) + (b) + (c). The net flux is the difference between the upward and downward fluxes and is given by the area (b) + (c) in Fig. 5, which may be measured in the manner indicated before.

In a similar fashion it is possible to take into account clouds present in the atmosphere. A cloud top as well as a cloud base represents a black surface and both are replaced by isothermal layers of infinite thickness. Thus, for instance, if the cloud *top* is located at the level of temperature T_0 in Fig. 5, the area (b) will represent the net loss of heat from the top of the cloud. If on the other hand the cloud base is at the level of temperature T_0, then the area (c) represents the net gain of heat at the cloud base due to radiation coming both from the ground and from the moist air below the cloud. The case of a ground inversion is represented in Fig. 6 with the reference level at the ground; the area to be evaluated consists now of two parts, one of which has negative sign.

Fig. 7 illustrates a direct way of obtaining cooling values from the chart. The two moisture-temperature distributions from the upper and lower boundaries of the slab in question are drawn and the area between shaded. This represents the difference of fluxes $F_1 - F_2$. The crosshatched strip to the right is again de-

termined from the auxiliary table as a difference of two wedge-shaped areas. The remainder of the area consists of two parts with opposite signs; it is seen, however, that if we go along the contour as indicated by the arrows, we encircle the two parts in opposite sense; we can therefore determine the area by a single

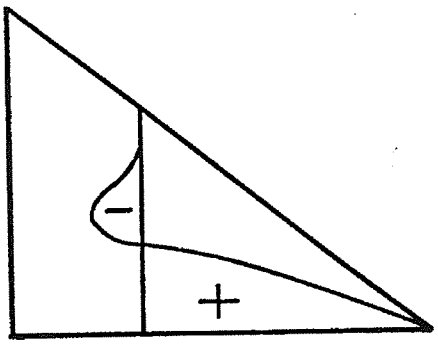

FIG. 6.

run of the planimeter. Using this method, one can plot the moisture curves of several successive levels on the same chart and rapidly obtain the cooling in each layer.

In the interior of a cloud we have black body radiation both in upward and downward direction and the resultant net flux which is the difference of the upward and

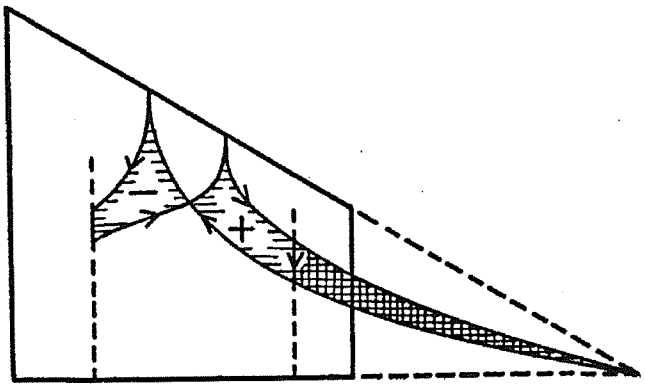

FIG. 7.

downward fluxes is extremely small. The loss or gain of heat which takes place at the boundary is usually distributed through the cloud by convective action. If we take F_1 and F_2 to mean the *net* fluxes at the base and the top of the cloud, respectively, formula (5.6) may still be applied to compute the cooling of the cloud by radiation.

Finally, the method of obtaining the $u(T)$ relationship which is plotted on the chart may be illustrated by an example. Table 2 gives an actual sounding, the

first three columns giving pressure, temperature, and specific humidity. The fourth column gives the mean specific humidity in each layer bounded by two points of the sounding. The fifth column indicates the thickness of each layer in millibars, the sixth column gives the pressure correction factor of the absorption $\sqrt{p/p_s}$, which was discussed at the beginning of this section. The effective amount of moisture in each layer is the product of the figures of columns 4, 5, and 6 divided by 1000 and is contained in column 7. By adding up the values in column 7 beginning from a given reference level and going either upward or downward from that level we obtain the values in the last three columns. These are the moisture thicknesses of the form (5.3). If they are plotted against the temperatures of column 2, curves of the type of Fig. 4 are obtained, and the areas under these curves can be evaluated in the manner indicated. It is often more convenient to plot the effective moistures as contained in column 7 on a sheet of graph paper and to obtain the values of column 8 by graphical integration.

TABLE 2

1	2	3	4	5	6	7	8	9	10
	Sounding		Mean			Eff.	u for reference level at		
p(mb)	t(°C)	w(gr/kg)	w	Δp	$\sqrt{p/p_s}$	moist.	1015	710	505
1015	10	6.7					0	1.36	1.56
			6.3	65	.99	0.41			
950	7	5.8					0.41	0.95	1.15
			5.5	30	.97	0.16			
920	7	5.3					0.57	0.79	0.99
			4.6	130	.93	0.56			
790	−1	3.9					1.13	0.23	0.43
			3.6	52	.87	0.16			
740	−4	3.3					1.29	0.07	0.27
			2.9	29	.85	0.07			
710	−2	2.5					1.36	0	0.20
			1.9	45	.83	0.07			
650	−8	1.3					1.43	0.07	0.13
			1.2	73	.78	0.07			
580	−14	1.1					1.50	0.14	0.06
			1.0	77	.74	0.06			
505	−16	0.9					1.56	0.20	0
			0.9	35	.69	0.02			
470	−18	0.8					1.58	0.22	0.02
			0.5	124	.64	0.04			
350	−34	0.3					1.62	0.26	0.06
			0.2	49	.57	0.01			
300	−44	..					1.63	0.27	0.07

PART II. STRUCTURE AND ABSORPTION OF INFRARED BANDS

6. Absorption of Spectral Lines

In texts on spectroscopy a number of effects are indicated which determine the width of spectral lines (9), (14). Among these, only two are of any importance for infrared lines under atmospheric conditions. These are first the disturbing effect upon radiating gas molecules of neighboring molecules known as impact broadening or pressure broadening of the lines. The second effect is the so called Doppler effect, which is due to the motions of the radiating molecules themselves. Under atmospheric conditions, however, the Doppler effect is usually much smaller than the pressure broadening effect and becomes indeed noticeable only if the pressure

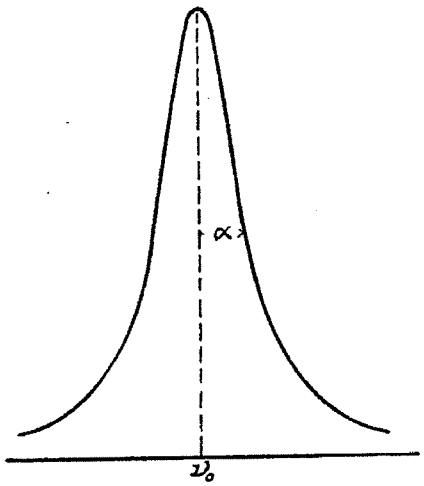

FIG. 8. Spectral line.

effect is sufficiently reduced. This is the case in the upper stratosphere, while in the lower stratosphere and the troposphere the shape of the spectral lines is practically determined by pressure broadening alone. Under these conditions it has been found that the shape of the line, i.e., the variation of the absorption coefficient with frequency is given by (Fig. 8),

$$k(\nu) = \frac{S}{\pi} \frac{a}{(\nu - \nu_0)^2 + a^2} \tag{6.1}$$

S is called the total intensity of the line; indeed,

$$\int_{-\infty}^{+\infty} k \, d\nu = S$$

and a is called the *half-width*. The maximum value of k is reached for $\nu = \nu_0$ and is equal to $S/\pi a$; for $\nu - \nu_0 = \pm a$ the intensity of absorption has sunk to $S/2\pi a$, one half of the maximum value.

We shall now calculate the fraction of incident radiation absorbed by a spectral line of the form (6.1) if a beam traverses a column of arbitrary thickness u. We assume that the incident intensity I_0 is constant within a certain interval $\Delta\nu$ of the spectrum and we make $\Delta\nu$ so large that outside of it the absorption of the considered line is negligible. The radiative energy incident in $\Delta\nu$ is $I_0 \Delta\nu$ and we define the *fractional absorption* in $\Delta\nu$ as

$$A = \frac{\int (I_0 - I)\, d\nu}{\int I_0\, d\nu} = \frac{1}{\Delta\nu}\int (1 - e^{-ku})\, d\nu \tag{6.2}$$

where k is given by (6.1). If we make the interval $\Delta\nu$ sufficiently wide we might without appreciable error introduce $-\infty$ and $+\infty$ as limits of the integral. We substitute (6.1) into (6.2), put for brevity

$$x = Su/2\pi a \tag{6.3}$$

and introduce a variable s by

$$\frac{\nu - \nu_0}{a} = \operatorname{tg}\frac{s}{2}, \quad \text{hence} \quad \frac{1}{(\nu - \nu_0)^2 + a^2} = \frac{1}{a^2}\cos^2\frac{s}{2} = \frac{1}{2a^2}(\cos s + 1)$$

(6.2) becomes now

$$A\Delta\nu = a\int_{-\pi}^{+\pi} (1 - e^{-x\cos s - x})\, \frac{d}{ds}\left(\operatorname{tg}\frac{s}{2}\right) ds$$

and by means of an integration by parts

$$A\Delta\nu = a\left| (1 - e^{-x\cos s - x})/\operatorname{cotg}\frac{s}{2}\right|_{-\pi}^{+\pi} + a\int_{-\pi}^{+\pi} x \sin s\, e^{-x\cos s - x} \operatorname{tg}\frac{s}{2}\, ds$$

The first term has the form $0/0$ at the boundaries and vanishes if numerator and denominator are differentiated. The second term may be written

$$A\Delta\nu = axe^{-x}\int_{-\pi}^{+\pi} (1 - \cos s)\, e^{-x\cos s}\, ds$$

This integral can be expressed in terms of *Bessel functions*.[1] A Bessel function of the order n is defined by the power series

$$J_n(z) = \frac{(z/2)^n}{0!\,n!} - \frac{(z/2)^{n+2}}{1!(n+1)!} + \frac{(z/2)^{n+4}}{2!(n+2)!} - \frac{(z/2)^{n+6}}{3!(n+3)!} + \cdots\cdots \tag{6.4}$$

[1] See for instance, Whittaker and Watson, *Modern Analysis*, ch. 17.

(where $0! = 1! = 1$); z might be a real or complex number. It is seen from (6.4) that

$$J_n(-z) = (-1)^n J_n(z) \tag{6.5}$$

The Bessel function may also be obtained by means of the following integral,[1] where $i = \sqrt{-1}$,

$$J_n(z) = \frac{1}{2\pi}\int_{-\pi}^{+\pi} e^{-ins + iz\cos s}\, ds \tag{6.6}$$

If we put $z = ix$ and make use of (6.5) we obtain finally for our integral (after Ladenburg and Reiche)

$$A\Delta\nu = 2\pi a x e^{-x}\left[J_0(ix) - iJ_1(ix)\right] = 2\pi a\, f(x) \tag{6.7}$$

where x is defined by (6.3). The Bessel functions appearing here have a purely imaginary argument. These functions are tabulated [2] and values of $f(x)$ are given in Table 3.

TABLE 3

$$f(x) = xe^{-x}\left[J_0(ix) - iJ_1(ix)\right]$$

x	$f(x)$	x	$f(x)$	x	$f(x)$	x	$f(x)$
0.01	0.0099	0.22	0.198	0.70	0.521	1.9	1.016
0.02	0.0198	0.24	0.214	0.75	0.548	2.0	1.048
0.03	0.0295	0.26	0.230	0.80	0.575	2.5	1.192
0.04	0.0392	0.28	0.246	0.85	0.601	3.0	1.320
0.05	0.0488	0.30	0.261	0.90	0.626	3.5	1.436
0.06	0.0583	0.32	0.276	0.95	0.650	4.0	1.543
0.07	0.0676	0.34	0.291	1.00	0.674	4.5	1.643
0.08	0.0769	0.36	0.305	1.1	0.719	5	1.734
0.09	0.0861	0.38	0.320	1.2	0.762	6	1.912
0.10	0.0952	0.40	0.334	1.3	0.803	7	2.072
0.12	0.1132	0.45	0.368	1.4	0.842	8	2.222
0.14	0.1309	0.50	0.401	1.5	0.879	9	2.360
0.16	0.1480	0.55	0.432	1.6	0.916	10	2.491
0.18	0.1652	0.60	0.463	1.7	0.950		
0.20	0.1818	0.65	0.492	1.8	0.984		

We shall first study the behavior of the expression (6.7) for small and large values of x. For small x we see from (6.4) that $J_0(ix) \to 1$ and $iJ_1(ix) \to -x/2$, which is small. Further $e^{-x} \to 1$. Hence for small x, using (6.3)

$$A\Delta\nu = 2\pi a x = Su \tag{6.8}$$

so that for small u (thin layers) the amount absorbed is equal to the product of the line intensity and the thickness of the layer.

For large values of x, on the other hand, we may use a formula which is proved

[1] Whittaker and Watson, ch. 17. 23.

[2] Jahnke-Emde, *Tables of Functions*, 2nd ed., Leipzig, 1933.

in the theory of Bessel functions. It is shown there that if x is large we have approximately

$$J_n(ix) \to \frac{(i)^n e^x}{\sqrt{2\pi x}} \tag{6.9}$$

which if applied to (6.7) yields immediately

$$A\Delta\nu = \sqrt{8\pi a^2 x} = 2\sqrt{Sau} \tag{6.10}$$

While the mathematical derivation of (6.9) implies that x is actually large, it is found that a good approximation obtains already for rather moderate numerical values of x, say $x = 3$. This means that for layers of moderate thickness (6.10) is a

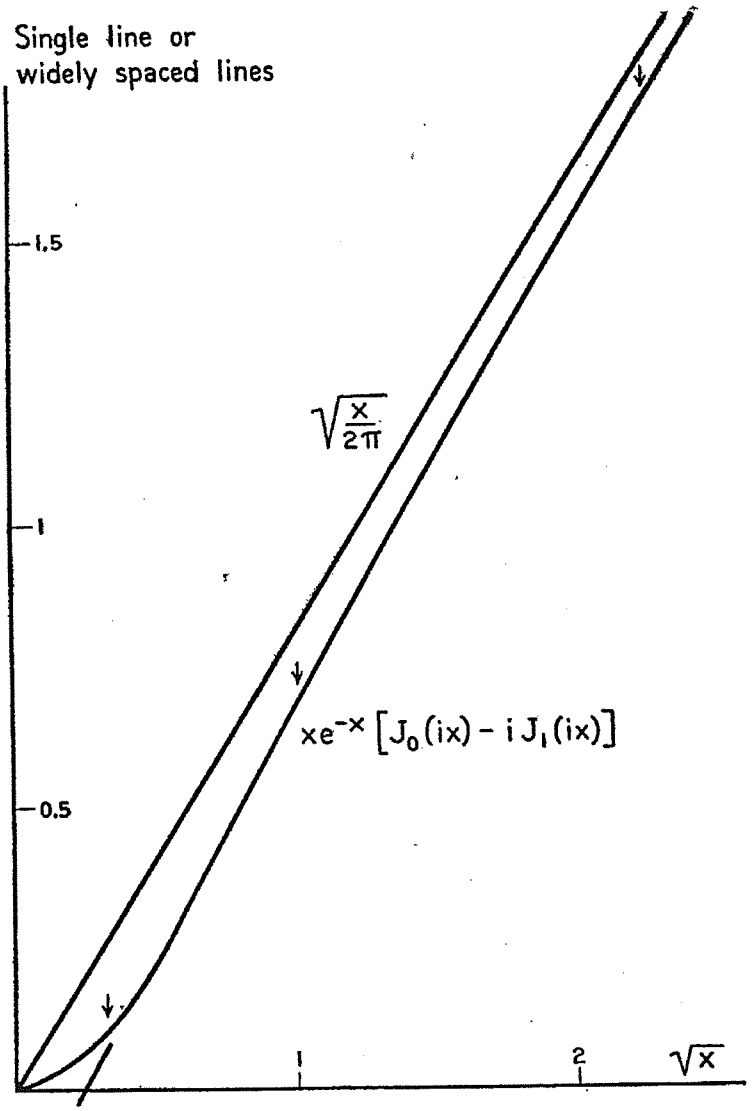

FIG. 9. Absorption of a spectral line, after Ladenburg and Reiche.

good approximation, and we see that for such layers the absorption is proportional to the *square root* of the thickness u and of the line intensity S.

On account of the great significance for the subsequent investigations of this type of absorption we give, in Fig. 10, a somewhat more detailed analysis. Fig. 10 shows the actual transmission as a function of ν for three different thicknesses corresponding to $x = 0.1$, $x = 1$, and $x = 5$, values which have been marked by small arrows in Fig. 9. For $x = 0.1$ we are obviously in the region of the linear absorp-

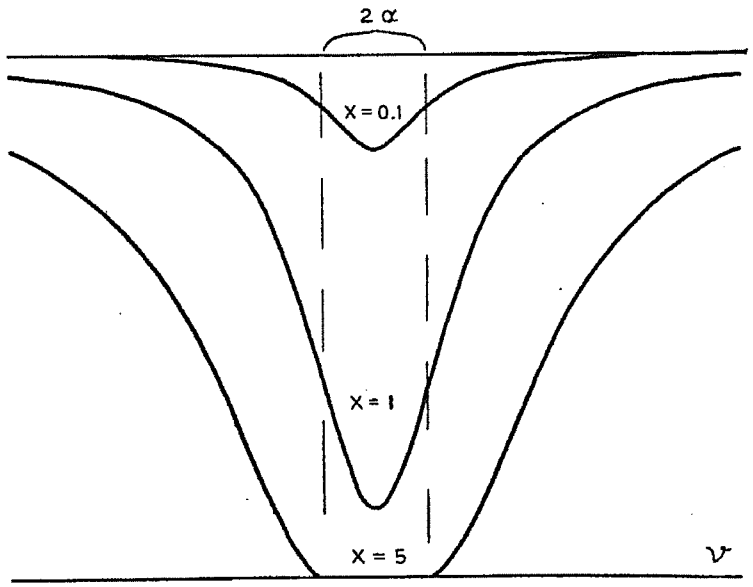

FIG. 10. Absorption of a spectral line.

tion law (6.8), the area above the curve which measures the total amount of radiation absorbed being proportional to x. For $x = 5$, on the other hand, we are in the domain of the square-root absorption law (6.10), and the physical significance of this may be inferred from the figure: The center of the line has been absorbed completely and any further increase of absorptions takes place in the *wings* of the line at a large distance from the center. We may express this mathematically by neglecting a^2 in the denominator of (6.1) as compared to $(\nu - \nu_0)^2$. We may then write, say,

$$ku = 2xa^2/(\nu - \nu_0)^2 = v,$$

and we have from (6.2):

$$A\Delta\nu = \sqrt{2xa^2}\int_0^\infty (1 - e^{-v})\,\frac{dv}{v^{3}}$$

$$= 2\left|\frac{\sqrt{2xa^2}}{\sqrt{v}}\,(1 - e^{-v})\right|_0^\infty + 2\sqrt{2xa^2}\int_0^\infty e^{-v}\,\frac{dv}{\sqrt{v}} = \sqrt{8\pi xa^2}$$

and this is indeed identical with (6.10).

The above analysis is due to Ladenburg and Reiche (51); the approximate proportionality of the absorption with the square root of the optical thickness for spectra of this kind has been verified in numerous spectroscopic investigations. The values of $f(x)$ as defined by (6.7) are plotted in Fig. 9 with $\sqrt{x}$ as abscissa. The straight line which goes through the origin of the coördinates represents the function $\sqrt{2x/\pi}$ which by (6.9) approximates $f(x)$ for large x. For intermediate values of x a better approximation may be obtained from the numerical formula

$$A\Delta\nu/2\pi a = 0.85\sqrt{x} - 0.17$$

which intersects the axis of abscissae at $\sqrt{x} = 0.20$ and can of course only be used for values of $\sqrt{x}$ larger than this.

* * *

The infrared absorption bands contain usually a very large number of lines of the type considered. In some important cases, for instance in the water vapor bands, the lines are so far apart from each other that each one absorbs independently of the others. The total amount of radiation absorbed is then a sum of individual contributions of the form (6.7). Experiments have shown that it is permissible to assume that the half-width a of the lines is roughly the same for all lines of one band. Let us now assume that there are N lines in a given interval of the spectrum, all having the same half-width a. Remembering that $x = Su/2\pi a$ we obtain from the preceding formula for the combined absorption of these lines:

$$A\Delta\nu = 0.85\sqrt{2\pi a}\,(\Sigma\sqrt{S_i})\sqrt{u} - 0.17\cdot 2\pi a N \tag{6.11}$$

This relationship represents a straight line in a diagram such as Fig. 9 where $A\Delta\nu$ is plotted against $\sqrt{u}$. We may write

$$A\Delta\nu = a\sqrt{u} - b$$

If the line intersects the $\sqrt{u}$ axis at $\sqrt{u_0}$ we have $b = a\sqrt{u_0}$ and since b is small we may write here in sufficient approximation $a = A\Delta\nu/\sqrt{u}$. Hence, using the numerical value of b from (6.11)

$$(A/\sqrt{u})\sqrt{u_0} = b\,\Delta\nu = 0.17\,(2\pi a/d) \tag{6.12}$$

where $d = 1/N\Delta\nu$ is the mean distance of consecutive lines in the spectrum. We can thus determine the ratio a/d by measurements which do not involve a spectroscopic resolution of the individual lines.

If u is sufficiently large, so that the somewhat simpler approximation (6.9) applies, we have

$$A\Delta\nu = 2\sqrt{a}\,(\Sigma\sqrt{S_i})\sqrt{u} \tag{6.13}$$

In infrared spectroscopy it is often impossible to measure the individual lines except with instruments of the highest resolving power. It is therefore difficult to decide whether a given absorption is of a continuous character or composed of the absorption of individual lines. If we plot the absorption against the square root of the optical thickness, we obtain a straight line in the case discussed here. If on the other hand the absorption is that of a continuous spectrum so that by (6.2)

$$I/I_0 = 1 - A = e^{-ku}$$

we obtain a straight line if we plot $\log I/I_0$ against the thickness u. This method has been extensively used by Strong (33). It was found from the observations that in cases of interest for atmospheric transfer the absorption is clearly of the square-root type.

In some cases it is possible to obtain more accurate information about the spectral lines from absorption plots of a related type. Matheson (52) has studied the

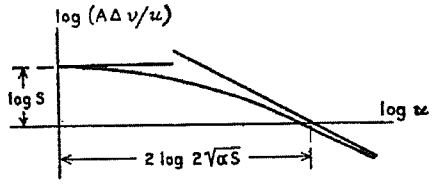

FIG. 11. Matheson diagram.

transition from the linear law (6.8) to the square-root law (6.10). If we take first a single line and plot $\log (A\Delta\nu/u)$ against $\log u$ (Fig. 11) we see from (6.8) that for small values of u the curve approaches asymptotically a horizontal straight line, while for large u it approaches a slanting line. The intersections of these lines with the axes determine the quantities indicated in Fig. 11 which are $2 \log 2\sqrt{\alpha S}$ and S, respectively. It is then possible to determine α from the plot. If we have a number of lines absorbing simultaneously, the corresponding quantities will be $2 \log 2\sqrt{\alpha}\, \Sigma\sqrt{S_i}$ and $\Sigma\sqrt{S_i}$, respectively. Assuming that in a certain interval the lines are of practically equal intensity S we see that $\Sigma\sqrt{S_i}$ and ΣS_i reduce to $\sqrt{NS}$ and NS respectively, where N is the number of lines in the interval. One can again obtain α from the plot if N is known; often N may be obtained from molecular theory. In this way Matheson determined the line width of carbon monoxide. The method seems to work well for diatomic molecules which have very regular spectra but would seem to break down for polyatomic molecules such as water vapor where the spectral lines are by no means of nearly constant intensity.

* * *

So far we have only discussed the absorption of a straight beam by a spectral line or a sum of lines. To conclude this section we shall briefly compare the absorp-

tion of straight columns and of slabs in the cases of exponential and square-root absorption.

For the absorption of a continuous spectrum of coefficient k we go back to Section 2. If we again define the beam and slab transmission functions by

$$\tau_I = I/I_0, \quad \tau_f = f/f_0$$

we have for a continuous spectrum

$$\tau_I = e^{-ku}$$

and by (2.8)

$$\tau_f = 2Ei_3\,(ku)$$

The function $2Ei_3$ has a shape very similar to that of an ordinary exponential. Roberts (89) found that a close numerical approximation is obtained by putting

$$\tau_f = e^{-3ku/2} \tag{6.14}$$

so that a slab of thickness u is practically equivalent to a linear column of length $1.5\,u$.

On the other hand, if we have a spectral line or a sum of lines, the absorption is proportional to the square root of u. If in (6.13) we put

$$2\sqrt{a}\,(\Sigma\sqrt{S_i}) = \sqrt{2l/\pi}$$

where l is a constant characterizing the intensity of the square root absorption, we may write

$$\tau_I = 1 - \sqrt{2lu/\pi} \tag{6.15}$$

and we obtain the transmission of a slab from (3.8) which yields

$$\tau_f = 1 - \frac{4}{3}\sqrt{2lu/\pi} = 1 - \sqrt{(1.78u)\cdot 2l/\pi}$$

Hence, in the case of square-root absorption a slab of thickness u is mathematically equivalent to a linear column of length $1.78\,u$. (On limited applicability, see Sec. 7.)

7. Absorption of a Band Spectrum

It is obvious that the increase of absorption with the square root of the thickness cannot go on indefinitely if several lines are present in the spectrum, as for sufficiently thick layers the absorption strips of neighboring lines must overlap. In other words, a thickness must finally be reached in which almost all the radiative energy has been absorbed from a given interval of the spectrum, and a further increase in thickness can produce only a smaller increase in absorption. Hence the square-root formula must fail when the absorption strips of neighboring lines begin to overlap appreciably.

This case has been treated by Schnaidt (55) and by Elsasser (42). Schnaidt uses a numerical approximation in order to account for the reduction in absorption due to the overlapping of neighboring lines while Elsasser develops a mathematical method for a somewhat idealized model of an absorption band. We shall now indicate the principle of the latter method; the numerical results obtained by the two authors show very little difference.

In place of one spectral line we introduce a periodical pattern of equal and equidistant lines (Fig. 12). In formulae, we assume the absorption coefficient to be

$$k(\nu) = \sum_{-\infty}^{+\infty} \frac{S}{\pi} \frac{a}{(\nu - nd)^2 + a^2} \tag{7.1}$$

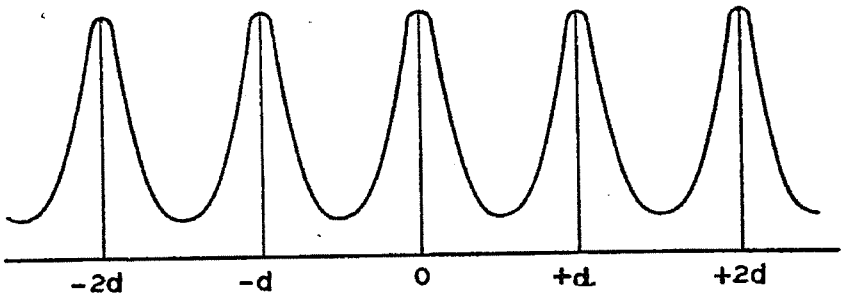

FIG. 12. Schematical "band spectrum."

where the individual line is again of the form (6.1) and where the line centers are located at 0, $\pm d$, $\pm 2d$, ... This expression can be brought into another, more convenient form. In the theory of functions it is shown that any periodic function, such as (7.1) can be expressed by means of trigonometric functions.[1] We shall omit the details here and simply indicate the result. If we put

$$s = 2\pi\nu/d, \quad \beta = 2\pi a/d \tag{7.2}$$

we find for (7.1)

$$k(\nu) = \frac{S}{d} \frac{\sinh \beta}{\cosh \beta - \cos s} \tag{7.3}$$

where as usual *sinh* and *cosh* designate the hyperbolic *sin* and *cos*. If we now assume the incident intensity to be constant throughout the spectrum, we may define the transmission functions as

$$\tau_I = \frac{1}{2\pi} \int_{-\pi}^{+\pi} e^{-k(s)u}\, ds \tag{7.4}$$

where k is given by (7.3).

[1] Whittaker and Watson, *Modern Analysis*, ch. 7. 4.

We consider first the special case in which the lines are far apart from each other, $d \gg a$, or β small. We have then $\cosh \beta = 1$ and $\sinh \beta = \beta$ and (7.3) becomes

$$k(\nu) = S\beta u/d \sin^2\left(\frac{s}{2}\right) = C/\sin^2\left(\frac{s}{2}\right) = C \cdot y \tag{7.5}$$

Introducing into (7.4) we find readily that

$$\tau_I = \frac{1}{\pi}\int_1^\infty \frac{e^{-Cy}\,dy}{y\sqrt{y-1}}$$

It follows that (with $z = y - 1$):

$$-\frac{d\tau_I}{dC} = \frac{1}{\pi}\int_1^\infty \frac{e^{Cy}\,dy}{\sqrt{y-1}} = \frac{e^{-C}}{\pi}\int_0^\infty \frac{e^{-Cz}}{\sqrt{z}}\,dz = \frac{e^{-C}}{\sqrt{\pi C}}$$

Integrating again with respect to C we find

$$\tau_I = \frac{1}{\sqrt{\pi}}\int_{\sqrt{C}}^{C} e^{-C}\frac{dC}{\sqrt{C}} = \frac{2}{\sqrt{\pi}}\int_{\sqrt{C}}^{\infty} e^{-x^2}\,dx$$

The upper limit of the last integral has to be chosen so that $\tau_I = 1$ for $C = 0$ which shows that the limit is $+\infty$. The function which appears here is known under the name of *probability integral*. It is usually defined as

$$\phi(x) = \frac{2}{\sqrt{\pi}}\int_0^x e^{-x^2}\,dx \tag{7.6}$$

and on using this symbol we have finally, in view of (7.2) and (7.5),

$$\tau_I = 1 - \phi(\sqrt{C}) = 1 - \phi(\sqrt{\pi S a u/d}) \tag{7.7}$$

The probability integral may be developed into the power series

$$\phi(x) = \frac{2}{\sqrt{\pi}}\left(x - \frac{x^3}{3} + \ldots\right)$$

and for small values of the argument (7.7) reduces therefore to

$$\tau_I = 1 - 2\sqrt{Sau}/d \tag{7.8}$$

Since there is one line per spectral interval of width d, the absorption of a single line is $2\sqrt{Sau}$ in agreement with (6.9). Formula (7.8) becomes identical with (6.15) if we define a *generalized absorption coefficient* of our band by

$$l = 2\pi a S/d^2 \tag{7.9}$$

On introducing this abbreviation into (7.7) we may write

$$\tau_I = 1 - \phi\left(\sqrt{\frac{lu}{2}}\right) \tag{7.10}$$

While this formula has been derived for a regular absorption pattern of the type represented in Fig. 11, we might also use as an approximation for bands of more irregular structure, such as the water vapor bands, in which the lines are no longer equidistant and of equal intensity.

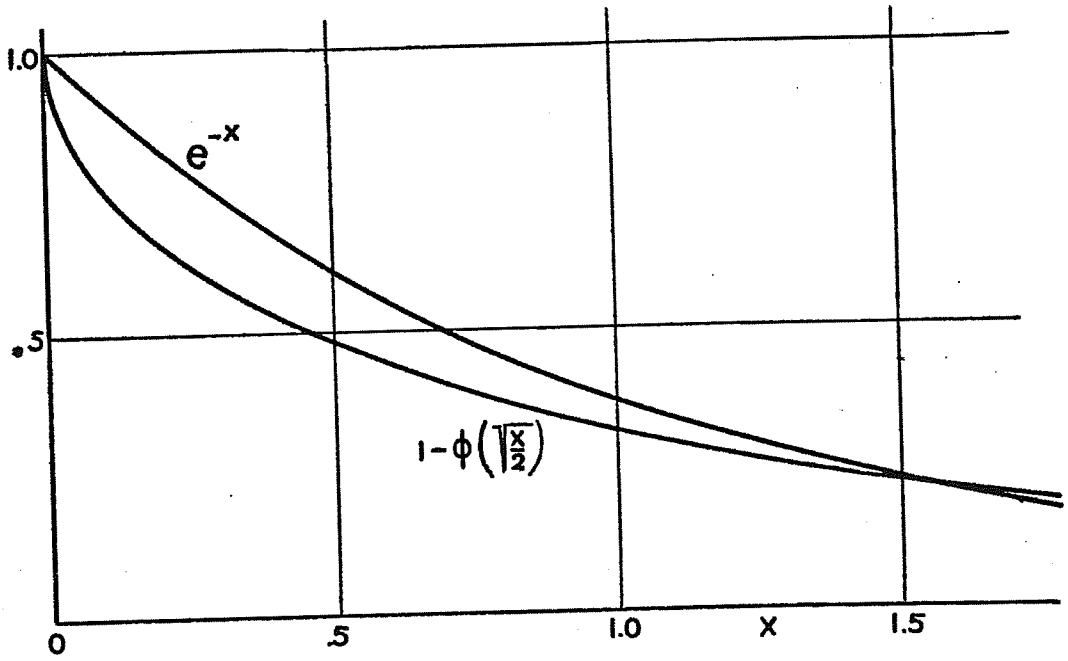

FIG. 13. Transmission functions of a straight column.

The transmission function is generally defined as the ratio of transmitted to incident intensity in a given spectral interval, and we have by (6.2)

$$\tau_I = \frac{1}{I_0 \Delta\nu} \int_{\Delta\nu} I d\nu = 1 - A$$

The transmission τ_I of a slab is again connected with τ_I by (3.8).

We have by (7.8) and (7.9) for sufficiently small values of u

$$\tau_I = 1 - \sqrt{2lu/\pi} \tag{7.11}$$

and hence the relation between A and l is in the region where the square-root law applies

$$A = \sqrt{2lu/\pi} \tag{7.12}$$

On the other hand, on using (7.12) we get from (6.13) for the transmission of a group of widely separated but otherwise arbitrary lines of intensities S_i

$$\tau_I = 1 - 2\sqrt{au}\,(\Sigma\sqrt{S_i})/\Delta\nu$$

and hence

$$\sqrt{l} = \sqrt{2\pi a}\,(\Sigma\sqrt{S_i})/\Delta\nu \tag{7.13}$$

The generalized absorption coefficient thus defined may now be inserted in (7.10) and we obtain a formula for the absorption of a band of arbitrary composition. It

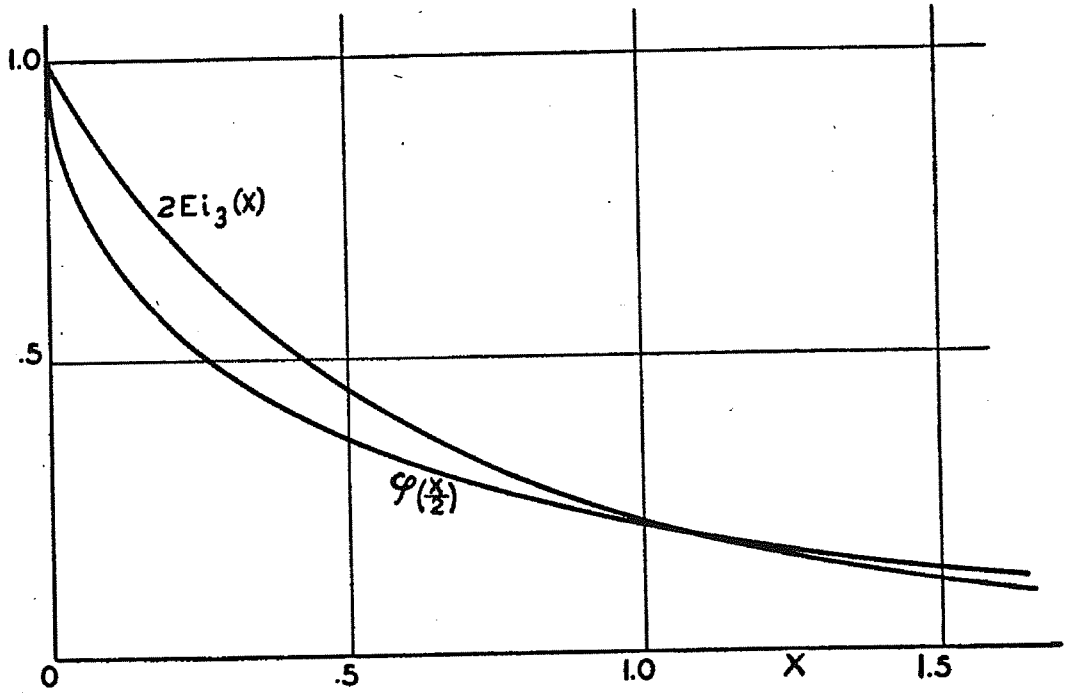

FIG. 14. Transmission functions of a slab.

is of course not to be expected that the absorption of such a band should follow (7.10) accurately, since the latter was derived for the regular pattern represented in Fig. 12, but it would be extremely difficult to derive mathematical expressions for the absorption of a more complicated band and (7.10) may be considered as an approximation of the general case with a suitably chosen value of l.

We can finally compute the transmission in a slab of absorbing material from (3.8) if we substitute the value (7.10) of τ_I. After a rather cumbersome but straightforward calculation we obtain, with $x = lu/2$,

$$\tau_f = \varphi(x) = (1 - \phi(\sqrt{x}))\left(1 - \frac{4x^2}{3}\right) + \frac{2e^{-x}}{3}\sqrt{\frac{x}{\pi}}\,(2x - 1) \tag{7.14}$$

Some of the transmission functions which appear in the present analysis are numerically given in Table 4. The first two columns give the functions $Ei_2(x)$ and $2Ei_3(x)$, while the next two columns give the band transmission functions $\tau_I(x) = 1 - \phi(\sqrt{x})$ and $\tau_f(x) = \varphi(x)$ defined by (7.14). In order to compare the transmission of a continuous and that of a band spectrum the functions e^{-x} and $1 - \phi(\sqrt{x/2})$ are plotted together in Fig. 13; in a similar fashion, the corresponding transmission functions for a slab, $2Ei_3(x)$ and $\varphi(x/2)$ are plotted in Fig. 14.

TABLE 4. TRANSMISSION FUNCTIONS (THE FIRST TWO FROM (8))

Ei_n is defined by (2.8), ϕ by (7.6), and φ by (7.14).

x	$Ei_2(x)$	$2Ei_3(x)$	$1-\phi(\sqrt{x})$	$\varphi(x)$	x	$Ei_2(x)$	$2Ei_3(x)$	$1-\phi(\sqrt{x})$	$\varphi(x)$
0	1.0000	1.0000	1.0000	1.0000	1.0	.1485	.2194	.1573	.0859
0.01	.9497	.9806	.8875	.8509	1.1	.1283	.1918	.1380	.0729
0.02	.9131	.9619	.8415	.7910	1.2	.1111	.1679	.1213	.0621
0.03	.8817	.9440	.8065	.7461	1.3	.0964	.1472	.1069	.0531
0.04	.8535	.9266	.7773	.7091	1.4	.0839	.1291	.0943	.0455
0.05	.8278	.9098	.7518	.6773	1.5	.0731	.1134	.0833	.0391
0.06	.8040	.8935	.7290	.6499	1.6	.0638	.0998	.0736	.0337
0.07	.7818	.8777	.7083	.6239	1.7	.0558	.0879	.0652	.0291
0.08	.7610	.8622	.6892	.6008	1.8	.0488	.0774	.0578	.0251
0.09	.7412	.8472	.6714	.5796	1.9	.0428	.0683	.0512	.0217
0.10	.7225	.8326	.6547	.5599	2.0	.0375	.0603	.0455	.0188
0.15	.6410	.7646	.5838	.4786	2.1	.0330	.0532	.0404	.0163
0.20	.5742	.7039	.5271	.4163	2.2	.0290	.0470	.0359	.0142
0.25	.5177	.6494	.4795	.3647	2.3	.0255	.0416	.0320	.0124
0.30	.4691	.6001	.4386	.3249	2.4	.0225	.0368	.0285	.0108
0.35	.4267	.5553	.4028	.2899	2.5	.0198	.0325	.0254	.0094
0.40	.3894	.5146	.3711	.2588	2.6	.0175	.0289	.0226	.0081
0.45	.3562	.4773	.3428	.2341	2.7	.0154	.0256	.0201	.0072
0.50	.3266	.4432	.3173	.2115	2.8	.0136	.0227	.0180	.0063
0.55	.3001	.4119	.2943	.1918	2.9	.0120	.0201	.0160	.0055
0.60	.2762	.3831	.2733	.1741	3.0	.0107	.0178	.0143	.0048
0.65	.2546	.3566	.2542	.1585	3.5	.0058	.0099	.0081	.0025
0.70	.2349	.3321	.2367	.1446	4.0	.0032	.0055	.0047	.0013
0.75	.2171	.3095	.2207	.1321	4.5	.0018	.0031	.0027	.0007
0.80	.2008	.2886	.2059	.1209	5	.0010	.0017	.0016	.0004
0.85	.1860	.2693	.1923	.1108	6	.0003	.0006	.0005	.0001
0.90	.1725	.2513	.1797	.1017	7	.0001	.0002	.0002	
0.95	.1600	.2348	.1681	.0934	8		.0001	.0001	

* * *

At this point we might perhaps enlarge somewhat on the physical interpretation of the transmission functions. We might define τ_I as the probability of a beam of radiation traversing a column of thickness u without being absorbed. If $\tau_I = e^{-ku}$ we have

$$\int_0^\infty e^{-ku}\, du = 1/k$$

hence ke^{-ku} is a probability in the ordinary sense. Correspondingly we find

$$\int_0^\infty (1 - \phi(\sqrt{lu/2}))\, du = 1/l$$

so that $l\,(1 - \phi(\sqrt{lu/2}))$ is the corresponding probability for a band absorption.

The *mean* penetration of a beam into the absorber may be defined in agreement with the ordinary rules of probability theory as

$$\bar{u} = \int_0^\infty u\tau_I\, du / \int_0^\infty \tau_I\, du$$

and we obtain for $\tau_I = e^{-ku}$

$$\bar{u} = 1/k$$

Furthermore for $\tau_I = 1 - \phi(\sqrt{lu/2})$ we get after a few simple calculations

$$\bar{u} = 3/2l$$

so that for $k = l$ the radiation penetrates further in the case of a band spectrum.

* * *

The band transmission functions (7.7) or (7.10) will reduce to the square-root formula (7.8) or (7.12) for small values of the thickness u. On the other hand we saw in the preceding chapter that for extremely small values of u the square-root law becomes again invalid. We shall see later that the same is true for the formulae (7.7) or (7.10) if u becomes very small. The question arises therefore of whether there exists an intermediate interval of u of appreciable magnitude in which the square-root formula is actually valid. This can be answered in the affirmative. It may be seen from an inspection of the numerical values of (7.10) given in Table 4 that the probability integral can be well approximated by the first term of its power series for a considerable interval. Up to an absorption of about 65% the deviations amount to only a few per cent. On the other hand, the deviation which occurs for very small values of the absorption, (where the simple square root has to be replaced by the expression (6.7),) depends on the line distance and line width of the particular spectrum. This deviation may be determined by substituting (7.12) into (6.12) which yields

$$\sqrt{lu_0} = 0.21\,\frac{2\pi a}{d} \tag{7.15}$$

where u_0 is a critical thickness for which the absorption becomes practically zero.

The transmission function (7.10) with the correction for small thicknesses just explained is plotted in Fig. 15 against the decadic logarithm, log lu, (the numerical value $2\pi a/d = 0.5$ being used for the cut-off was obtained by assuming $a = 0.25$ as

explained in Section 9 and counting the number of lines per unit spectral interval of the water vapor spectrum in Fig. 16, which gives about $d = 3$). This curve is designated by "beam"; the dashed curve is the unmodified transmission curve (7.10) and in the region where the dashed curve deviates from the solid curve the latter represents the function (6.7) adjusted so that it will practically vanish at the value (7.15). The curve designated by "slab" is derived from transmission function (7.14) with a similar correction for small thicknesses, the function represented for thicker layers being $\varphi(lu/2)$. This plot was used in the numerical computations for the radiation chart. It is seen that in the average the distance of the two curves is about 0.21 on the logarithmic scale which corresponds to a ratio of thicknesses of about $5/3 = 1.66$. This is intermediate between the values given in (6.14) and (6.15) while somewhat closer to the latter. It may be concluded that for most practical purposes in radiation transfer problems the radiation of two-dimensional slabs may be reduced to that of linear columns by the substitution $u \to 1.66\, u$ without too much loss of accuracy.

* * *

We shall close this section [1] by deriving a formula for band absorption in the most general case. We go back to the expression (7.3) for the absorption coefficient. If we put

$$\frac{1 - \cosh\beta \cdot \cos s}{\cosh\beta - \cos s} = \cos\varphi, \quad \text{and} \quad \frac{\sinh\beta - \sin s}{\cosh\beta - \cos s} = \sin\varphi$$

it follows that

$$\frac{\sinh\beta}{\cosh\beta - \cos s} = \frac{\cosh\beta - \cos\varphi}{\sinh\beta} \quad \text{and} \quad ds = \frac{\sinh\beta}{\cosh\beta - \cos s}\, d\varphi$$

On introducing these expressions into (7.4) and writing for brevity $y = Su/(d \sinh\beta)$ we find

$$\frac{d\tau}{dy} = \frac{\sinh\beta}{2\pi}\int_{-\pi}^{+\pi} e^{-y\cosh\beta + y\cos\varphi}\, d\varphi = \sinh\beta\, e^{-y\cosh\beta}\, J_0(iy)$$

the last equality by (6.6) and in view of (6.5). Integrating this with respect to y and taking the limits of integration so that $\tau_I = 1$ for $y = 0$ and $\tau_I = 0$ for $y = \infty$ we obtain

$$\tau_I = \sinh\beta \int_{y = Su/(d\sinh\beta)}^{\infty} e^{-y\cosh\beta}\, J_0(iy)\, dy \tag{7.16}$$

A number of previously discussed cases can readily be derived by specialization of (7.16). For widely spaced lines β and hence $\sinh\beta$ is small so that y is large. We

[1] The remainder of the section contains mathematical details which will not be referred to later.

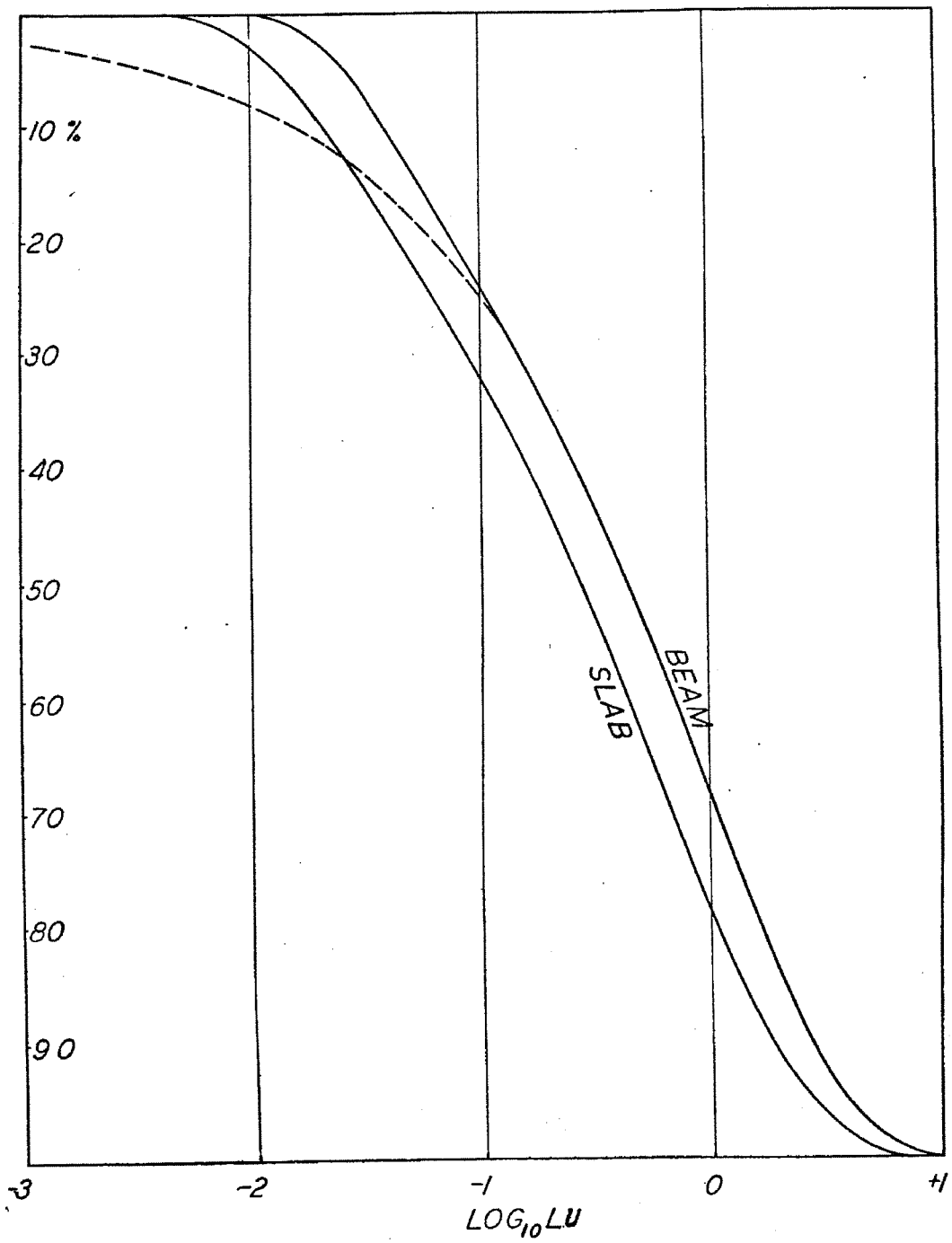

FIG. 15. Corrected transmission functions (logarithmic scale).

can then use the approximate expression (6.9) for $J_0(iy)$ and since for small β we have $\cosh\beta - 1 = \beta^2/2$ we are left with

$$\tau_I = \sinh\beta \int_y^\infty e^{-y\beta^2/2} \frac{dy}{\sqrt{2\pi y}}$$

which is readily seen to be identical with (7.7).

If the spectral lines are close together we have the other extreme in which β is large. Then $\cosh\beta$ is appreciably larger than unity and hence the exponential decreases more rapidly than the Bessel function increases. If we write

$$1 - \tau_I = \sinh\beta \int_0^y e^{-y\cosh\beta} J_0(iy)\, dy$$

we see that most of the contribution to the integral comes from small values of y. Now $J_0(0) = 1$, and the function increases very slowly in the beginning so that we may replace J_0 by unity under the integral. Since further for large β we have $\sinh\beta = \cosh\beta$ we get

$$\tau_I = e^{-Su/d}$$

the transmission is that of a continuous spectrum of absorption coefficient $k = S/d$. The last result may be derived more directly from (7.3) which gives $k = S/d$ for large values of β. Numerically, this is a rather good approximation for, say, $\beta \geqq 2$. For $\beta = 2$ we see from (7.2) that $d = \pi a$, so that if the line distance is about three times the half-width the mean absorption is very little different from that of a continuous spectrum. On the other hand for $\beta \leqq 1/2$ the approximation (7.7) holds good and for $\beta = 1/2$ we have $d = 4\pi a$ so that for a mean line distance twelve times the half-width or more formula (7.7) is applicable.

Finally we can derive a generalization of (6.7) from our formula (7.16). In this case β is again small (distant lines), but now u is assumed to be small too. Hence y in (7.16) is not in general small, but we can put $\cosh\beta = 1$. Then

$$\tau_I = \beta \int_y^\infty e^{-y} J_0(iy)\, dy \tag{7.17}$$

By means of the relations

$$\frac{dJ_0(z)}{dz} = -J_1(z), \qquad \frac{dJ_1(z)}{dz} = -\frac{J_1(z)}{z} + J_0(z)$$

which may readily be proved from (6.4) we find

$$e^{-y} J_0(iy) = \frac{d}{dy}\left[ye^{-y}\left(J_0(iy) - iJ_1(iy)\right)\right]$$

and (7.17) becomes

$$1 - \tau_I = \frac{Su}{d} e^{-y}\left[J_0(iy) - iJ_1(iy)\right] \tag{7.18}$$

But $y = Su/(d \sinh \beta) = Su/d\beta$ for small β; and since $\beta = 2\pi a/d$ by (7.2) we see that now $y = x$, where x is defined by (6.3). Hence (7.18) is identical with (6.7) apart from a factor $1/d$, which gives the number of lines per unit frequency interval in the spectrum.

We might say that formula (7.18) for small u in conjunction with the probability integral (7.7) for moderate values of u yields an excellent approximation of the true absorption curve up to, say, 85–90% absorption even if the spectrum is highly irregular, provided only the line distance is large compared to the half-width, as in water vapor. For very thick layers the probability integral (7.7) will tend to give somewhat too intense absorption for a spectrum of irregular structure. The reason for this is that with an irregular distribution of the lines, there will occasionally be wider gaps in the sequence of lines and comparatively thick layers will be required until the absorption is complete in these gaps. This is, however, only a qualitative argument, and the computation of an absorption curve in which both the distances and the intensities of the lines are distributed irregularly must remain to the future. A direct experimental determination of the transmission curve for a given spectrum, such as that of water vapor, is of course possible if the slit-width of the spectroscope is suitably chosen, but might be difficult on account of the considerable interval of thicknesses that has to be covered.

8. Pressure and Temperature Corrections

So far we have implicitly assumed that the absorption coefficient is independent of pressure and temperature so that the influence of temperature upon radiation is entirely due to the variation of the Planck function (1.6) with temperature, and the influence of the air pressure upon the radiation is nil. We shall now investigate the influence of pressure and temperature upon the absorption coefficients.

We first consider the pressure effect. For the subsequent presentation we have made frequent use of a paper by Schnaidt (55). It has been found that the total line intensity S is nearly independent of the pressure while the half-width a is a function of the pressure and increases with the latter, (9), (14). This effect is called pressure broadening of the spectral lines. It is of course understood that we compare conditions in which the total optical thickness u of the radiation remains the same while the pressure is changed either by compressing the radiating gas or by adding a transparent gas such as air. It is found that the half-width produced depends on the chemical nature of the broadening gas. Thus for instance in a measurement of Fowle (22) on the 6μ band of water vapor under atmospheric conditions the transmission values obtained are practically identical with those which Rubens and Aschkinass (29a) had found in steam with only one half the amount

of precipitable water in the path. From the results of the preceding section we might safely conclude that, apart from a small temperature influence, the broadening power of water vapor upon water vapor is just about twice that of air upon water vapor. Fortunately the gases optically active in the atmosphere are only small admixtures to the air so that their broadening influence upon themselves and upon each other is practically negligible. The line widths to be discussed refer therefore to air as broadening agent and their change refers to a change in air pressure.

According to the theory of Lorentz, confirmed by experiments on spectral lines in the visible spectrum, the broadening is caused by the impacts which the radiating molecule undergoes due to the presence of other molecules and a is directly proportional to the number of impacts. We know from the kinetic theory of gases that the number of impacts is directly proportional to the pressure and inversely proportional to the square root of the absolute temperature. Hence if p_s and T_s designate standard pressure and temperature and if a_s is the half-width under these standard conditions, we may write:

$$a = a_s \frac{p}{p_s} \sqrt{\frac{T_s}{T}} \tag{8.1}$$

There are only a very few direct observations of the pressure and temperature dependence of spectral lines in *infrared* bands. There seemed at first sight little reason why the theory of Lorentz expressed by (8.1) should not apply to the infrared band lines. Direct measurements (36a) of the individual lines of a HCl band at 1.75μ made under air pressures ranging from 4 to 12 atm. gave a close proportionality between pressure and half-width, while earlier measurements (36) on another band of HCl had shown a decrease of half-width slightly slower than proportional to p. There seem to be no other direct measurements of pressure broadening in the infrared, but it is possible to obtain rather reliable indirect evidence. We know that for layers which are neither very thin nor very thick the square-root absorption law is an excellent approximation of the true behavior of the absorption. We see from (7.13) that $\sqrt{lu}$ contains a factor $\sqrt{a}$, so that in the region where the square-root law holds, the absorption is proportional to $\sqrt{a}$. Hence it follows from (8.1) that in this region the absorption should, for constant u, be proportional to the *square root of the total pressure.* This rule can be tested by experiments of a rather simple kind, as they do not involve the use of powerful spectroscopes.

In 1938 Falckenberg (46) measured the absorption of heat radiation by a column of moist air 2.35 meters long; while the moisture was kept constant he varied the air pressure from 1 atm. to 1/4 atm. It has recently been conclusively shown by Brooks (37) that for the length of column used by Falckenberg water vapor follows the square-root law of absorption very closely, and Falckenberg's measurements

must therefore be considered as significant even though they were carried out without any spectroscope, with black radiating and receiving surfaces. Falckenberg found that the absorption varies with the *fourth* root of the air pressure, a result which would indicate that the half-width a is proportional to the square root of the pressure and not to the pressure itself.

Schnaidt (55) subsequently was able to show that similar results are implied in the work of a number of earlier investigators hitherto not interpreted quantitatively. The measurements of E. v. Bahr (35) on the 2.7μ band of water vapor show that the ratio of absorptions for various pressures is very nearly equal to the ratio of the square roots of the pressures. A similar result, though a less good quantitative agreement, was found in the measurements of Kühne (49) on the absorption of water vapor between 43 and 90μ. We verified a similar behavior for the band of carbon dioxide at 14μ in the measurements of Hertz (47). The same result appears from the careful measurements of Wimmer (58) on the carbon dioxide band at 4.3μ. Quite recently Strong and Watanabe (57) in measurements on ozone found a corresponding result. We have therefore a considerable body of indirect but definite evidence in favor of the conclusion that the half-width of the lines is proportional to the square root of the total pressure. The subject badly needs further investigation, but until new results are available we may take the last-mentioned rule as the expression of our actual knowledge of the pressure influence.

It must be borne in mind that a pressure effect can only appear if the individual spectral lines are well separated from each other. As the pressure increases the lines grow broader and they will finish up by overlapping so completely that a continuous spectrum with exponential absorption results. The absorption then becomes independent of a (as shown in the previous chapter). It appears from Strong's measurements (31) that for ozone this point is reached at about atmospheric pressure, while for considerably lower pressures the absorption is proportional to the square root of the thickness, corresponding to separate lines. For water vapor the lines are still completely separated at atmospheric pressure, while for carbon dioxide they are closer together but here also the square root law of absorption holds at atmospheric pressure, as has been shown directly by Falckenberg (45).

In the absorption formulae of the preceding chapter only the product lu appears and l is proportional to a by (7.13). For actual computations it is more convenient to assume l constant and introduce an equivalent variation of u with pressure. We may now account for the variation of absorption with atmospheric pressure by multiplying u with a factor

$$\frac{a}{a_s} = \sqrt{\frac{p}{p_s}}\,\sqrt[4]{\frac{T_s}{T}}$$

The factor containing the fourth root of the temperature is usually very close to unity and may be disregarded. Our correction factor is then simply $\sqrt{p/p_s}$. In the atmosphere we do not deal with columns of constant pressure as in the laboratory; instead, the pressure changes continuously with height. The pressure correction factor must then be applied at each level. This leads finally to formula (5.3) for the computation of the corrected optical thickness.

* * *

Up to now we have assumed that the absorption coefficient k is independent of the temperature, the temperature entering into our formulae by way of the black body flux f_b. Indeed, the whole theory of transfer as developed in Part I of this paper was based on the assumption that k is constant, being only a function of the frequency ν. While this is a first approximation under atmospheric conditions, it is not rigorously true. We shall now investigate the actual dependence of k upon the temperature in general terms, the numerical values for water vapor being given later on.

In any atmosphere the temperature is a function of the optical thickness, or vice versa, $u = u(T)$. Hence, in any atmosphere the absorption coefficient k, being a function of T, is a given function of u. We consider a straight column of absorber for which the transfer equation (1.5) applies. If we write $du = \rho\, ds$ by (2.2), formula (1.5) reads

$$\frac{dI}{du} = -k(I - I_0) \tag{8.2}$$

where now k is a given function of u. In the theory of differential equations it is shown that the solution of (8.2) is

$$I(u) = -e^{\int_{u_1}^{u} k\,du} \int_{u_1}^{u} kI_0\, e^{-\int_{u_1}^{w} k\,dw}\, dw \tag{8.3}$$

It may be verified by substituting (8.3) in (8.2) that this is a solution of the equation; but it is not the most general solution of (8.2); the latter is found by adding to (8.3) a term

$$I = I' e^{-\int_{u_1}^{u} k\,du}$$

where I' signifies the radiation incident at the boundary u_1. The solution (8.3) corresponds to $I' = 0$. Since in our analysis of atmospheric radiation we usually have only black boundaries which we replace by radiating layers of infinite thickness, we may put $I' = 0$ without loss of generality. We may write (8.3)

$$I = -\int_{u_1}^{u} kI_0\, e^{-\int_{u}^{w} k\,dw}\, dw = \int_{u_1}^{u} I_0 \frac{d}{dw} e^{-\int_{u}^{w} k\,dw}\, dw$$

We can now proceed in exactly the same way as in Sections 2 and 3 to obtain the total flux crossing a horizontal surface in the atmosphere. This involves an integration over the angles and over the frequency; in addition we introduce the generalized absorption coefficient l in place of k in the same manner as before. The details may be omitted, the final result is a formula which is perfectly analogous to (4.1):

$$F(u) = -\int_0^\infty dv \int_{u_1}^{u} f_b \frac{d}{dw} \tau_f \left(\int_u^w l \, dw \right) dw \tag{8.4}$$

We introduce now a mean value of the absorption coefficient by writing

$$\int_u^w l dw = l_m (w - u) \tag{8.5}$$

and (8.4) becomes formally identical with (4.1), except that u and w stand for u_0 and u, respectively, and that l_m stands in place of l. While l is independent of the temperature, l_m is a function of T. As a first approximation we might assume that value of l_m which would prevail in the middle of the layer considered, that is at $\frac{1}{2}(w - u)$. If we take $u = 0$ and write u again in place of w, we may put in generalization of (4.3)

$$\int_0^\infty \frac{df_b}{dT} \tau_f (l_m u) \, dv = Q \left(u, T; T \left(\frac{u}{2} \right) \right)$$

In order to apply the radiation chart to this case it may be convenient to derive the new Q from the old one by a change in moisture u. We may therefore write

$$Q \left(u, T; T \left(\frac{u}{2} \right) \right) = Q (u - \delta u, T)$$

where now δu is a function of two variables, u and $T \left(\frac{u}{2} \right)$. If δu is known as function of these variables, proper corrections can be applied to the moisture values u before they are entered into the radiation chart. However, the actual variation of the absorption with temperature, especially in the region near where it is most important for atmospheric transfer, is very little known.

9. The Water Vapor Spectrum

We shall now discuss the actual structure of the far infrared spectrum of water vapor. For the study of radiative heat transfer it is sufficient to know quantitatively the course of the generalized absorption coefficients; the data of the radiation chart which in turn solve the transfer problem may then be computed. The whole infrared spectrum is schematically represented in Fig. 1, and the generalized absorption

coefficients finally adopted are plotted in Fig. 19, the ordinates in this figure representing the decadic logarithms of l. Most striking in this diagram is the enormous range of variability of l. Indeed, from the top of the long wave absorption band to the bottom of the transparent region there is a difference of about 4.5 corresponding to a ratio of absorption coefficients of 30,000. Hence, in order to produce a certain fractional absorption at 8–12μ a layer about 30,000 times thicker than at 50–100μ is required. While the existence of such intense variations has been known in the

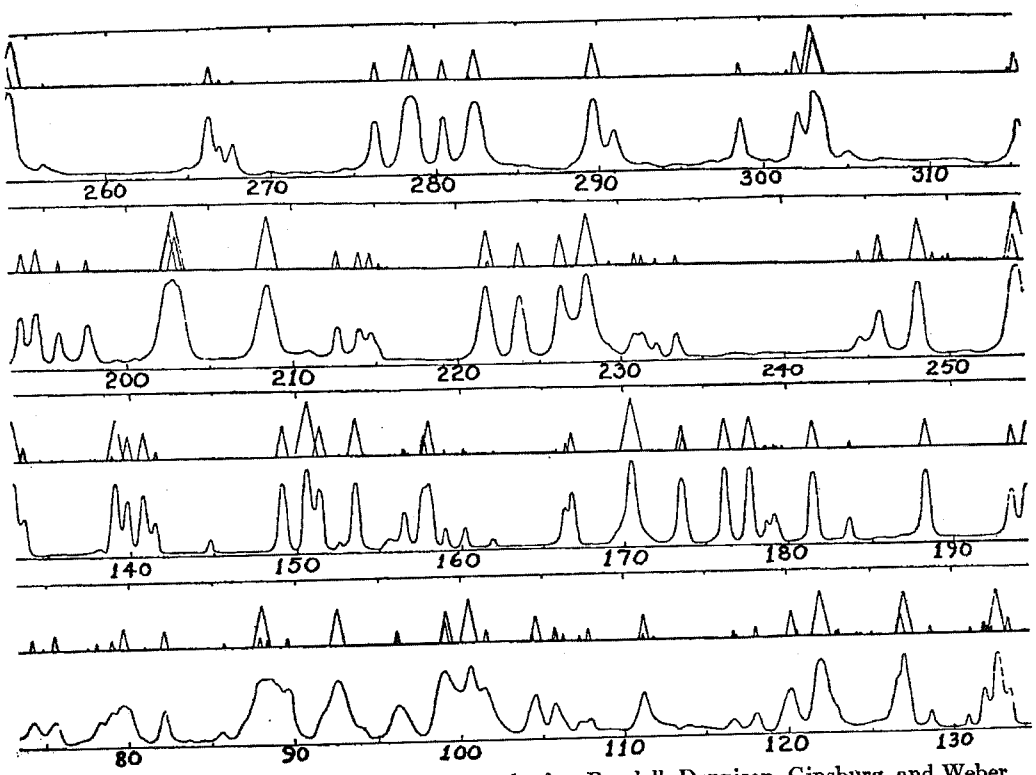

FIG. 16. A section of the rotational water band, after Randall, Dennison, Ginsburg, and Weber.

laboratory for many years, it remained to the fundamental investigations of Simpson in 1928 (56) to discover the fact that the heat balance of the atmosphere could not be explained without taking into account the existence of a band of great transparency of water vapor near 10μ. Since that time our understanding of radiative heat exchange has made rapid strides; the large variability of the absorption coefficients has proven more and more to be of basic importance for the understanding of the atmospheric heat balance.

We begin our discussion of the spectrum at the long wave side where the most intense band is located. It is the so-called *rotational* band; it originates by a pure rotation of the water molecule while all the other bands originate by a combination

of rotation and vibration of the molecule, (3), (7), (12). An exhaustive spectroscopic analysis of this band was given by Randall, Dennison, Ginsburg, and Weber (29). Fig. 16 is taken from their paper and shows part of the spectrum with the extraordinary spectral resolution obtained by their instrument. The numbers indicated are wave numbers. Above the line on which the spectrum is drawn there is another line on which small triangles are placed. These triangles represent line intensities calculated from formulae of quantum mechanics, the area of each triangle being proportional to the intensity of the line. It is seen that there is practically perfect agreement between the observed and calculated positions of the lines in the spectrum. The intensities, on the other hand, are more difficult to compare; the drawn contour of the spectrum represents an estimate rather than a measurement of the intensity of absorption. It is extremely difficult to obtain quantitative information about intensities in this region of the spectrum, since the quantities of water vapor producing the absorption are minute. The computed theoretical intensities on the other hand may be considered as fairly reliable; [1] moreover they involve only one well-known empirical constant, the electric moment of the water molecule ($1.84 \cdot 10^{-18}$ electrostatic units). Errors in the computations should be reduced by the process of averaging over many lines and by the fact that the absorption is proportional to the square root of the line intensity rather than to the intensity itself.

If the line intensities are known, we may compute the generalized absorption coefficient from (7.13), provided that the half-width α is also known. There is no direct measurement of the half-width in this particular band. Cornell (38) has measured the half-width of a considerable number of lines in two bands of water vapor in the near infrared at 0.9μ and 1.1μ. He finds that the line width is fairly constant for the lines in each band and the mean values for the two bands are $\alpha = 0.28$ cm^{-1} and $\alpha = 0.20$ cm^{-1}, respectively. Since there seems to be no particular reason why the line width in the rotational band should be essentially different from these values, a value of $\alpha = 0.25$ cm^{-1} was taken for the latter. Any errors will be reduced by the fact that only the square root of α enters into the calculations. It is not impossible that this figure is appreciably too large, since Matheson (52), by the indirect method referred to in Section 7, found 0.10 and 0.12 cm^{-1} for the half-width of lines in two infrared bands of carbon monoxide.

It is evident from Fig. 16 that in the water vapor spectrum the mean distance of consecutive lines is much larger than the half-width and consequently we can compute the generalized absorption coefficient from (7.13). The calculations, using Dennison's values for the line intensities have been carried out by the author (41), and some of the results are given in Table 5. The variation of the intensities with

[1] According to a personal communication from Professor Dennison.

temperature was also computed and values for two temperatures, 300° abs. and 220° abs., are reproduced in Table 5. The values scatter appreciably in each column, owing to the irregular distribution of the lines in the spectrum. The analysis of the

TABLE 5. GENERALIZED ABSORPTION COEFFICIENTS FOR THE ROTATIONAL WATER BAND

Interval, cm^{-1}	l_{300}	l_{220}	Interval, cm^{-1}	l_{300}	l_{220}
75–100	2280	2880	225–250	1550	1000
100–125	2430	2410	250–275	390	243
125–150	2970	2940	275–300	1130	690
150–175	3690	3340	300–325	283	134
175–200	1310	780	325–350	149	62
200–225	2980	2510	350–375	141	43

spectrum extends much farther out to shorter waves and ends at 550 cm^{-1}; absorption coefficients were also calculated for this region, but it is found that the values obtained are too small and become gradually more and more inadequate as one goes

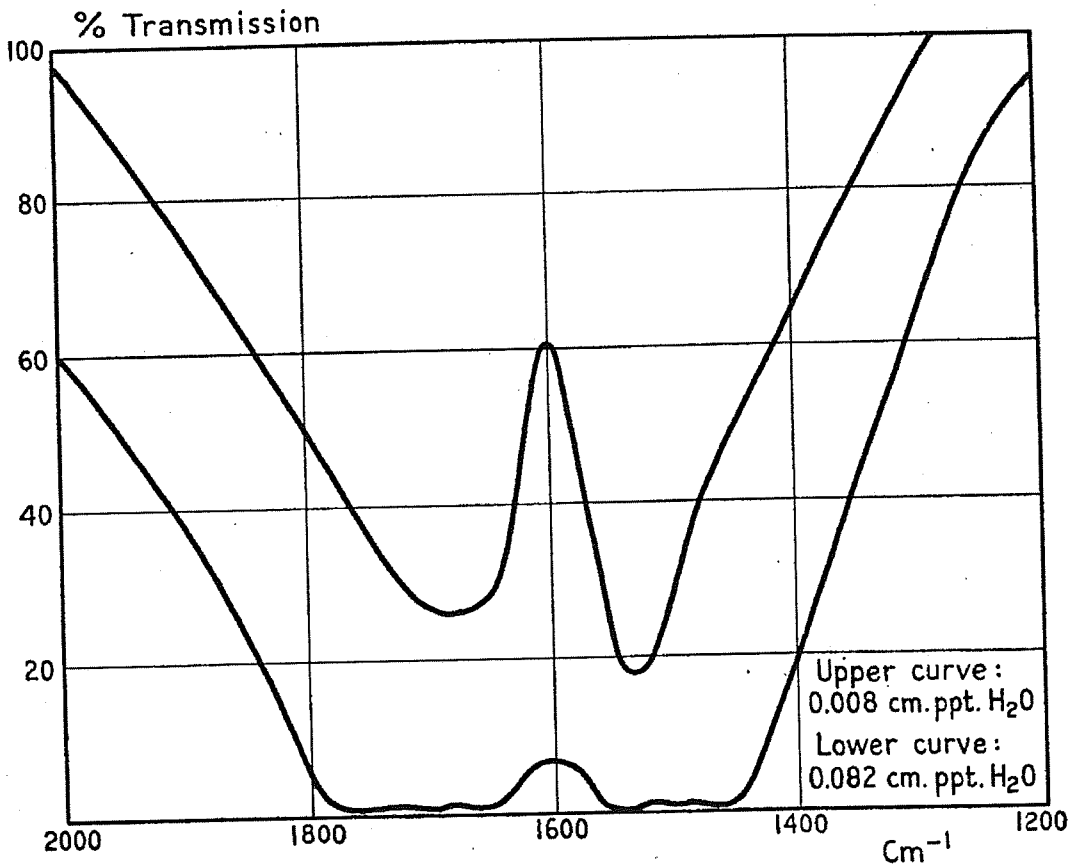

FIG. 17. Transmission in the 6μ band of water vapor, after Fowle.

farther out towards the edge of the band. The calculated values may be tested indirectly by the emissivity measurements discussed in section 12. Strong (33) has measured the absorption in the neighborhood of 21μ (480 cm^{-1}) as a function of the thickness and has directly verified the validity of the square-root law of absorption there. The generalized absorption coefficient obtained from these measurements is $l = 17$.

We go next to the water vapor band at 6μ. No similarly exhaustive analysis of this band is available. The band is very nearly symmetrical about a center located at 1595 cm^{-1}. The course of the absorption may be obtained from the measurements of Fowle (22). His results are represented in Fig. 17, the ordinates giving the transmission for two different thicknesses of water vapor which are 0.008 gr/cm^2 for upper and 0.082 gr/cm^2 for the lower curve, the abscissae being wave numbers. If we assume that the transmission is given by the formulae and curves developed in Section 7, the generalized absorption coefficients can be computed from the observed absorption. The band is slightly asymmetric, but averaging over the two branches we find for the peak absorption approximately $l = 125$.

We turn now to the region of great transparency which goes from about 8μ to about 14μ. Here we have the extensive recent measurements of Adel and Lampland (16). These measurements were made in the atmosphere with a spectroheliscope, the amount of water vapor overhead being simultaneously determined by the method of Fowle (22). The latter consists in a measurement of the intensity of absorption in the ϕ-band at 1.12μ which has been accurately calibrated by Fowle. Table 6 gives the results in form of mean transmissions for certain representative

TABLE 6. PERCENTAGE TRANSMISSIONS IN THE TRANSPARENT REGION. SPECTROHELIOGRAPHIC OBSERVATIONS (16)

Curve	8–9μ	9–10μ	10–11μ	water	air mass
A	47.9	39.3	54.9	4.15	1.6
B	61.3	47.2	69.5	2.14	1.6
C	78.4	57.7	80.6	1.08	1.4
D	84.8	64.0	91.8	0.61	1.3
E	88.2	60.1	93.3	0.32	1.6
F	91.8	61.9	97.2	0.21	1.5
Curve	**11–12μ**	**12–13μ**	**13–14μ**	**water**	**air mass**
A	66.3	59.7	22.1	2.33	1.2
B	70.3	62.9	23.1	2.03	1.3
C	72.9	65.1	18.7	1.79	2.1
D	87.3	81.1	32.5	0.65	1.3
E	91.3	84.8	32.9	0.41	1.4
F	95.8	94.2	38.7	0.13	1.4

runs. The water is in g/cm² and the quantity designated by "air mass" gives the length of path traversed by the beam in the atmosphere as compared to a vertical path in a standard atmosphere. The "air mass" is therefore $(p/p_s)\sec\theta$ where p_s is standard pressure and θ the zenith distance of the sun.

It is seen from Table 6 that from about 8μ to about 13μ the absorption varies little with wave length, with the exception of the interval 9–10μ, where the observations include the absorption produced by the ozone band. Beyond 13μ the carbon dioxide absorption becomes appreciable. The actual observations on which

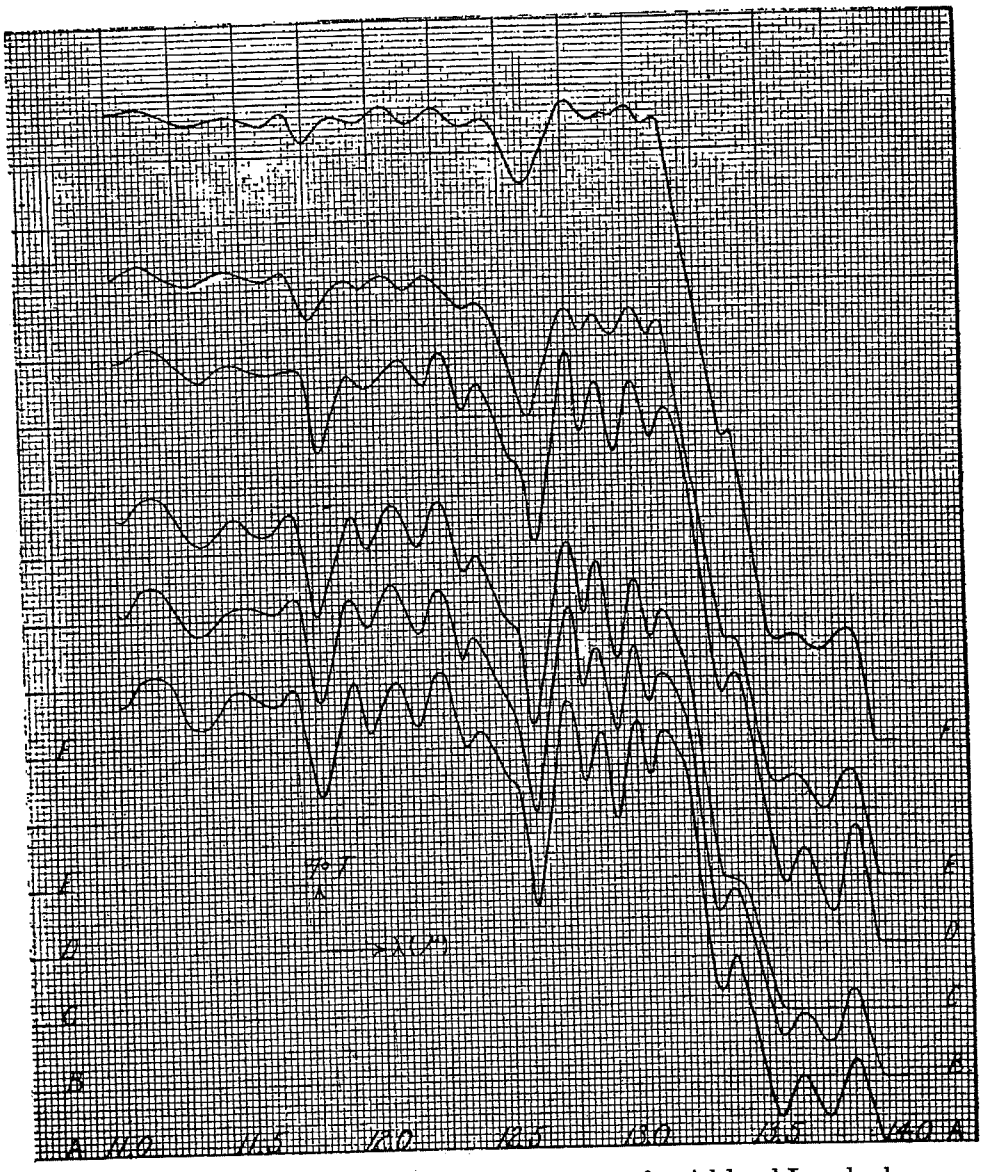

FIG. 18. Transmission of solar radiation, 11–14μ, after Adel and Lampland.

the values in the lower part of Table 6 are based are shown in Fig. 18, which is reproduced from the authors quoted. The letters labeling the spectra in Fig. 18 correspond to those given in the lower half of Table 6.

Strong (33) has plotted the values of Table 6 against the square root of the thickness and has shown that within a reasonable margin they are approximated by a straight line. On the other hand, if the logarithm of the transmission is plotted against the thickness itself, a slightly curved line obtains. This indicates that the absorption is due to individual lines and is of the square-root rather than of the exponential type. The generalized absorption coefficient, which is nearly constant throughout the region, is about $l = 0.10$. It should be mentioned that Elsasser (40) had shown previously that there ought to exist, in this part of the spectrum, a continuous absorption which originates as follows: The lines at the peak of the rotational band are extremely intense; on the other hand at points of the spectrum far removed from the line center, the absorption coefficient of a line is by (6.1) approximately $k = Sa/\pi\ (\nu - \nu_0)^2$. If this expression is summed up over all the strong lines of the rotational band we obtain a formula for the absorption coefficient outside of the band proper, caused by the line wings:

$$k = \sum_i \frac{S_i a}{\pi\ (\nu - \nu_i)^2}$$

This absorption coefficient, valid at great distance from the lines, changes only very slowly with ν and the absorption is therefore of the continuous type. Adopting a value of $a = 0.25$ cm^{-1} and carrying out the summation it is found that for $\nu > 500$ cm^{-1} the absorption coefficient may be approximated by the formula

$$k = (7800 - 24t)/(\nu - 200)^2$$

where t is the temperature in centigrade. The effect is therefore the same as that of a single very intense spectral line located at 200 cm^{-1}. For $t = 20°$ C and 1 cm of precipitable water this formula gives an absorption of 9% at 9μ and of 19% at 12.5μ. While these absorptions are smaller than those given in Table 6, they still are of the order of one half of the latter. On the other hand, as pointed out above, the half-width of the lines might be appreciably smaller than assumed and this would correspondingly reduce the absorption. Spectroscopists seem to agree that the extrapolation of formula (6.1) to large distances from the line center is legitimate and it must therefore be considered possible that the spectrum in this region is a line spectrum with a slight continuous background, the lines being preponderant as evidenced by the fact that the absorption follows very nearly the square-root law. A decision might be obtained from the observation of very thick layers, since in this

case the transmission of a continuum falls to zero more rapidly than that of a line spectrum (Fig. 13). In practice however it will be sufficient to apply to this region the transmission function (7.10) valid for the rest of the spectrum.

We shall finally discuss the temperature dependence of the absorption coefficients. Unfortunately very little is known about this subject. The peak of the band absorption is relatively insensitive to temperature, the main temperature effect taking place at the edges of the bands. It is of course difficult to observe this variation directly at low temperatures; on the other hand the existing measurements in steam are of no avail since it is certain that the half-width of the lines in steam is different from that in air (see Section 8). While the absorption of the rotational band, computed from the theoretical line intensities (29), is unreliable beyond about 350 cm^{-1}, it was thought that the computed ratio of the absorption for two different temperatures should be far more accurate. In Table 7 the ratio of the generalized

TABLE 7. COMPUTED TEMPERATURE DEPENDENCE OF GENERALIZED ABSORPTION COEFFICIENTS

Interval, cm^{-1}	l_{300}/l_{220}	Interval, cm^{-1}	l_{300}/l_{220}
350–375	3.3	450–475	3.8
375–400	4.7	475–500	9.6
400–425	4.7	500–525	4.8
425–450	3.5	525–550	3.0

absorption coefficients for 300° abs. and 220° abs. is given (41). Direct measurements of the dependence of the absorption of the water vapor bands upon temperature are highly desirable, since the knowledge of this variation is of considerable importance for the analysis of radiative transfer in the upper atmosphere.

* * *

On the basis of the data collected earlier in this section, a curve of the generalized absorption coefficients is now constructed. The final curve is shown in Fig. 19. We have several pivotal points which determine the shape of the spectrum in its main outline. They may be summarized as follows:

1. Peak of the rotational band, $l = 3000$, computed from line intensities of Dennison
2. Peak of the 6μ band, $l = 125$, measured by Fowle
3. Region near 21μ, $l = 17$, measured by Strong
4. Region from 8 to 13μ, $l = 0.10$, measured by Adel and Lampland

We get the slope of the rotational band by fitting No. 3 to No. 1; furthermore, the long wave slope of the 6μ band can be obtained by fitting the measurements of

Fowle together with those of Adel and Lampland. Still, it is felt that our knowledge of the spectrum is inadequate and furthermore not much is known about the accuracy of the individual measurements involved. A valuable aid for the construction of the absorption curve comes from the result of the spectroscopic analysis of the water vapor molecule. It is found that, apart from minor disturbances, the 6μ band should be symmetrical about its center at 1595 cm^{-1}, furthermore each of the two branches of the band, measured from the center outwards, should be similar to the rotational band measured from $\nu = 0$ upwards, in the sense that the absorption of corresponding points should differ only by a constant factor. On a logarithmic diagram like Fig. 19 the contour of the branches of the 6μ band should result from that of the rotational band by a vertical displacement. In reality there are

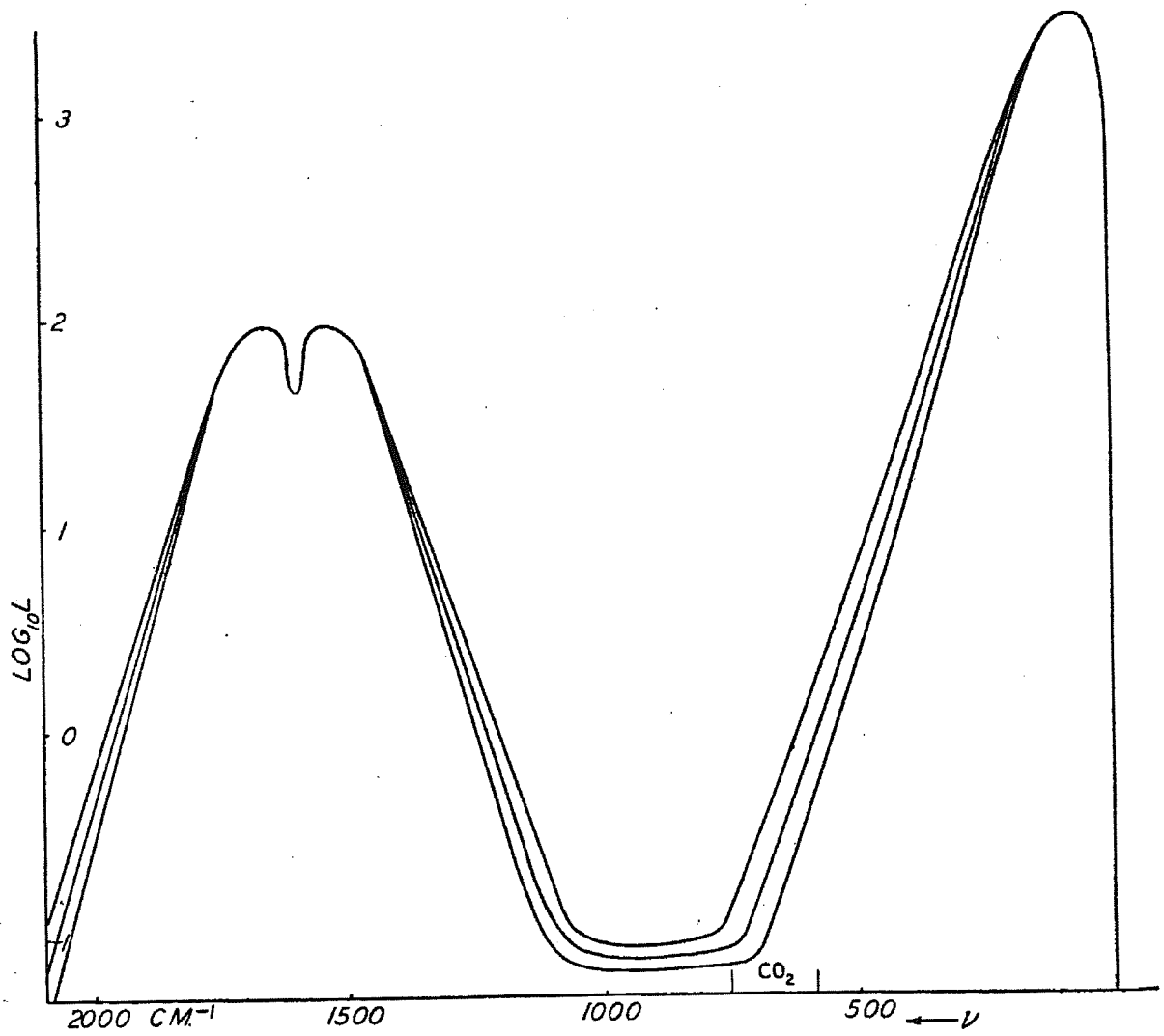

FIG. 19. Generalized absorption coefficients for water vapor.

deviations from this simple behavior, and their magnitude may be inferred from the deviations from perfect symmetry of the absorption contour of Fig. 17.

In view of our inadequate knowledge of the spectrum, rather rigorous simplifications seemed appropriate, especially since the use of a simple contour greatly facilitates the subsequent numerical work. Therefore the following rules were applied: (1) The spectrum to be constructed should have the rigorous character of symmetry just described. (2) The slope of the band edges should be linear on the logarithmic diagram of Fig. 19 (this might not be quite true in reality, but greatly simplifies the calculations). A number of stencils were drawn with slightly different band contours and slightly different slopes. From each stencil a spectrum was drawn by putting the stencil at the proper height for the top of the rotational band and then shifting it to the 6μ band with a proper peak value. Slight deviations of the peak values from the ones tabulated above were permitted. For each of the curves thus obtained a number of trial emissivities were computed and the results compared with the measured emissivity curve (Section 12). This procedure is fairly critical, and it is found that the actual emissivity curve is fairly well defined by the spectroscopic data. The curve finally adopted is shown in Fig. 19. In this curve the peak value of the 6μ band is at $l = 100$, slightly lower than measured by Fowle; at 21μ we have $l = 13$ as compared to Strong's $l = 17$. The slope of the curve at the latter point however is so steep that a slight deviation of the curve would produce a considerable change in absorption. This point proved extremely valuable in determining the general slope of the curve, but a very accurate numerical coincidence might not be required at the present stage of the work. The reduction of the peak of the 6μ band as compared to Fowle's values, however, appears from more recent information [1] to be unjustified. This will be discussed further in Section 12.

An attempt is also made to take into account the variation of absorption with temperature. The three curves of Fig. 19 are supposed to correspond approximately to temperatures of $+20°$ C, $-10°$ C and $-40°$ C. The assignment is merely tentative, and the calculations were carried through in order to get an idea of the effect of this variation upon the transfer rather than in the belief that these curves represent the true absorption. The temperature variation at the bottom of the figure, in the 10μ region is entirely fictitious and not founded upon fact or theory; fortunately this has little practical consequence as only at high temperatures the air contains enough water vapor to produce appreciable absorption in this region.

* * *

[1] The work just described was done about a year earlier.

It is now possible to compute the quantities which appear on the radiation chart. The ordinates of the chart are proportional to (4.3):

$$Q(u, T) = \int_0^\infty \frac{df_b}{dT} \tau_f(lu)\, d\nu$$

Now l is given by Fig. 19, τ_f by Fig. 15, and df_b/dT is obtained from Table 1 and is plotted in Fig. 1. The results of the integrations are collected in the three parts of Table 8, each of which correspond to one of the three curves of Fig. 18. The values are given in per cent, the quantity tabulated being thus 100 $Q(u, T)/Q(0, T)$, where $Q(0, T) = 4\sigma T^3$. In addition we are interested in the quantity

$$\int_0^T Q(0, T) = \int_0^\infty f_b \tau_f(lu)\, d\nu$$

whose physical significance is that of the transmission of an isothermal layer for radiation of its own temperature (triangular areas of Fig. 4). This quantity is given

TABLE 8. RADIATION CHART VALUES FOR PURE WATER VAPOR IN PER CENT

A. Upper curve of Fig. 18

Water	+40°	+20°	0°	−20°	−40°	−60°	−80°	$f_b(-80°)$
0.00025	97.2	97.0	96.8	96.5	96.0	95.1	93.5	88.3
0.0004	96.0	95.8	95.6	95.2	94.6	93.6	91.8	84.8
0.0006	94.8	94.7	94.5	94.1	93.3	92.0	90.1	81.7
0.001	92.7	92.6	92.4	92.0	91.1	89.7	87.4	77.6
0.0015	90.9	90.8	90.6	90.2	89.1	87.5	85.0	74.2
0.0025	88.2	88.1	88.0	87.4	86.3	84.6	81.8	69.6
0.004	85.2	85.1	85.0	84.5	83.4	81.7	78.6	65.3
0.006	82.8	82.7	82.6	82.0	80.8	78.7	75.5	61.6
0.01	79.0	78.9	78.9	78.4	77.2	75.0	71.3	56.8
0.015	75.6	75.7	75.7	75.5	74.1	71.7	67.9	53.0
0.025	71.1	71.3	71.4	71.0	69.7	67.3	63.4	48.3
0.04	66.8	67.0	67.2	66.8	65.4	63.0	59.0	44.0
0.06	62.9	63.2	63.4	63.0	61.6	59.1	54.8	40.2
0.1	57.9	58.2	58.3	57.8	56.4	53.9	49.6	35.6
0.15	53.7	53.9	53.9	53.4	52.1	49.7	45.6	32.1
0.25	48.3	48.3	48.2	47.6	46.3	44.1	40.4	27.8
0.4	43.3	43.2	42.9	42.1	40.9	38.9	35.4	23.9
0.6	38.9	38.8	38.4	37.6	36.4	34.5	31.3	20.8
1	33.3	33.0	32.5	31.8	30.7	29.0	26.2	17.2
1.5	29.0	28.6	28.1	27.4	26.3	24.8	22.3	14.4
2.5	23.6	23.1	22.5	21.8	21.0	19.6	17.5	11.1
4	18.8	18.2	17.6	17.0	16.3	15.0	13.3	8.5
6	14.9	14.2	13.6	13.1	12.4	11.5	10.2	6.3
10	10.3	9.4	8.8	8.3	7.8	7.3	6.4	3.9
15	7.3	6.4	5.7	5.2	4.8	4.4	4.0	2.4
25	4.8	3.9	3.2	2.6	2.2	1.9	1.7	1.3

TABLE 8. — *Continued*

B. Middle curve of Fig. 18

Water	+40°	+20°	0°	−20°	−40°	−60°	−80°	f_b (−80°)
0.00025	97.6	97.5	97.3	96.9	96.4	95.7	94.6	89.6
0.0004	96.5	96.4	96.3	95.9	95.3	94.4	93.0	86.5
0.0006	95.2	95.1	95.0	94.7	94.1	93.0	91.3	83.6
0.001	93.4	93.3	93.2	92.9	92.1	90.8	88.9	79.8
0.0015	91.8	91.7	91.6	91.3	90.4	88.8	86.7	76.6
0.0025	89.3	89.3	89.2	88.9	87.9	86.3	83.8	72.5
0.004	86.8	86.8	86.8	86.5	85.4	83.7	81.0	68.6
0.006	84.3	84.3	84.4	84.2	83.1	81.3	78.4	65.2
0.01	80.8	80.9	81.0	80.9	79.9	78.0	74.8	60.9
0.015	77.9	78.1	78.3	78.2	77.1	75.1	71.7	57.4
0.025	74.0	74.2	74.4	74.3	73.2	71.1	67.4	52.9
0.04	70.1	70.3	70.5	70.4	69.3	67.2	63.3	48.6
0.06	66.6	66.9	67.1	66.9	65.7	63.5	59.6	44.8
0.1	62.0	62.4	62.6	62.4	61.0	58.7	54.8	40.1
0.15	57.9	58.3	58.5	58.2	56.9	54.7	50.9	36.4
0.25	52.5	52.8	53.0	52.6	51.4	49.2	45.5	31.7
0.4	47.5	47.7	47.7	47.2	46.0	44.0	40.4	27.7
0.6	43.0	43.1	43.0	42.4	41.3	39.4	36.0	24.4
1	37.1	37.1	36.8	36.5	35.4	33.6	30.5	20.5
1.5	32.6	32.6	32.3	31.9	30.8	29.1	26.3	17.5
2.5	27.2	27.0	26.7	26.2	25.2	23.7	21.2	13.9
4	22.2	21.8	21.5	20.9	20.0	18.8	16.6	10.8
6	18.0	17.3	16.8	16.4	15.7	14.8	13.0	8.3
10	12.9	12.0	11.3	10.8	10.3	9.8	8.6	5.5
15	9.4	8.4	7.7	7.1	6.7	6.3	5.6	3.7
25	6.0	5.0	4.3	3.8	3.4	3.2	2.8	2.0

C. Lower curve of Fig. 18

Water	+40°	+20°	0°	−20°	−40°	−60°	−80°	f_b (−80°)
0.00025	97.9	97.8	97.7	97.3	97.0	96.4	95.5	91.1
0.0004	96.9	96.8	96.7	96.3	95.9	95.2	93.9	88.1
0.0006	95.8	95.7	95.6	95.3	94.8	93.9	92.4	85.4
0.001	94.0	94.0	93.9	93.7	93.1	92.1	90.2	81.8
0.0015	92.4	92.5	92.5	92.3	91.6	90.5	88.3	78.9
0.0025	90.2	90.3	90.3	90.2	89.5	88.1	85.8	75.1
0.004	87.9	88.1	88.2	88.1	87.3	85.8	83.3	71.5
0.006	85.7	85.9	86.0	85.9	85.1	83.5	81.0	68.5
0.01	82.6	82.9	83.1	83.0	82.2	80.6	77.9	64.5
0.015	80.0	80.5	80.8	80.6	79.8	78.1	75.2	61.2
0.025	76.4	77.1	77.5	77.3	76.4	74.7	71.6	56.9
0.04	72.9	73.6	74.1	74.1	73.1	71.2	68.0	52.9
0.06	69.8	70.5	71.0	71.0	69.9	68.0	64.7	49.4
0.1	65.5	66.3	66.9	66.7	65.7	63.6	60.2	44.9
0.15	61.8	62.6	63.0	62.9	61.9	59.8	56.1	40.5
0.25	56.9	57.4	57.7	57.5	56.5	54.5	50.7	36.2
0.4	52.0	52.2	52.2	51.9	51.0	49.2	45.6	32.2
0.6	47.6	47.7	47.5	47.1	46.1	44.4	41.1	28.8
1	41.9	41.8	41.5	41.0	40.0	38.3	35.5	24.5
1.5	37.2	37.0	36.8	36.3	35.3	33.6	31.0	21.0
2.5	31.2	31.0	30.8	30.3	29.3	27.7	25.5	16.8
4	25.9	25.6	25.2	24.7	23.9	22.4	20.5	13.2
6	21.2	20.7	20.3	19.9	19.2	17.9	16.3	10.4
10	15.5	14.8	14.3	14.0	13.5	12.5	11.1	7.2
15	11.2	10.5	10.0	9.6	9.2	8.5	7.5	4.9
25	7.1	6.5	5.8	5.2	4.8	4.5	4.1	2.7

in the last column for $-80°$ C; the values for higher temperatures can be computed from the tables by numerical integration. Each figure in the three parts of Table 8 represents the result of one integration of the form (4.3). This calculating work has been carried out with a mechanical device whose construction is described in the appendix. The results obtained involved errors of computation of the order of one per cent; they were subjected to a twofold smoothing process by plotting them first as function of the temperature and smoothing and by plotting the corrected values as function of $\log u$ and smoothing again. The figures in the last column could of course only be smoothed once, with respect to $\log u$.

Only one more step is necessary to bring the radiation chart to its final form: this is to account for the radiation of carbon dioxide. It is clear that in principle a radiation chart functions only for one radiation substance (for several substances only if their relative proportions remain constant). In the atmosphere the ratio of water to carbon dioxide is extremely variable. On the other hand, while carbon dioxide absorbs only within two narrow bands (Fig. 1) the intensity within these bands is extremely high. In this case the heat transfer within the band becomes small, as was shown in the beginning of Section 5. The only (though perhaps not very satisfactory) way in which carbon dioxide is introduced into the radiation chart without giving rise to additional complications is by the assumption that the parts of the spectrum occupied by the carbon dioxide band are completely opaque, i.e., that even very thin layers radiate as black bodies within these bands. For almost all practical problems in the lower atmosphere to which the radiation chart is applied this is a reasonably good approximation. Among the infrared bands of carbon dioxide that at 15μ is vastly preponderant for atmospheric radiation and was the only one to be taken into account for the construction of the chart. According to spectroscopic analysis it is symmetrical about a center at 668 cm^{-1}. From the observations of Adel and Lampland represented in Fig. 18 we see that the band cuts off rather sharply at about 13.3μ (752 cm^{-1}). This being taken as the short wave edge, the long wave edge comes at 584 cm^{-1}. Most of the curves in Fig. 18 refer to an air mass of 1.3–1.4, while curve C represents an air mass of 2.1. It is seen that the shift of the band edge to shorter waves owing to the increase of the length of path is extremely small. Since the radiation chart represents the radiation of slabs rather than columns, the equivalent length of a column corresponding to the flux from the atmosphere should be about 1.66 air masses, according to Section 7. Hence, in assuming a stretch from 584 to 752 cm^{-1} as opaque we get an approximately correct estimate of the sky radiation in the lower atmosphere contributed by carbon dioxide.

There is also a certain amount of water vapor radiation within this band. In

order not to count this amount twice, one should treat the water vapor as if it was transparent within the band.[1] For practical reasons, however, the integrations for pure water vapor whose results appear in Table 8 were simply carried through without regard to the effect of carbon dioxide. The mean transmission of water vapor in the band, that is $\int \tau_f (lu)\, dv$ (where the integration extends over the width of the band) was computed separately and is given in Table 9. Since the absorption coefficients are highly hypothetical in this region, these figures are considered merely as an intrinsic correction of the chart and not as representative of the true absorption of water vapor in this part of the spectrum. If now F_{CO_2} designates the fraction of the black body flux contained in the limits of the band and τ the correction given in Table 9, the final chart ordinates are obtained by subtracting from the figures of Table 8 the quantity $F_{CO_2} \cdot \tau$.

TABLE 9. PERCENTAGE TRANSMISSION OF WATER VAPOR (SLABS) IN THE CO_2 BAND AT 14μ

Water	a	b	c	Water	a	b	c
0.01	98	100	100	0.6	49	59	70
0.015	97	99	100	1	39	50	61
0.025	93	97	100	1.5	31	42	53
0.04	88	94	98	2.5	22	32	43
0.06	83	91	96	4	13	23	33
0.1	77	85	92	6	8	16	25
0.15	72	80	88	10	3	9	16
0.25	64	73	82	15	1	5	10
0.4	56	66	76	25	0	2	4

For the construction of the chart a definite set of absorption coefficients must be chosen, corresponding to a reasonable average temperature of the atmosphere. The values finally adopted were obtained by interpolating between the figures of Table 8A and 8B in the ratio 2 : 3. If the figures of these tables correspond to temperatures of $+20°$ C and $-10°$ C, the chart would be correct at about $+8°$ C. It appeared, however, after the numerical work had been carried out, that the values used are slightly too low (see Section 12) and therefore the chart would be correct at appreciably lower temperatures. A final decision should be made by comparison with further observations.

In the actual radiation chart the unit flux chosen is one calorie per cm^2 per three hours. The abscissae and ordinates are given by formula (4.6). Putting there $a = 12.50\sigma$ we have for the actual abscissae and ordinates of the chart

$$x = 12.50\sigma T^2, \quad y = Q/25\sigma T = 0.160\, T^2\, Q\,(u, T)/Q\,(0, T) \times \frac{1}{5}$$

[1] See, however, the more complete treatment of this overlapping by Hottel and Mangelsdorf (48).

The chart ordinates are given in Table 10. The triangular areas of Fig. 4 which represent the transmission of isothermal layers for radiation of their own temperature are now obtained by numerical integration. They are given in Table 11.

TABLE 10. ORDINATES OF THE RADIATION CHART

Water	+40°	+30°	+20°	+10°	0°	−10°	−20°	−30°	−40°	−50°	−60°	−70°	−80°
black	3138	2941	2750	2566	2388	2216	2051	1892	1740	1594	1454	1321	1194
CO_2	2708	2518	2332	2155	1989	1828	1676	1533	1399	1273	1156	1046	943
0.00025	2627	2438	2255	2081	1917	1760	1608	1466	1332	1206	1088	975	870
0.0006	2551	2371	2192	2024	1862	1709	1559	1419	1287	1162	1045	935	831
0.001	2489	2312	2137	1970	1815	1664	1520	1381	1251	1128	1012	903	800
0.0025	2350	2182	2019	1863	1714	1569	1430	1296	1171	1052	941	836	735
0.004	2266	2103	1942	1788	1648	1507	1374	1247	1124	1009	900	798	700
0.006	2187	2029	1873	1727	1590	1456	1325	1200	1080	967	861	759	665
0.01	2073	1923	1776	1637	1506	1378	1255	1137	1023	913	808	712	619
0.015	1985	1843	1702	1568	1443	1319	1201	1088	978	872	771	675	584
0.025	1863	1729	1600	1475	1357	1240	1128	1019	915	814	719	628	539
0.04	1750	1625	1502	1386	1277	1167	1061	957	859	764	673	585	499
0.06	1651	1536	1420	1310	1207	1102	1002	904	808	716	629	546	461
0.1	1523	1417	1313	1211	1114	1017	922	829	740	655	574	495	417
0.15	1416	1318	1221	1126	1033	941	853	767	684	604	530	457	382
0.25	1279	1185	1096	1008	927	844	764	684	610	539	469	402	337
0.4	1154	1069	987	908	831	753	679	609	532	477	416	356	296
0.6	1043	970	892	819	748	679	611	547	485	428	373	318	264
1	907	838	772	706	645	587	528	474	421	369	320	271	225
1.5	804	743	684	626	572	518	467	417	369	324	281	239	198
2.5	678	624	573	521	476	431	388	347	308	269	232	197	163
4	561	513	468	432	391	355	318	283	252	220	189	161	133
6	458	415	378	342	312	281	254	227	201	177	153	131	107
10	331	294	263	237	212	189	170	152	134	119	104	90	75
15	247	216	188	164	145	128	114	101	89	78	68	59	50
25	164	139	116	98	84	73	64	53	45	38	33	29	24

10. Spectra of Other Atmospheric Gases; Absorption of Sunlight

Next to water vapor the most important agent for radiative heat transfer in the atmosphere is carbon dioxide. It has three absorption bands in the far infrared region, two very intense bands at about 4μ and 15μ and a very faint one near 10μ. The band at 4μ is just at the upper end of the black body curve for ordinary temperatures and in the computations for the radiation chart it has been neglected. This might give rise to slight errors for temperatures above about 10° C. The most important band is that near 15μ; according to the spectroscopic analysis (25) it is symmetrical about a center at 668 cm^{-1}. The manner in which it was introduced into the radiation chart has been discussed in the previous chapter. The fraction of

the black body radiation taken up by this band is appreciable; at ordinary temperatures it is of the order of 18% for a radiating layer of the thickness of the atmosphere. As we go upwards in the atmosphere we must finally reach a height where this radiation flows out to space without compensation by downward radiation. This takes place in the stratosphere, and it is found that the radiative effects of carbon dioxide in the stratosphere become as strong as or stronger than those of water vapor.

TABLE 11. AREAS OF THE RADIATION CHART

Water	+40°	+30°	+20°	+10°	0°	−10°	−20°	−30°	−40°	−50°	−60°	−70°	−80°
black	141.1	124.2	108.6	94.5	81.9	70.5	60.4	51.4	43.5	36.5	30.4	25.0	20.5
CO_2	117.4	102.6	89.3	77.4	66.8	57.4	49.1	41.8	35.4	29.8	24.9	20.7	17.1
0.00025	111.0	96.7	83.8	72.4	62.2	53.1	45.1	38.1	32.0	26.7	22.1	18.1	14.8
0.0006	106.8	92.9	80.4	69.2	59.3	50.5	42.7	36.0	30.0	24.9	20.5	16.7	13.5
0.001	103.5	89.9	77.7	66.9	57.2	48.6	41.1	34.5	28.7	23.7	19.4	15.8	12.7
0.0025	96.6	83.7	72.2	61.9	52.8	44.7	37.6	31.4	26.0	21.3	17.3	13.9	11.1
0.004	92.4	80.0	68.9	59.1	50.3	42.5	35.7	29.7	24.5	20.0	16.2	13.0	10.2
0.006	88.6	76.7	66.0	56.4	48.0	40.5	33.9	28.1	23.1	18.8	15.2	12.1	9.5
0.01	83.4	72.1	62.0	53.0	44.9	37.8	31.6	26.1	21.4	17.3	13.9	11.0	8.6
0.015	79.5	68.7	59.0	50.3	42.6	35.8	29.9	24.6	20.1	16.2	12.9	10.2	7.9
0.025	74.2	64.1	54.9	46.8	39.6	33.2	27.5	22.6	18.4	14.8	11.7	9.1	7.0
0.04	69.4	59.8	51.3	43.6	36.8	30.8	25.5	20.9	17.0	13.6	10.7	8.3	6.3
0.06	65.2	56.2	48.1	40.8	34.4	28.7	23.7	19.4	15.6	12.4	9.7	7.5	5.7
0.1	59.7	51.4	43.9	37.2	31.3	26.0	21.4	17.4	14.0	11.1	8.6	6.6	4.9
0.15	55.1	47.4	40.5	34.3	28.7	23.9	19.6	15.9	12.7	10.0	7.8	5.9	4.4
0.25	49.2	42.2	36.0	30.4	25.5	21.1	17.3	14.0	11.2	8.8	6.7	5.1	3.7
0.4	43.9	37.6	32.0	27.0	22.5	18.6	15.2	12.3	9.8	7.6	5.8	4.4	3.2
0.6	39.5	33.8	28.7	24.1	20.1	16.6	13.5	10.9	8.6	6.7	5.1	3.8	2.8
1	34.0	29.1	24.7	20.8	17.3	14.3	11.6	9.4	7.4	5.7	4.4	3.2	2.3
1.5	30.0	25.7	21.8	18.3	15.2	12.5	10.2	8.2	6.5	5.0	3.8	2.8	2.0
2.5	25.0	21.3	18.1	15.2	12.6	10.4	8.4	6.8	5.3	4.1	3.1	2.3	1.6
4	20.5	17.5	14.8	12.4	10.3	8.5	6.9	5.5	4.4	3.4	2.5	1.9	1.3
6	16.5	14.0	11.9	9.9	8.3	6.8	5.5	4.4	3.5	2.7	2.1	1.5	1.1
10	11.4	9.6	8.1	6.7	5.6	4.6	3.8	3.0	2.4	1.9	1.4	1.0	0.7
15	7.9	6.6	5.5	4.5	3.7	3.1	2.5	2.0	1.6	1.2	0.9	0.7	0.5
25	4.6	3.8	3.1	2.5	2.0	1.6	1.3	1.0	0.8	0.7	0.5	0.4	0.3

If we want to compute the radiative transfer by carbon dioxide, a graphical method presents itself naturally, similar to that for water vapor. The procedure is comparatively simple due to the fact that the radiation is confined to a narrow band, and one may replace the black body flux by its value at the band center. The formulae of Sections 3 and 4 are then replaced by much simpler expressions. We shall however not enter into the mathematical details. The total emission of layers of carbon dioxide has been computed by several writers. This quantity can also be

measured directly with far less difficulty than for water vapor and we shall come back to this topic in Section 12 where numerical values will be given.

A very faint absorption band of carbon dioxide is found near 10μ; it has been resolved and identified by Barker and Adel (20). According to Schnaidt (55) the contribution of this band is about 0.4% of the black body radiation so that it is negligible except for very accurate investigations.

The half-width of the lines in carbon dioxide is not known; however Rubens and Ladenburg (30) have shown that the broadening effect of air upon carbon dioxide is almost exactly equal to that of carbon dioxide upon itself, a fact which

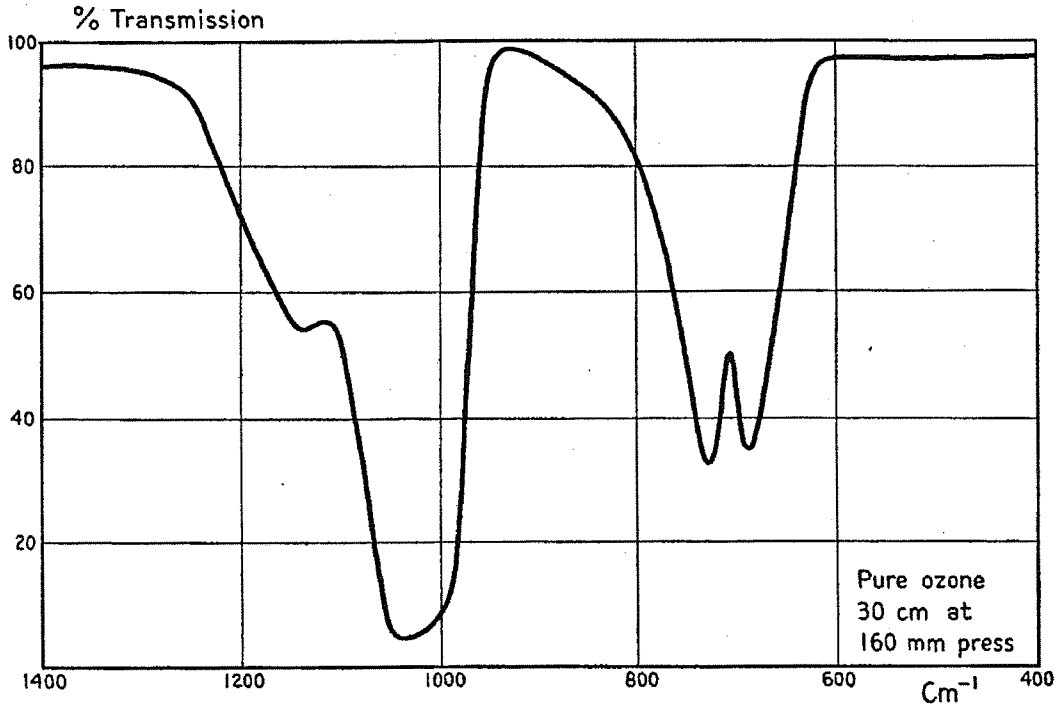

FIG. 20. Transmission of ozone, after Hettner, Pohlmann, and Schuhmacher.

permits the direct application to the atmosphere of measurements made in pure carbon dioxide. The measurements of Falckenberg (45) show that under atmospheric pressure the absorption follows the square-root law for moderately thick layers so that the bands are composed of distinct lines. The latter fact is in accordance with direct spectroscopic investigation (25). The pressure dependence, (47), (58) of the absorption seems to be the same as for water vapor; hence formula (5.3) should apply to carbon dioxide.

Next in importance for infrared atmospheric radiation is ozone. Its infrared spectrum has been measured by Hettner, Pohlmann, and Schuhmacher (24). Fig. 20 shows the transmission curve which is obtained from a column of 30 cm of

practically pure ozone under a pressure of 160 mm of mercury. The band near 1000 cm^{-1} falls into the region where water vapor is highly transparent, and may therefore be observed in the atmosphere itself; it has been studied by Adel and Lampland (16) and, very extensively, by Strong (32). The absorption curve of Fig. 20 corresponds to a much larger amount of ozone than is ever found in the atmosphere. The peak transmission at the 10μ band in Fig. 20 is about 5% while in the measurements of Adel and Lampland it is about 40%. If we assume that formula (7.10) applies for the transmission function, we find from Table 4 that atmospheric ozone corresponds to a column of about one tenth the length of that in Fig. 20. This is however an "equivalent" column and the true amount can be different, owing to the fact that the line-broadening effect of ozone upon itself may be different from that of air upon ozone.

There is another band visible in Fig. 20 which has its center at about 710 cm^{-1} and coincides almost completely with the 15μ carbon dioxide band whose center is at 668 cm^{-1}. The peak transmission is about 34% and the peak transmission for one tenth of the column would come to about 77%. This band must play a certain role in the heat transfer of the stratosphere, where it coöperates with the carbon dioxide band in producing a radiative flux in this part of the spectrum, but owing to its overall weakness which is indicated by the estimate just made it should be of but minor importance for the radiative heat balance.

Strong (32) has shown that for air pressures appreciably lower than one atmosphere the absorption of the 10μ band follows the square-root law so that the band consists of separate lines. Strong and Watanabe (57) have demonstrated that under these conditions the pressure dependence of the absorption follows a law similar to that of water vapor.

While ozone is of course of great importance for the heat balance of the stratosphere, owing to its absorption of sunlight, it is of minor significance for the radiative balance of the lower atmosphere, especially since the effective temperature of the ozone layer is in general much smaller than that of the ground and of the lower atmosphere. For average temperatures prevailing in the stratosphere the flux due to the 10μ band of ozone is slightly less than 1% of the black body flux of these temperatures. The contribution of ozone to the incoming sky radiation is therefore a fraction of 1% of the black body flux corresponding to the ground temperature in middle latitudes.

A number of minor bands in the far infrared absorption spectrum of the sun have recently become known through the investigations of Adel. A narrow but distinct absorption band is located at 7.8μ and is due to the pentoxide of nitrogen (17). One might presume that this gas is located at the very top of the atmosphere

where oxygen is dissociated by the ultraviolet rays of the sun. For the atmospheric heat transfer this band is probably negligible, unless the temperatures of the layer where it originates should come out to be exceedingly high. A very faint band, also due to an oxide of nitrogen, is found at 12.6μ (18). It may be recognized in Fig. 18. In very moist air Adel (19) has been able to identify and to resolve a band due to heavy water (HDO) located at 7.12μ and corresponding to the 6μ band of ordinary water vapor.

A word might be said about the possibility of infrared emission and absorption by the main constituents of the atmosphere, nitrogen and oxygen. The optical thickness of these gases in the atmosphere is so large that it seems unjustified to infer from their transparency in common laboratory tests the complete absence of infrared emission and absorption of a dry atmosphere. The absorption or emission, even of the whole atmosphere, must in any case be very small, and in the regions of the spectrum where water vapor and carbon dioxide radiate appreciably the superposition of a very small absorption of the air would leave the existing radiation balance practically unaltered. Such an absorption should show up in the solar observations of Adel and Lampland in the 10μ region and give rise to a residual absorption if the obtained curves are extrapolated to zero moisture content. There appears to be no such effect of any appreciable magnitude and it seems safe to assume in the theory of radiative transfer that dry air is completely transparent.

* * *

The depletion of solar radiation by the atmosphere by absorption and scattering is an important problem of meteorology; although it does not belong to our subject proper, the absorption of solar radiation by atmospheric gases, in practice almost exclusively by water vapor, will be briefly discussed here. Our quantitative knowledge is due to Fowle (22), whose laboratory investigations in this field will remain a classic of the experimental art. The light of a Nernst glower was sent through a tube of about 60 meters length and then into the slit of an infrared spectroscope. By means of mirrors the light could be passed four times through the tube and an optical path of about 240 meters was thus achieved, giving, with the amount of water vapor present under laboratory conditions, sufficient absorption even in the weaker bands to obtain the transmission contours of the bands. The details of the work cannot be discussed here. The final results of Fowle have been put in a form convenient for numerical computation by Mügge and Möller (83), who showed that within the range of 0.5 cm to 8 cm of precipitable water which Fowle's measurements cover, the latter can be represented by the formula

$$a(u) = 0.172\, u^{0.308} \tag{10.1}$$

where a is the solar energy absorbed in calories per cm^2 per minute and u the column of precipitable water in gr/cm^2. Formula (10.1) fits Fowle's observations everywhere within 1% or less, but should not be extrapolated far beyond the interval for which it is derived. If the zenith distance of the sun is θ, and if now u designates the amount of precipitable water in a *vertical* column, we must write $u \sec\theta$ in (10.1) in order to use this formula in the atmosphere. The amount absorbed in a thin layer of the atmosphere of vertical thickness du is then seen to be

$$du \frac{d\, a(u \sec\theta)}{d\,(u \sec\theta)} = 0.0521\ (u \sec\theta)^{-0.697}\, du$$

and this must be equal to the increase of heat content of the layer $c_p\, \Delta T\, dm$ where dm is the mass of air in the layer per cm^2. We have $du/dm = w/1000$ where w is the specific humidity; if we express the heating in degrees centigrade per 3 hours we have numerically (with an accuracy which might suffice for most practical purposes)

$$(\Delta T)_{3\ \text{hours}} = 0.039\ (u \sec\theta)^{-0.70} \tag{10.2}$$

where u is the total precipitable water above the considered level. The height of the sun does not of course remain constant, and (10.2) must be integrated over the course of the sun's height during the day in order to obtain the total heating (93).

In Fig. 21 is plotted Fowle's curve (10.1), together with two other curves which represent the absorption of atmospheric water vapor as determined directly as an average from a large number of solar radiation observations. The two lower curves are due to Kimball (76) and Hoelper (75), the diagram being taken from Hoelper's paper. According to the latter the two curves are practically in agreement within the observational errors. The lowest curve runs at about 80% of Fowle's values while the curve of Kimball is nearer to 90% for small moistures. Fowle himself has estimated the pressure correction of his transmission curve from the measurements of E. v. Bahr (35) and finds that for typical atmospheres it reduces the moisture values to 89–90% of the uncorrected amounts. The pressure dependence, as we know, is very nearly of the square-root type discussed in Section 7. In addition, all the bands will become narrower with lower temperature in the same way as indicated in Fig. 16 for two of them. This will lead to a further reduction of the observed absorption and it might appear that in this way the difference between Fowle's curve and the two lower curves of Fig. 21 reduces to an almost insignificant amount. The loss of radiation due to scattering in the atmosphere which is very large in the blue and violet part of the spectrum is almost negligible in the red and completely negligible in the infrared (unless of course dust or haze is present). We might conclude that in a clear atmosphere our formula (10.2) with a suitable pres-

sure correction factor $\sqrt{p/p_s}$ for each level and, if a high degree of accuracy is desired, with a temperature correction factor which might vary between, say, 0.95 and 1, should give quite satisfactory values for heating of the atmosphere by solar radiation.

It was noted by E. v. Bahr (35) that all the infrared bands of water vapor show nearly the same pressure dependence. Until more accurate measurements are

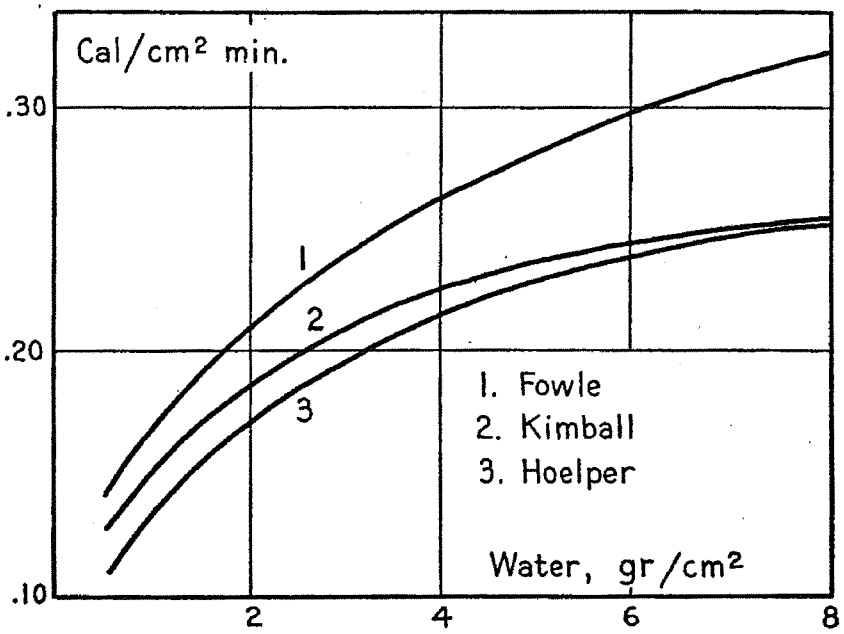

FIG. 21. Absorption of sunlight by the atmosphere, after Hoelper.

available this statement may be taken with a certain reserve so far as the water vapor bands in the visible and the very near infrared are concerned. It may be inferred from general considerations of quantum theory that, whatever the physical explanation of the square-root law of line broadening may be, it must eventually yield to a law of broadening which is linear with pressure when we go to absorption bands of shorter and shorter wave length. Just where this transition may take place is of course difficult to say. Such an effect would tend to increase the pressure correction factor of the total absorption, but this increase would presumably be slight.

PART III. THE MEASUREMENT OF ATMOSPHERIC EMISSION

11. Instruments for Atmospheric Radiation Measurements

If a horizontal black plate is exposed to the sky at night it will cool. This effect is the basis of numerous meteorological phenomena of great practical significance, such as the formation of inversions, of ground fogs, nocturnal frosts, etc. Sky radiation measurements have therefore early received attention. It is obvious that the heat loss of the black plate is equal to the defect of the incoming sky radiation relative to the black body radiation emitted towards the sky by the black plate itself. We shall briefly discuss the various instruments used for the purpose of such measurements and then say a few words about spectroscopic measurements of sky radiation.

The non-spectroscopic instruments operating with a black receiving surface are of three types: (1) the open instrument with a horizontal black surface receiving radiation from the whole sky; (2) the box-type instrument in which the receiver is placed at the bottom of a box with a hole at the top; (3) the telescope-type instrument in which the receiver is located in the focal plane of a concave mirror. The last two types have a mechanical suspension which permits setting of the instrument at any desired angle of elevation. All three types have been used extensively for sky radiation observations. Apart from some primitive instruments using the blackened bulb of a thermometer and having a low accuracy, the temperature is measured by means of thermoelectric elements. In the open-type instruments the fall of the temperature of the black plate is compensated by artificial heating in order to eliminate the influence of the wind. This is done electrically, and the heat flow is determined by measuring the heating current after the instrument has reached temperature equilibrium with the surrounding air. In place of thermocouples, resistance thermometers have occasionally been used.

The construction of a radiation instrument would be comparatively simple if the receiver could be completely enclosed rather than exposed to the atmospheric air. Extensive investigations of infrared spectra (2) show however that there is no solid which is completely transparent throughout the far infrared region of the spectrum. In order to obtain accurate results, windows are avoided, and consequently the receiving surface finds itself in a space which communicates directly with the atmosphere. The receiver should be constructed so that it is insensitive to short-period local fluctuations of the temperature due to adiabatic compression or expansion of the surrounding air. This is achieved either by giving the receiver a comparatively large mass, or by using a compensation method in which the hot

and cold junctions of the thermocouples are attached to two equal plates, one plate being blackened or exposed to the sky and the compensating plate being made reflecting or shielded from the sky.

One of the most important features of the receiver is its "blackness." We saw in Section 1 that a black body will absorb any radiation falling upon it and will emit radiation of its own temperature according to Planck's law. Since all actual surfaces show a certain regular or diffuse reflection, no surface is completely black. For laboratory purposes a black body is realized by means of an opening in a wall of a closed vessel, preferably of conical form (Fig. 22), which is blackened at the inside and kept at a constant temperature. It is seen that a beam of radiation which enters the diaphragm has only a very small probability of leaving the vessel again because of reflection or scattering; in this way the ideal black body is closely approached.

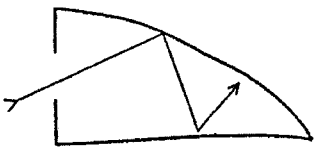

FIG. 22. Black body.

An efficient method of producing a black body is to use a fluffy substance which at the same time has a high coefficient of absorption throughout the spectrum. This is the reason why a cloud or a fog is black in the far infrared even if it is comparatively thin. According to Falckenberg (44) snow is 99.5% black in the far infrared, that is absolutely black within the errors of his measurement. The powdery substances such as lamp-black, platinum black, zinc black, etc., which are applied to surfaces in order to blacken them do not show an equally high absorption. They are usually between 92% and 96% black. Two properties are important in practice. First, the coat should have approximately the same power of absorption for all wave lengths involved, and secondly, it should be a good conductor of heat. If the latter condition is not fulfilled, a temperature gradient will be established between the body of the receiver where the temperature is measured and the actual radiating surface which determines the temperature of the outgoing radiation. This reduces the sensitivity of the receiver in the case of the box-type instrument where the incident radiation and the change in temperature produced are very small. In open-air instruments with compensatory heating the wind influences the temperature of the radiating black surface, and if a temperature gradient develops in the blackening coat, the body of the receiver will in equilibrium be at a higher temperature than the surrounding air. This seems to be a frequent source of errors. For the technical procedure of blackening a surface we refer to the comprehensive treatises (6), (13).

The Ångström instrument, called pyrgeometer, is the simplest open-surface instrument. It consists essentially of four thin strips of manganin which are exactly equal and of which two are blackened while the two others are kept reflecting. The strips have a surface of 2×0.3 cm each and during the observations they are set in the direction of the wind. The junctions of the thermoelements are alternately fastened to the black and the reflecting strips and the former are electrically heated until all strips are at the same temperature. In spite of the compensation the wind influence upon this instrument seems to be considerable. Fig. 23 shows measurements of Süssenberger (122) who compared the readings of the Ångström instrument with those of an instrument of the telescope type. The wind velocity during these observations did not surpass 5 m/s. In windy weather the readings of the Ångström instrument are consistently too low by large percentages. We mention

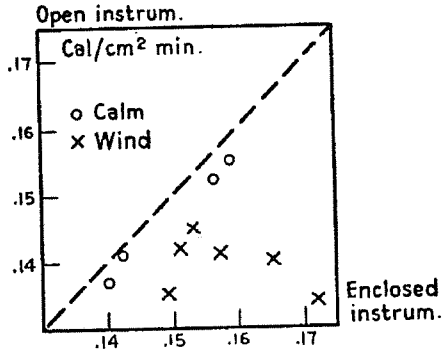

FIG. 23. Comparison of two instruments.

this fact here because the Ångström instrument has been widely used for sky observations. It seems probable that this effect is due to the existence of a temperature gradient across the coat of blackening in the manner outlined.

Albrecht has devised some ingenious compensating methods for the elimination of the wind influence. In a first instrument (95), two equal and equally exposed black plates are used, one of which carries a 3-junction and the other a 6-junction thermopile. The cold junctions of the thermoelements of both plates are reflecting and are exposed to the air in an enclosure underneath the plates which is ventilated but protected against radiation. The thermopiles are in series with opposite polarities. The plate with 6 junctions is heated until the thermo-current vanishes (if there is more incoming than outgoing radiation the other plate is heated). The radiative heat loss per plate is now equal to twice the energy supplied by the heating current. This instrument is based on the assumption that the heat conveyed to each plate by the wind is proportional to the difference between the air temperature and the measured temperature of the plate. Another instrument (95a) of

Albrecht is based on the same assumption. It uses one plate which in short succession is heated by two different currents producing the amounts of heat H_1 and H_2, say. If R is the radiative heat loss, we have

$$H_1 - R = C \cdot t_1 \quad \text{and} \quad H_2 - R = C \cdot t_2$$

where t_1 and t_2 are the temperature differences between the plate and the air, C being a coefficient which depends on the wind velocity but is assumed to remain constant during the measurements. We find

$$R = (H_2 t_1 - H_1 t_2)/(t_1 - t_2)$$

In practice a ratio $H_1/H_2 = 0.4$ is proposed. This instrument was tested in a wind tunnel with velocities up to 8 m/s and the proportionality of heat transfer with temperature was verified. In place of one plate, two equal plates may be used which are permanently heated with two different currents while the galvanometer is periodically switched from one to the other plate. In this form the instrument was used by Albrecht for recording purposes.

Of a somewhat similar but in many respects more refined type than the Ångström instrument is the instrument of Aldrich (96) which is called the Melikeron (honeycomb). Fig. 24 shows its design. Here the black-body principle is realized in an open-surface instrument. The essential part is a honeycomb-like structure, (a) built of individual metallic strips of which one is shown in the lower left-hand corner of the figure. The strips are made of a special alloy and are 1.2 cm wide and 0.05 mm thick. The individual strips are insulated from each other by a shellac cover and are electrically in series so that the compensating current which passes through them heats them homogeneously. A 4-junction thermoelement is used, the hot junctions being fastened to the strips and the cold junctions to the under side of the glass plates (e) which hold the honeycomb in place. The lower two thirds of the width of each strip are blackened, the upper third being left reflecting. In this way only the part of the honeycomb which is fairly well enclosed and may therefore be assumed to have a homogeneous and well-defined temperature, absorbs and emits radiation. Rays which arrive almost vertically and pass through the meshes of the honeycomb are reflected back into the latter by a slanting mirror (b). A hemispherical cover (d), blackened at the inside, is provided which can be flapped over the instrument. (c) is a removable glass hemisphere which is used only for solar radiation measurements. In the Melikeron the influence of the wind upon the temperature is greatly diminished since the essential radiating part of the instrument is well enclosed and it should therefore be much nearer to internal thermal equilibrium than a level plate which is heated and exposed to air. This instrument

has been extensively used by the United States Weather Bureau for nocturnal radiation measurements (see for instance (123)). When the various open surface instruments are compared with each other it seems to the writer that the melikeron combines a maximum of desirable features with a simple principle of operation and relatively inexpensive auxiliary apparatus.

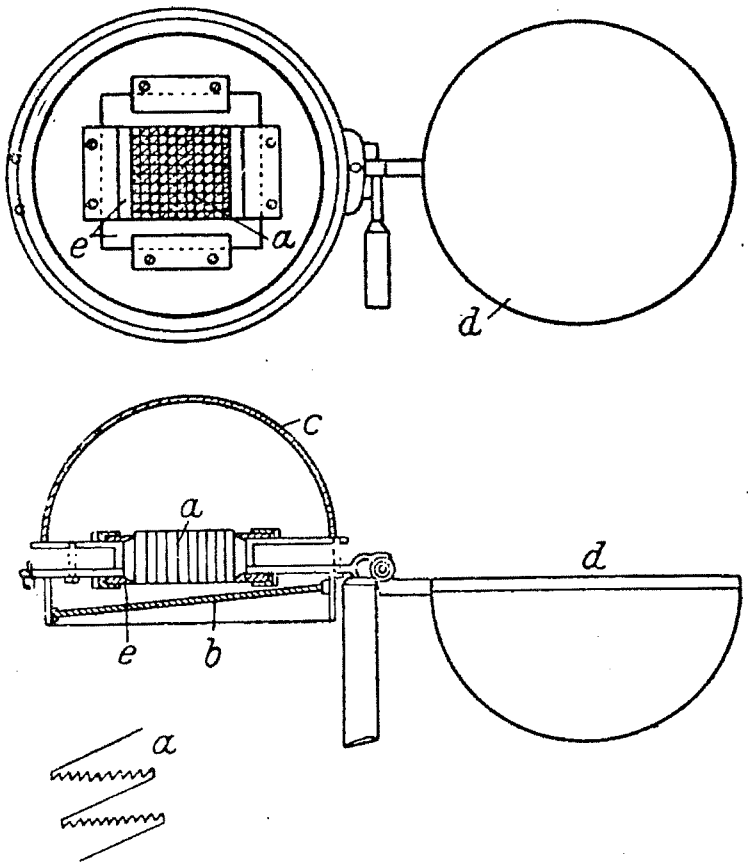

FIG. 24. The Aldrich radiation instrument (Melikeron).

The box-type radiation instrument was extensively used by Dines (104), Ramanathan and Desai (116), and others. Dines's instrument consisted of a 120-element thermopile located at the bottom of a tubular vessel of 60 cm length at the top of which an opening of 10 cm diameter was provided. The instrument was placed underground and surrounded by tanks of water in order to insure constancy of temperature. Measurements were made at various angles of elevation.

Instruments of the telescope type have been constructed by Dubois (105), the author (43), and others. In Dubois's instrument a sensitive thermopile was located at the focus of a concave mirror. These instruments are fairly well shielded from the

wind but they require galvanometers of a much higher degree of sensitivity than the open-air instruments and they are therefore better suited for laboratory measurements than for field use.

We may mention here that Ångström has made radiation measurements in a free balloon (98). An ordinary open-surface instrument was used, and in order to eliminate the radiation from the balloon itself, one half of the sky was screened off by a hemispherical black screen. The instrument could be pointed upwards and downwards so that both the upward and downward flux could be measured.

A word might be said in passing about the calibration of black-body radiometers. Usually these instruments are calibrated by putting them opposite a black body of well-defined size and of known temperature, higher or lower than that of the instrument itself. It may be seen from Fig. 27 of Section 12 that the infrared emissivity of ordinary air is appreciable even in thin layers; a column of 1 meter of moist air under average laboratory conditions has an emissivity of 7–10% of the black body radiation. Calibrations are therefore either carried out in completely dry air or a correction must be applied for the absorption and thermal emission of the air between the standard black body and the instrument.

Automatic recording devices for sky radiation have been constructed by a number of meteorologists (95a), (99), (108). Among other instruments we mention an apparatus of Falckenberg for the measurement of the infrared absorption of objects of small heat capacity (44). The measurement of leaves showed that they were 96% black, the same as water.

We know of only one attempt at observing the infrared emission of the nocturnal sky directly with a spectroscope, by Deveaux (21). The radiative intensity available is minute and the observations had to be made with a very wide slit so that not much detail could be secured. Deveaux indicates that he was able to identify the major features of the water vapor spectrum, the strong band at 6μ and the region of low emission from 8 to 13μ; he also could distinguish clearly the ozone emission at 9μ. An extensive study of infrared atmospheric radiation by an entirely different method has been made by Strong (33). His instrument (31) uses the method of residual rays: It is known that practically all crystals have bands of selective reflection in the far infrared (2). These bands are of various widths and in general comparable in extension and shape with the infrared absorption bands of gases (except that they have no line structure). At the peak of these bands the reflectivity of the crystal is usually very high. If a beam of infrared radiation undergoes several successive reflections at crystals of the same kind, a spectral selection of radiation takes place (Fig. 25). Indeed, if r is the reflectivity for any given frequency, the incident radiation I of this frequency will after n reflections be reduced to Ir^n; if n is not too

small this will be small unless r is close to unity. In this way an originally rather broad and diffuse band can be appreciably sharpened. In Strong's instrument up to five successive reflections can be produced. A number of bands in various parts of the spectrum are obtained by a selection of suitable crystals. The reflected intensity is measured with a vacuum thermopile. We have already made ample use in the preceding chapters of some of the results obtained with this instrument. The residual rays of apophyllite are located near 9μ and coincide with the ozone band of this region. Measurements of atmospheric ozone both in solar absorption and in emission have been made with the instrument (32).

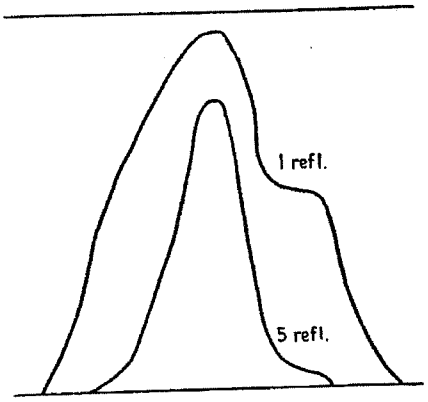

FIG. 25. Residual rays.

There is of course the vast field of solar spectroscopy which for the far infrared has been developed in recent years by Adel (16)–(19). We have had numerous opportunities already to make use of the results of these investigations. The technique is identical with that of ordinary infrared spectroscopy and its discussion is outside the scope of the present study.

12. Measurement of Isothermal Emissivities

The measurement of sky radiation by means of black body instruments represents the most straightforward, but neither the most simple nor the most accurate, test of the properties of atmospheric radiation. Indeed, the atmosphere is so complex in its constitution and in the variety of occurring temperature and moisture distributions that any attempt at connecting the spectroscopic properties of radiating gases directly with the emissive power of the atmosphere is subject to serious difficulties. The method to be described now affords a laboratory or semi-laboratory test of the heat transfer properties of the atmosphere. The method seems to have been invented by Arrhenius (34a) in connection with his well-known suggestion that

the ice ages might be due to a change in the radiative properties of the atmosphere caused by a change in its carbon dioxide content, an idea which has long since been abandoned as an untenable speculation. In more recent years the method has been applied by Hottel and Mangelsdorf (48) and by some others to the measurement of the infrared emission of hot furnace gases. The principle is very simple: the total infrared radiation emerging from a column of gas kept at a constant temperature is measured by means of a black body receiver; in order to shield off all radiation which might come from beyond the column of radiating gas, a black body (Fig. 22) of very low temperature is provided at the far end of the column. Arrhenius used a black body at $-80°$ C while more recent investigators used a black body chilled by liquid air. In the latter case the radiation emerging from this background is about 1% of the black body radiation at room temperature and gives rise to only a very small correction.

We shall first briefly outline the relation of this method to the theoretical conceptions given in Part I which led up to the construction of the radiation chart. We define the emissivity ϵ_I of an *isothermal* column of radiating gas as the ratio of the total radiation emitted by the column longitudinally to the total black body radiation at the temperature of the column. If again τ_I designates the transmission of the column for radiation of a given wave length and if I_b is the black body intensity at that particular wave length, we know from Kirchhoff's law (1.3) that the emission of the column is $I_b\,(1 - \tau_I)$. The total black body radiation is $(\sigma/\pi)T^4$ by (1.7). Hence the emissivity of the isothermal column

$$\epsilon_I\,(u,\ T) = \frac{1}{(\sigma/\pi)\,T^4}\int_0^\infty I_b\,(T)\,[1 - \tau_I\,(u)]\,d\nu$$

If ϵ_I is known, the emissivity ϵ_f of a *slab* of radiating matter may be calculated by (3.8) and is

$$\epsilon_f\,(u,\ T) = \int_0^1 \epsilon_I\,(u \sec\theta,\ T)\,d\,(\sin^2\theta)$$

Now ϵ_f has a very simple connection with the variables Q which form the ordinates of the radiation chart. This relation is derived from (4.3) and (4.7):

$$Q\,(0,\ T) - Q\,(u,\ T) = \frac{d}{dT}\,[\epsilon_f\,(u,\ T)\,\sigma T^4]$$

The triangular areas on the radiation chart which are tabulated in Table 11 are equal to

$$\int_0^T Q\,(u,\ T)\,dT = \sigma T^4\,[1 - \epsilon_f\,(u,\ T)]$$

Hence all the construction elements of the radiation chart may be obtained from the emissivities ϵ_I of isothermal columns by simple mathematical operations. Since ϵ_I is the quantity measured in the experiments just referred to, we have here a means of checking directly the quantities which determine the radiative heat transfer.

A slight generalization of the Arrhenius experiment is achieved if, instead of protecting one face of the radiating column from all incident radiation, we cover it with a black body of the temperature T_1, say. If the other face of the column is bounded by a black plate of the same temperature T as the gas, the net loss or gain of heat of the latter plate is found to be

$$(\sigma/\pi)\,(T_1^4 - T^4) + (\sigma/\pi)\,[T^4\,\epsilon_I\,(u, T) - T_1^4\,\epsilon_I\,(u, T_1)]$$

In such experiments one may take for T_1 either a higher or a lower temperature than T. Expressions of this type also have a simple geometrical interpretation on the radiation chart.

We see from these considerations that the radiation chart is completely determined if the emissivities of isothermal columns are known for all thicknesses u and for all temperatures T. If the emissivities have been measured for both water vapor and carbon dioxide and for the range of thicknesses and temperatures obtaining in the atmosphere, the transfer problem is completely solved with an accuracy exactly equal to that of these measurements — apart from a fourfold correction. The correction terms involve, according to Part II of this paper: (1) the variability of the absorption coefficients with temperature; (2) the effect of pressure upon the absorption coefficients; (3) the overlapping of the water vapor and carbon dioxide radiation bands; (4) the presence of minor radiators, such as ozone in the stratosphere and haze and dust in the troposphere.

We shall first discuss the measurements on carbon dioxide, which are of a comparatively simple character. The results are shown in Figs. 26 and 27. A great simplification is achieved by the fact, discovered by Rubens and Ladenburg (54), that the pressure effect upon the spectral lines of carbon dioxide is very nearly the same whether the pressure is exerted by air or by carbon dioxide itself. In other words a column of pure carbon dioxide under the pressure of one atmosphere will have the same emissive properties as the same amount of carbon dioxide spread over a long column of dry air under atmospheric pressure. In the experiments of Rubens and Ladenburg tubes filled with carbon dioxide were used closed by windows transparent for the carbon dioxide band; the reflectivity of the windows was determined separately and corrections for it were applied. In the experiments of Hottel and Mangelsdorf (48) and of Falckenberg (45) the use of windows was circumvented

by methods which we shall not discuss here. The point in the figures attributed to Hertz was computed (48) from the spectroscopic data of the latter (47).

In Fig. 26 the emissivity in per cent is plotted against the square root of the thickness, and in Fig. 27 against the logarithm of the thickness. The unit thickness

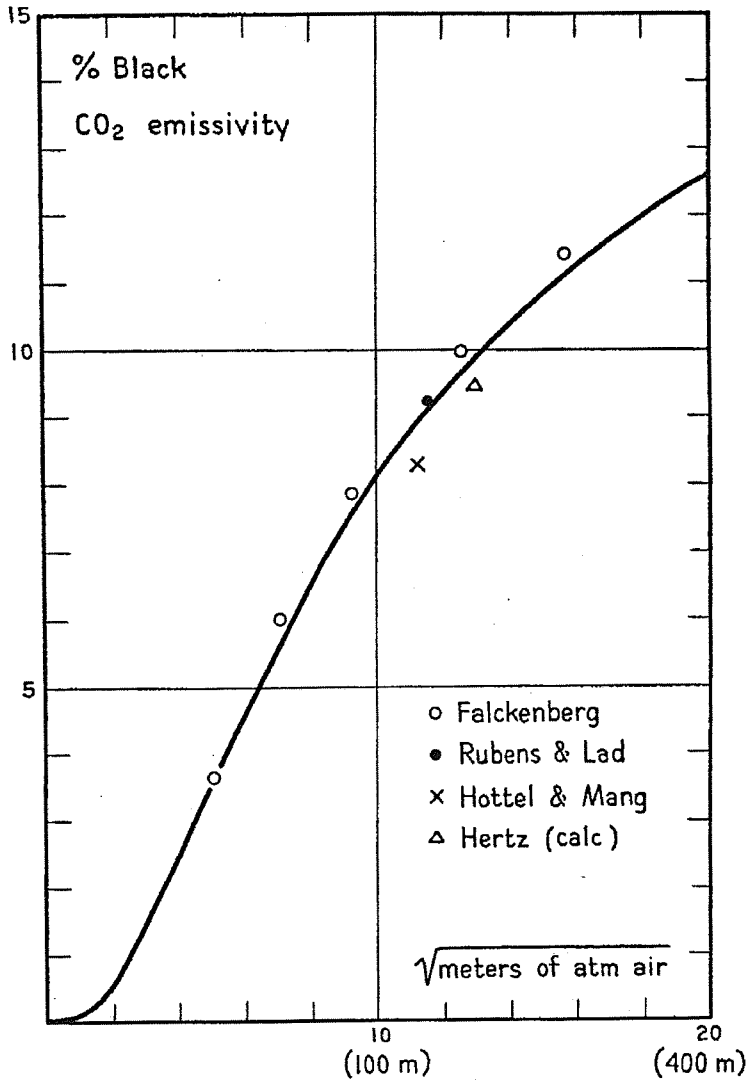

FIG. 26. Emissivity curve of carbon dioxide.

has been taken as one meter of dry air which contains 0.03% of carbon dioxide by volume.[1] We see that for small thicknesses, up to about 50 m of air, the emission is very nearly a linear function of the square root. For longer columns the emission

[1] F. A. Paneth, The Chemical Composition of the Atmosphere, Quart. Journ. Roy. Met. Soc. 63: 433. 1937.

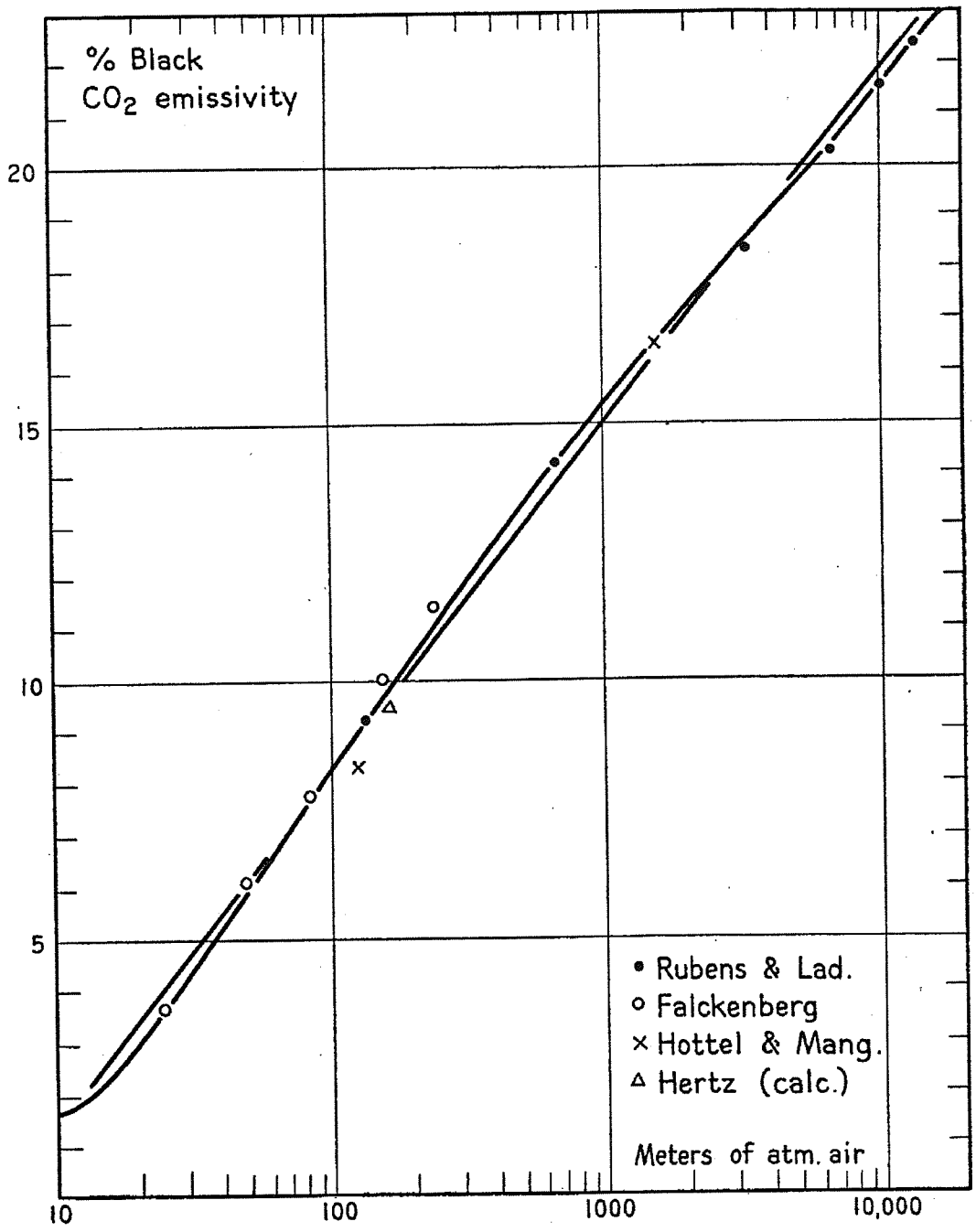

FIG. 27. Emissivity curve of carbon dioxide.

increases much less rapidly and is nearly a linear function of the logarithm of the thickness. In Fig. 27 a curve which fits the observations closely has been drawn and also a straight line. If ϵ_I designates now the emissivity in per cent, the straight line is

$$\epsilon_I = 6.8 \log_{10} u - 5.4$$

We can readily compute from this the emissivity of a slab if we assume that, as shown in Section 7, a slab of thickness u is nearly equivalent to a column of length $1.66\,u$. We obtain

$$\epsilon_I = 6.8 \log_{10} u - 3.9$$

The fact that the emissivity increases first according to a square-root law and later according to a logarithmic law might require some comment. In an absorption band there is a central region where the intensity is fairly constant over a certain interval of the spectrum, while at both sides of the center the intensity decreases very rapidly (about exponentially). This may for instance be seen for the water vapor bands in Fig. 19. As we have seen in Section 7 the absorption (or emission) of a line spectrum follows in any given part of the spectrum a square-root law until in that particular region the absorption or emission is fairly complete. Therefore a square-root law is found at the beginning of the emissivity curve until the absorption or emission is nearly complete in the central part of the band. The decrease of intensity at the edges of the band is extremely steep as, for the carbon dioxide band at 14μ, may be seen from the absorption curves of Fig. 18. As the emitting column grows still thicker, additional emission is due to the gradual appearance of progressively weaker lines at the band edges, and since the intensity of these lines decreases exponentially with distance from the band center, the increase of the emissivity becomes linear on a logarithmic plot. This is the behavior to be expected if the spectrum is dominated by a single band as in the case of carbon dioxide; if there are several strong bands as in water vapor, the emissivity curve becomes more complicated.

We shall now turn to the measured emissivity curves for water vapor which are represented in Fig. 29. Emissivity measurements have been made by Falckenberg (45), F. A. Brooks (37), and Elsasser (43).

Falckenberg used a tube 2.35 meters long which was set up vertically and had a chilled black body at the bottom and a black receiver at the top. Carbon dioxide was removed from the moist air before it entered the apparatus. With this tube, determinations of the pressure dependence of the absorption were also made which have already been discussed (Section 8). Brooks's measurements given in Fig. 28 were made in ordinary laboratory air. The receiving instrument used was of the

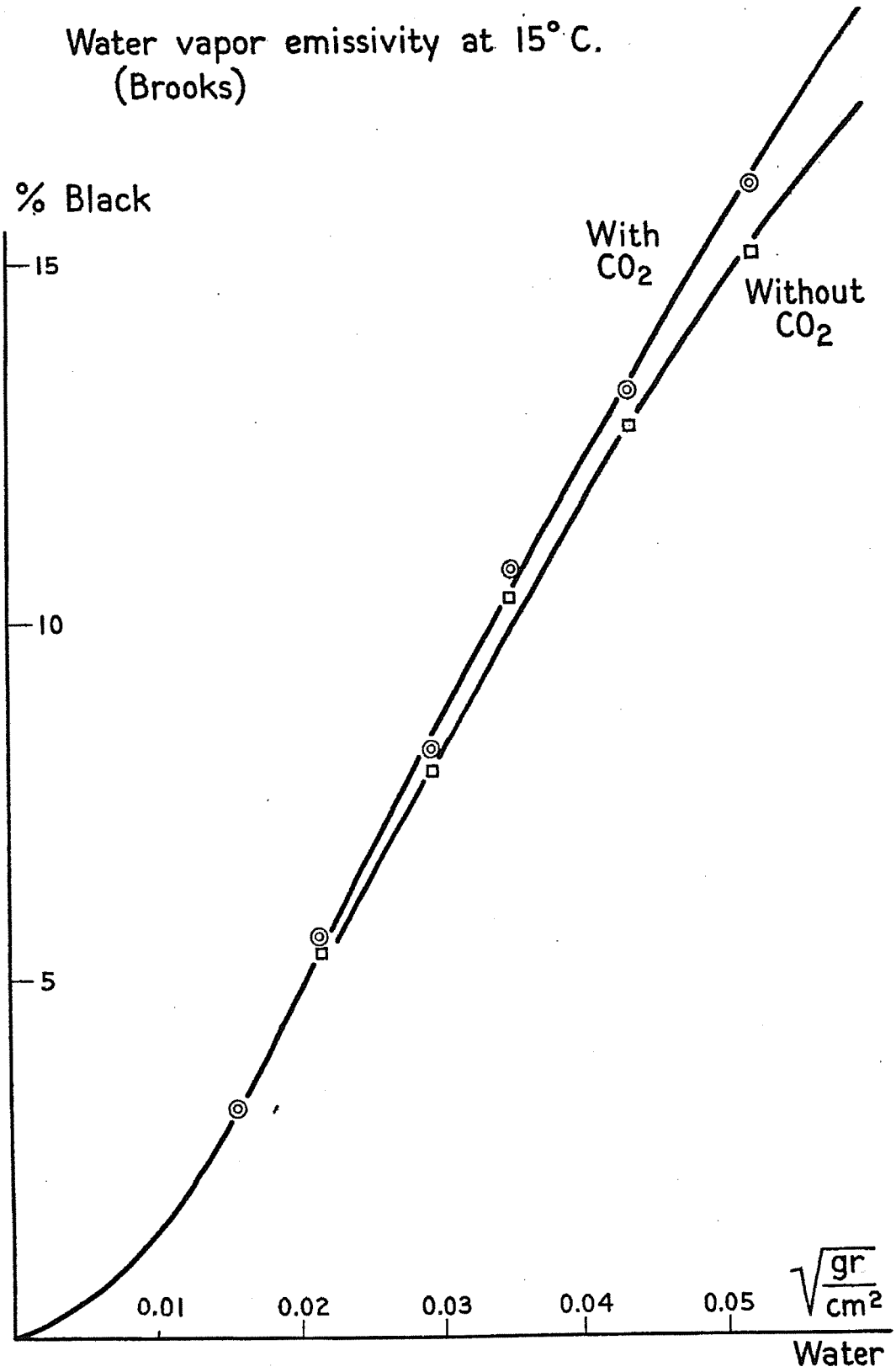

FIG. 28. Emissivity of water vapor, after Brooks.

telescope type with a 6-junction thermopile in the focal plane of a concave mirror. This receiver was built by Hottel and Mangelsdorf (48) for the measurement of heat radiation of furnace gases and is very carefully shielded from stray radiation. It is probable that these measurements are more accurate than those of the two other observers, especially since the author's own instrument was designed to cover a very large interval of path lengths and did not give the same accuracy for short paths. In Fig. 28 we have deducted the carbon dioxide emission as obtained from the curve of Fig. 26. The remaining water vapor emissivity (in per cent) between about 0.0001 and 0.0025 cm of precipitable water may be represented by the formula [1]

$$\epsilon_I = 340\sqrt{u} - 2.0$$

and for the emissivity of a slab, assuming a slab of thickness u equivalent to a linear column of length 1.66 u, we have correspondingly

$$\epsilon_f = 435\sqrt{u} - 2.0$$

These formulae, with proper correction for the pressure and temperature dependence of the emission, might prove useful for the investigation of radiative cooling in the stratosphere.

The author's measurements which are represented in Fig. 29 were made with a telescopic instrument in which two small black disks, each with a thermocouple attached to it, were located in the focal plane of a concave mirror. By means of a small 45° mirror and an eyepiece at the side of the instrument it was possible to see the black disks simultaneously with the image of an object in the focal plane. For the measurement of short optical paths (up to 2 m) the interior of a Dewar bottle filled with liquid air was used as a black body. For longer path (2m – 50m) a small chilled black body was placed at the focus of a concave mirror. A searchlight mirror, 80 cm in diameter and aluminized at the front side, was used for this purpose. The longest paths (50m – 350m) were obtained by combining the receiving instrument with an astronomical mirror of 55 cm diameter; hereby the magnifying power of the instrument was increased by about a factor seven. In each case, while one of the black disks was made to cover the image of the black body the compensating disk was made to cover the image of a cardboard or wooden plate having the temperature of the air. The measured values were corrected for reflective loss at the mirrors and the carbon dioxide emission was deducted according to Fig. 26.

[1] It does not appear possible to apply to this formula the method explained in Section 7 of determining the quantity $\beta = 2\pi a/d$. This method applies only to the case of a well-defined interval of the spectrum while here we are dealing with ratios of the whole black body emission.

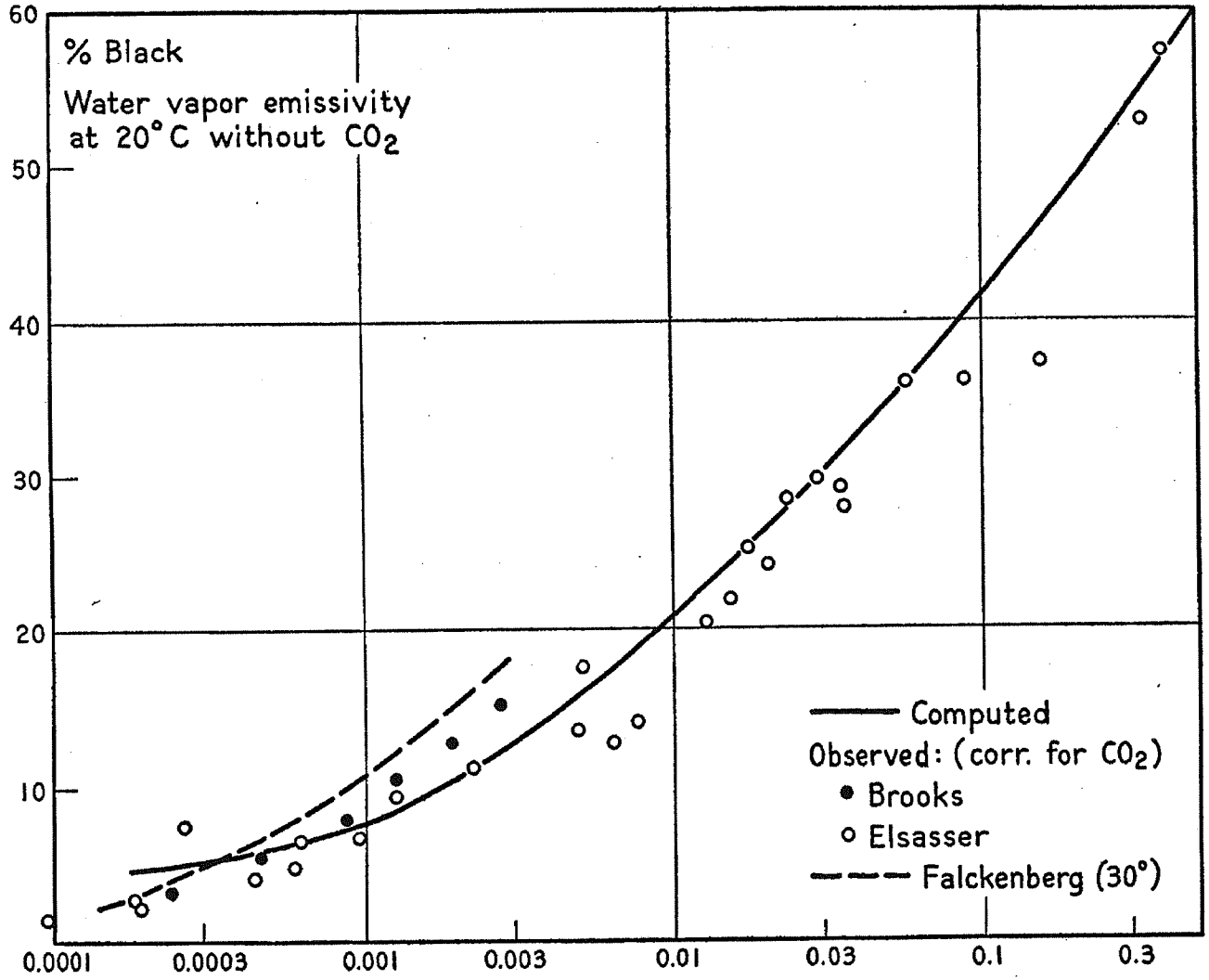

FIG. 29. Emissivity of water vapor (abscissae in g/cm² logarithmic scale).

The curve designated as "computed" in Fig. 29 is obtained from the data given in Section 9. Since all calculations for the radiation chart were carried out for radiating slabs only, the values were again reduced to those for a straight column by assuming that a slab of thickness u is equivalent to a column of length $1.66\ u$. When the calculations for the radiation chart were carried out, some adjustments of the curve of the absorption coefficients, Fig. 19, were made so that the resultant emissivity curve should fit our measured values. Details have been given in Section 9. At that time the measurements of F. A. Brooks had not yet been published. It would now appear that the computed curve is somewhat too high for very low moisture values and somewhat (about 2–3% of the black body intensity) too low in the center part of Fig. 29. This indicates that the intensity of the 6μ band as assumed in Fig. 19 is somewhat too small and that the intensity assumed at the top of the rotational band is too high. Neither result is unexpected according to the discussion in Section 9. In the light of the results obtained it may now be evident that by combining good spectroscopic intensity measurements with the measurements just described, one can arrive at reliable emissivity values and thus solve the radiative transfer problem. It could be argued that this is trivial since the total emission of any radiator is the sum of the emissions of all the parts of the spectrum. The total emissivity is, however, not only dependent upon the intensities of the spectral lines in all parts of the spectrum, but also upon the course of the transmission functions (Fig. 15) which, on account of the complicated nature of the spectrum, can only be approximations. The already fairly satisfactory agreement between the actual emissivities and the computed ones which might be improved by the corrections of the spectrum referred to can be taken as an indirect check of the correctness of the transmission curves. One might envisage the measurement of an emissivity curve of moist air for path lengths ranging over the whole scale of moisture-thicknesses covered by the radiation chart, and it might then appear as if a spectroscopic analysis could be omitted altogether. But it would be very difficult to make such emissivity measurements for the range of temperatures and pressures prevailing in the middle and upper atmosphere. On the other hand, we may hope that by means of a judicious analysis of the pressure and temperature dependence of the spectral lines we can determine corrections which will give us the emissivities under the conditions of the middle and higher atmosphere with an adequate degree of accuracy.

It may be mentioned here that a number of emissivity measurements of gases at high temperatures have been carried out for engineering purposes (literature in (45) and (48)). The results have a bearing on the problem of heat transfer in furnaces and steam boilers. The extrapolation of emissivity curves from high temperatures to room temperature has occasionally been tried. It might be justified for

carbon dioxide with its comparatively simple spectrum, but reliable measurements at room temperature are available. In the case of steam emissivities the spectrum and its variations are much more intricate, and the situation is further complicated by the fact that, as we have seen in Section 9, the width of the spectral lines in steam is about twice that in water vapor under atmospheric conditions. A straightforward extrapolation of steam emissivity values is therefore liable to lead to results which are seriously in error.

The emissivity values of Fig. 29 go up to about 3 mm of precipitable water. A determination of emissivities of thicker columns has been tried by F. A. Brooks

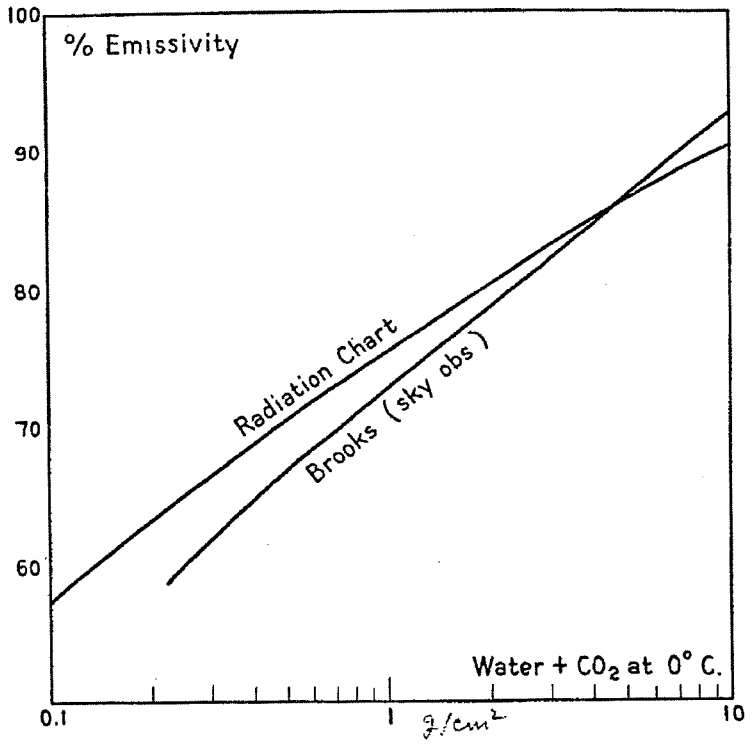

FIG. 30. Emissivity of water vapor, thick layers.

(37) on the basis of sky radiation measurements carried out with his telescopic instrument. The procedure followed was that of assuming a trial emissivity curve, then computing the sky emission and correcting the emissivity curve until the computed emissivities fitted the observations. This method disregards the small change of emissivity with temperature (it may be recalled that emissivity is defined as the ratio of gas emission to black body emission so that the main part of the change of emission with temperature is due to the change of the black body emission with T^4, while the change of emissivity with temperature reflects only the shift of the

position of the black body curve relative to that of the absorption bands and is comparatively small). More serious is the fact that the emissivity corresponds to a mixture of water vapor and carbon dioxide in proportions which have not been specified. The emissivity curve thus obtained was extrapolated on double logarithmic paper so as to pass into the emissivity values for low moistures represented in Fig. 26. Brooks's curve is compared in Fig. 30 with an emissivity curve drawn from the radiation chart. Brooks's values correspond to a ratio of water vapor to carbon dioxide which, so far as it is defined, should correspond to their mean proportion under average conditions near the earth's surface, while, as we know, the radiation chart is constructed so that the carbon dioxide radiation represents a constant amount for all moistures, being about equal to the carbon dioxide radiation emitted by the whole atmosphere. Hence for smaller moistures the chart values must lie above Brooks's values, since in the limit of zero moisture the chart gives about 18% emissivity corresponding to the carbon dioxide band alone while Brooks's curve gives zero emissivity. This behavior is verified from Fig. 30. In the region from, say, 5 mm to 10 cm of precipitable water which corresponds to the amounts of water vapor overhead found in the atmosphere under average conditions the two curves agree fairly well and the deviations are probably within the errors induced by the reduction of the sky radiation measurements. Hence, Fig. 30 may be taken as a test of the new radiation chart yielding a fairly good agreement between sky radiation computed from the chart and sky radiation observed.

13. Nocturnal Radiation Measurements

Sky radiation measurements are of practical interest in connection with the problems of nocturnal frosts and nocturnal fogs produced by the radiative cooling of the ground. Besides, if carried out in conjunction with upper air soundings, they provide valuable information about the dependence of the radiative heat flux on the distribution of the temperature and moisture aloft and thus allow us to draw indirect conclusions about the effects of this flux in the free atmosphere. Such combined measurements were carried out in the early work of Ångström (97) and in the more recent observations of the United States Weather Bureau in Alaska and North Dakota (123). While the amount of heat lost by the ground during any short period of time is comparatively small, radiative cooling of the ground is nevertheless a very powerful agent in the heat balance of the atmosphere, since it acts continuously, night and day. Reports of a rather sudden change of the amount of outgoing radiation at certain times of the day (107) are probably induced by wind influence upon the instrument or by other spurious effects. In a record of sky radiation made at Pasadena (unpublished) the author found that whenever the air was

stable enough to prevent day-time convection, the radiation from the sky at sufficient distance from the sun was very little different from that at night.

With clear skies the incoming radiation is practically always between 50% and 85% of the black body flux corresponding to the temperature of the air near the ground and is most commonly between 65% and 75% of this flux. It is seen from this fact that sky radiation observations in the presence of upper air soundings furnish a highly critical test of the calculations of radiative heat transfer: a relative error in emissivities referring to black body emission will produce a relative error in the rate of nocturnal cooling which is from three to four times larger. The figures mentioned refer to sky radiation with perfectly clear sky; any cloud present greatly reduces the heat loss of the ground and with a solid overcast the outgoing flux is only of the order of 5–10% of the black body flux.

On account of the great variety of moisture and temperature distributions found in the atmosphere the incoming sky radiation does not follow any very simple law. Since upper air soundings are not always available, observers early tried to correlate the incoming radiation with elements of observations at the ground, such as temperature, moisture, etc. These efforts have led to a number of empirical formulae for sky radiation, all of which agree only statistically with the observations but provide a valuable guide for the estimate of the sky radiation under given meteorological conditions. The two principal formulae of this type are due to Ångström (97), (100), and to Brunt (66), (1); we shall also briefly discuss a formula of Robitzsch (120). We express the incoming sky radiation R by means of the ratio R/F_b where $F_b=\sigma T^4$ is the black body flux corresponding to the temperature of the air near the ground. The empirical formulae give the sky radiation as function of the water vapor pressure e in the air near the ground; we express e in millibars.

In the following discussion we make frequent reference to a paper of Raman (116) from which many of the numerical values indicated below are drawn. The formula of Ångström reads

$$R/F_b = a - b\cdot 10^{-\gamma e}$$

Ångström has several times changed the values of the constants in order to achieve a better fit with the increasing number of observations; the latest values seem to be (8):

$$a = 0.806 \qquad b = 0.236 \qquad \gamma = 0.052$$

The figures represent quite well the original data of Ångström and of Asklöf (101); in addition Raman has calculated coefficients from a number of other series of observations:

	a	b	γ
Kimball (109) on Mt. Weather (540m)	0.80	0.325	0.070
Eckel (106) on Kanzelhöhe (1500m) Austria	0.71	0.24	0.074
Ramanathan and Desai (117) Poona (564m) India	0.78	0.27	0.040
Raman (116) Poona	0.79	0.273	0.051

Usually the individual observations show a fairly wide scatter about these curves.

Malurkar (112) has tried to modify the Ångström formula by introducing the function Ei_3 in place of the exponential. Since however $Ei_3(x)$ is numerically very close to $e^{-3x/2}$, no essential advantage results.

Brunt (66) has proposed another formula for sky radiation and found that in a number of series of observations the individual data scattered much less about his formula than about that of Ångström. Brunt's formula is

$$R/F_b = a + b\sqrt{e}$$

For the very extensive series of observations by Dines (104) he finds $a = 0.256$ and $b = 0.065$. Brunt (1) has calculated coefficients a and b from other series of observations and the list has been amplified by Raman. Below, we have also indicated the coefficient of correlation r between the observed values and those obtained from the formula. All these values are the result of comparatively lengthy series of observations.

	a	b	r
Dines (104), Benson, England	.53	.065	.97
Asklöf (101), Upsala, Sweden	.43	.082	.83
Ångström (97), Bassour (1160m), Algeria	.48	.058	.73
Ångström (97), Mt. Whitney (4420m), Calif.	.50	.032	.30
Boutaric (102), Montpellier (2860m), France	.60	.042	...
Robitzsch (120), Lindenberg, Germany	.34	.110	1.0
Kimball (109), Washington, D. C.	.44	.061	.29
Kimball, Mt. Weather (540m), Virginia	.52	.066	.84
Kimball, various places in U. S.	.53	.062	.88
Eckel (106), Kanzelhöhe (1500m), Austria	.47	.063	.89
Ramanathan and Desai (117), Poona (560m) India	.55	.038	.63
Raman (116), Poona	.62	.029	.68

Raman has pointed out that the measurements of Robitzsch might be influenced by systematic errors and the high coefficient of correlation would therefore not be significant.

A third empirical formula, finally, has been suggested by Robitzsch (120); it reads

$$R/F_b = (0.135\,p + 6.0\,e)/T$$

where p is the air pressure in millibars. In Fig. 31, taken from Robitzsch, the water vapor pressure is plotted against the value of the numerator on the right-hand side of this formula. The Lindenberg observations and those of Ångström at high elevations (97) were used; the latter were reduced to standard pressure $p_0 = 1000$ by adding the term $0.135\ (p_0 - p)$ to the numerator. Although the Lindenberg observations have been criticized by Raman (116) the fit with Ångström's observations deserves attention and invites further critical investigations of this formula.

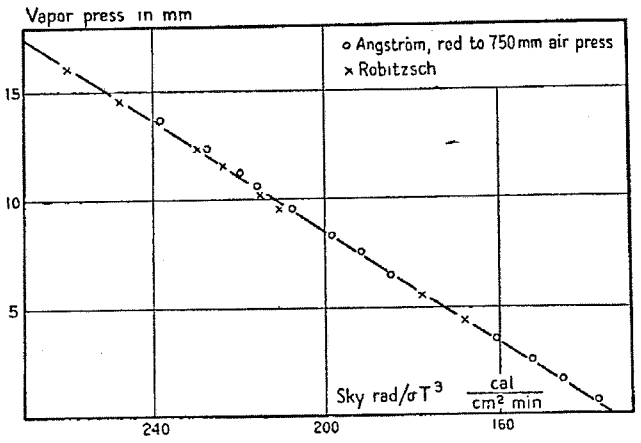

FIG. 31.

Attempts have been made by Ångström and others (87) (118) to give a theoretical justification of the empirical relationship expressed in Ångström's formula. One may take as a starting point the fact that the spectrum of the atmosphere consists of a highly opaque part and a semi-transparent part in the neighborhood of 10μ. The opaque portion may be regarded as a black radiator with a temperature nearly equal to that of the air near the ground. If we write Ångström's formula

$$R = F_b\,(a - b) + F_b\,b(1 - 10^{-\gamma e})$$

the first parenthesis would correspond to the contribution of the opaque part. The second term might be interpreted as the emission of an isothermal layer with a constant absorption coefficient (provided the spectrum is of a continuous and not of a line character), it being assumed that the total moisture overhead is proportional to the water vapor density near the ground. In addition, the formula interpreted in this way implies that the opaque and the semi-transparent parts of the spectrum

are distributed so that their relative proportion does not depend upon the temperature. (In reality the emissivity for a given moisture increases slowly with temperature as may be seen from Table 11.)

We know that the spectrum of water vapor is not a continuous but a line spectrum and does not obey an exponential but a square-root law of absorption and emission. Strong (33) has given a derivation of Brunt's formula based essentially upon the preceding arguments but using the square-root law in place of an exponential. Indeed if we replace $(1 - 10^{-\gamma e})$ in the above expression for the sky radiation by const $\cdot \sqrt{e}$ we obtain Brunt's formula. Raman (116) has pointed out that the two formulae are not so different as it might appear at first sight. Thus the expressions $0.28\,(1 - 10^{-0.055e})$ and $0.06\sqrt{e}$ do not differ from each other by more than 10% for an interval of e ranging from $e = 2$ to $e = 40$. On the other side we have Brunt's finding (1), that a considerably better correlation is found in some series of observations with the square-root than with the exponential formula.

The actual spectral structure of the emission of the sky is quite complex, and one would want to compare the formulae for sky radiation with the actual emissivity curve of an isothermal slab. The emissivity for the range of moistures with which we are dealing here is shown in Fig. 30, and the relation seems to be nearly linear on a logarithmic plot. Hence, assuming again that the total moisture overhead is proportional to the moisture near the ground, we are led to a formula for sky radiation

$$R/F_b = a + b \log e$$

This again is not so different from Brunt's formula as might be expected. The functions $0.21 + 0.22 \cdot \log e$ and $0.06\sqrt{e}$ do not differ by more than 10% in the interval $e = 3$ to $e = 40$. If the emissivity curve of Fig. 30 is plotted against the square root of the moisture, the curve obtained will have considerably more curvature than that on the logarithmic diagram. Under these circumstances, Brunt's formula can hardly be considered as much more than an empirical relationship, and if the premises are accepted upon which the theoretical derivation outlined above was based, a logarithmic formula would appear as a rather logical approximation.

In view of the empirical character of these relations a formula such as Robitzsch's might also deserve attention. The other two formulae do not take into account the height of the observer, and it might be assumed that with equal temperature and moisture at the ground the total amount of moisture overhead will be less at a higher elevation than at sea-level. The introduction of a pressure term seems therefore not altogether unjustified. The appearance of the temperature in the denomina-

tor seems to correspond to the fact that the emissivity decreases slowly with increasing temperature (as may be verified from Tables 8 and 11).

The formulae for sky radiation which have been proposed do not take into account the existence of ground inversions. One might be inclined to think that a better representation of empirical data by means of such formulae could be achieved if the case of inversion is treated separately. The decrease of moisture and temperature with height in an average atmosphere is fairly regular and uniform, and it is therefore understandable that the average sky radiation may be approximated by a simple function of temperature and moisture near the ground. One would not, however, expect such a formula to apply without further corrections to the case where a strong inversion is present in the lowest layers of the atmosphere. So far this question has apparently not been investigated.

If clouds are present, the amount of incoming radiation is greatly increased and the cooling of the ground is correspondingly reduced. Systematic observations have been made by Asklöf (101) and Ångström (100), and the following figures refer to a fully overcast sky. If R is again the incoming sky radiation and if R_0 is that incoming radiation which is computed from Ångström's formula for a clear sky, we write for the net loss of radiation:

$$L = F_b - R = \lambda (F_b - R_0)$$

where λ is a numerical factor which is found to depend principally on the height of the cloud deck. The following values of λ are reported:

cloud height	1.5	3	7 km
λ	0.14	0.25	0.80

Philipps (87) has derived a similar formula from theoretical arguments and finds

cloud height	2	5	8
λ	0.17	0.38	0.45

For low clouds the agreement between the observed and calculated values is quite satisfactory; in order to explain the discrepancy for high clouds Philipps suggests that the high overcast observed by Asklöf during the night was not in general thick enough to be entirely black and might have had occasional breaks. According to Dines's observations (104) the average heat loss of the ground for overcast skies is one sixth of that for clear skies.

We turn now to the dependence of the incoming sky radiation upon the angle θ of zenith distance. Spectroscopic measurements of the angular dependence for various wave lengths have been made by Strong (33) and observations with black

body instruments are due to Dines (104), Süssenberger (121), and Ramdas, Sreenivasiah and Raman (119). On increasing the distance from the zenith it is found that the incoming radiation increases very slowly and at 30° zenith distance it is still nearly the same as in the vertical. Only very near to the horizon does the incoming radiation increase rapidly towards the full black body value. As an example we give the yearly mean values of Dines in calories per cm² per day:

7.5°	22.5°	37.5°	52.5°	67.5°	82.5°
490	493	503	522	553	674

The values of Süssenberger show a very similar course except that above 80° they give much less incoming radiation. This might be attributed to the relatively large opening angle of Dines's instrument which could bring obstacles into the cone of sight near the horizon, whereas Süssenberger used a telescopic instrument with nearly parallel beam. Strong found (33) that the angular dependence of Dines's values can be rather accurately represented by a formula of the type

$$I_\theta = a + b\sqrt{\sec\theta}$$

where a and b are empirical constants. We found the same to be true for the measurements of Süssenberger up to 80°, while the values given for 85° were lower than would follow from such a formula. Strong also discovered that if the winter and summer values of Dines are plotted separately two curves result which have nearly the same b but different values of a.

Following Linke (100) we may determine the two coefficients in such a formula as the preceding one from two measurements, one at 0° and one at 60°. We may then compute the radiation falling upon a horizontal plate from the whole sky by using (2.4). If the simple calculations are carried out we obtain the result

$$R = 2.53\, I_{60} + 0.61\, I_0$$

Linke himself has tried to express the heat loss of the black instrument under the angle θ by an expression of the form

$$l_\theta = l_0 \cos^r\theta$$

where l_0 is the loss in vertical direction. The exponent r is found from two measurements, one at 0° and one at 60°:

$$r = \log(l_{60}/l_0)/\log\cos 60° = 3.32 \log(l_{60}/l_0)$$

and the net loss of a horizontal black plate follows as

$$L = 2\pi l_0/(2 + r)$$

Süssenberger indicates that the approximate curves thus obtained give a very good fit except at angles over 80° where the values computed from the formula are too large (i.e., the computed incoming radiation is too small). In the average over a large number of observations the total net loss L computed from the above formula was only about 3% higher than that obtained by graphical integration of the curves of angular distribution.

We see from (2.4) that in the integration over the hemisphere the incident intensity is multiplied by $\sin\theta \cos\theta$, a function which has a maximum at 45° and vanishes at 0° and 90°. Hence the part of the sky near the horizon contributes little to the total sky radiation and the assumption that the approximative formulae given above should come close to the true radiation of the whole sky is theoretically justified.

14. Notes on Radiative Cooling of the Free Atmosphere

The most significant meteorological applications of the methods developed on these pages are those dealing with the cooling of the free air. Here we enter the field of meteorological thermodynamics; unfortunately our knowledge of the cooling phenomena is still in a rather rudimentary state. We shall therefore confine ourselves to some very brief and general remarks. The relation of radiative cooling to the dynamics of the atmosphere is readily understood. The circulation of the atmosphere is due to two main causes, the difference in heat received from the sun in different geographical latitudes and the difference in heat gained or lost at different heights of the atmosphere. While the former cause is the primary agent that determines the atmospheric circulation, the radiative heat balance of the free air is a secondary controlling factor which does not yield much to the former in profound influence upon the dynamics of the air. Since, as we shall see, the atmosphere is continuously losing heat by infrared radiation into space (and the quantities of heat lost in this way are large) the mechanical motions of the air, due mainly to horizontal temperature gradients at the surface, must have vertical components of such magnitude that they can supply, in the average, the equivalent of the radiative loss at any level aloft. A variety of meteorological aspects of radiative transfer can only be lightly touched upon in the present paper; for a particularly complete treatment of infrared radiation in its various meteorological implications we refer to chapters 5–7 in the well-known treatise of Brunt (1). This book has played an outstanding role in the development of our subject and it has drawn the attention of many meteorologists to phenomena of infrared radiation.

It was found concordantly by Möller (80) who used the Mügge and Möller radiation chart (83), and by the calculations (70) carried out with the first edition

of our radiation chart, that the net effect of infrared radiation upon the free atmosphere is universally a *cooling*. This result is not essentially modified if the absorption of solar radiation by the free atmosphere is taken into account since the heating produced by the latter is always much smaller than the cooling due to the infrared emission of the atmosphere itself. The amount of cooling found from the first edition of the radiation chart varies in general between about 1° C and 3° C per day, depending mainly on the humidity and increasing regularly with the latter. The numerical values need revision and it is seen from a comparison of the first and second editions of the chart that the figures obtained were too large. Computations of the radiative heat balance by Möller (80) are shown in Figs. 32 and 33. Fig. 32 refers to mean conditions with a clear sky over Lindenberg in June; Fig. 33 to conditions of mean cloudiness for the same time and location. The cloud distribution assumed was the same as used by Baur and Philipps (64). The figures are reproduced here not so much on account of the numerical values for the cooling contained in them, but in order to illustrate the typical radiative heat balance prevailing in the free atmosphere in middle latitudes. The relative constancy of the radiative cooling over the larger part of the troposphere indicated in Fig. 32 is rather surprising. In our own calculations it was found on the contrary that the radiative cooling decreases rather rapidly with moisture and therefore with height. This work was done with the first edition of the radiation chart and new calculations are now required to bring about a decision. It seems fairly probable, however, that even with the new values radiative cooling will be found to decrease with height. This effect is of great importance in that it leads to a stabilization of the air in vertical direction since it tends to decrease the vertical temperature gradient. The heating of the atmosphere by absorption of solar radiation was also computed by Möller by means of formula (10.2) and is shown in Fig. 32. Similar, more extensive computations on the effect of sunlight were carried out by Tanck (93); he found that the heating effect due to the absorption of sunlight varies between about 0.3° and 0.6° C per day according to conditions. The pressure correction of the absorption was neglected in this work, but this should not modify the results by more than 10–15%.

It is seen from Fig. 33 that the picture of the clear sky is rather thoroughly altered if clouds are taken into account. It was found in our calculations that clouds cool appreciably because of their own emission, and this is also clearly recognized from the emission curve of Fig. 33. The solar absorption is not much changed as compared to Fig. 32, but the heat of condensation which now appears is so large that a balance of an entirely different type results, giving a rapid increase of cooling with height and thus a pronounced destabilization of the air in the middle troposphere. While these figures are probably far from definitive, they may give an idea

of the phenomena and problems related to heat transfer in the free atmosphere.

A number of meteorological papers have been devoted to the problem of radiative cooling in the free air and its dynamical implications (see Part 4 of the bibliography), but in view of our rapidly increasing knowledge of the infrared emissivities of water vapor and carbon dioxide it is perhaps premature to discuss this subject

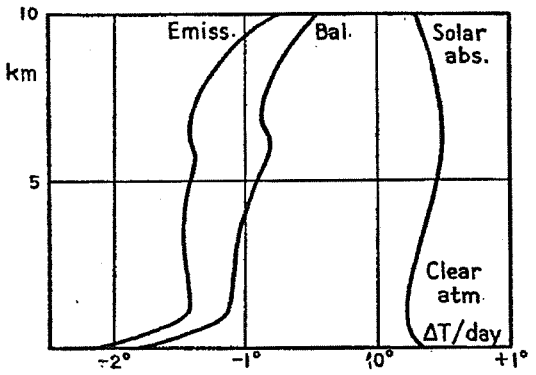

FIG. 32. Heat balance of the free air over Lindenberg in June, clear sky; after Möller.

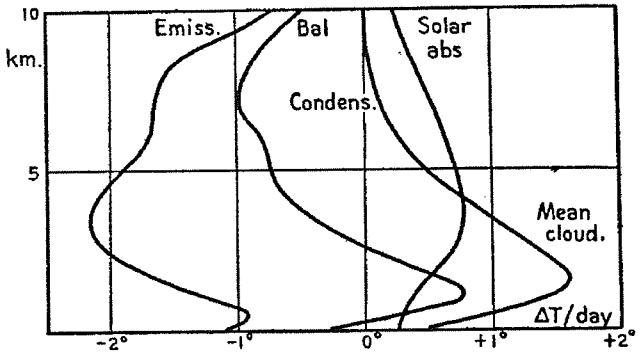

FIG. 33. Heat balance of the free air over Lindenberg in June, mean cloudiness; after Möller.

at present in more detail. We shall say a few words about ground inversions. The primary cause of most inversions is the radiative cooling of the ground itself. The main problem of the inversions lies in the understanding of the mechanism by which the lower strata of the atmosphere in turn transfer heat to the ground. This takes place partly by radiation and partly by turbulent transfer. The mechanism has been investigated by Brunt (65) and by Philipps (87). Most of the radiative cooling of the free air is due to a loss of radiation upwards to space, but in this respect the lowest layers do not behave differently from the air aloft, and no inversion will be

created; in addition there is a radiative flux from the lowest layers of air downwards to the ground if the latter is cold enough. It was clearly shown by Ashburn (63) and verified by the author (70) that this radiative transfer is relatively small and is quite negligible compared to the turbulent transfer at heights above about 50 m. This rule may suffer exception for the very pronounced inversions in polar regions over a snow surface where the snow becomes exceedingly cold and where there might be an appreciable radiative transfer from the air in the lowest layers to the ground, as has been found by Wexler (94).

In the lower atmosphere the outgoing flux is carried almost exclusively by water vapor radiation, and the contribution of carbon dioxide radiation to the cooling is small. This is different in the stratosphere. The stratosphere being almost isothermal, an emissivity curve of the type of Fig. 27 must apply to the carbon dioxide radiation; the pressure and temperature are of course different from those to which Fig. 27 refers. In the stratosphere the contributions of water vapor and carbon dioxide to the cooling appear to be of the same order of magnitude. The cooling, which seems to have a minimum in the upper troposphere, increases again as we go upwards in the stratosphere as Möller has found and as may be inferred from the carbon dioxide emissivity, Fig. 27. In order to get a rough estimate of the total cooling of the stratosphere, let us assume that the outgoing flux is, say, 20% of the black body flux at $-55°$ C. This gives us 53 calories per cm^2 per day and if we distributed this evenly over a layer of the thickness of the stratosphere, say 200 millibars, we would by (5.6) obtain a mean cooling of 1.1° per day. In reality the cooling will be much less in the lower stratosphere and will increase as we go upwards. It has been pointed out by Professor Strong that if the top layers of the stratosphere are very warm, as is probable, a downward flux of radiation in the carbon dioxide band must obtain. We can expect this effect to reduce considerably the radiative cooling of the stratosphere in the layers directly underneath the warm top layer.

It is an open question whether the heat lost by infrared radiation of the stratosphere may in part be replenished from the warm layers on top by turbulent motions of the air. (Notice that in a medium which has a stable stratification, the flow of heat produced by turbulence is always directed downwards.) It seems that the heat lost by the thermal emission of the stratosphere is in the main supplied through the absorption of ultraviolet and visible sunlight by ozone. The ozone problem is too complex to be even touched upon here; for the convenience of the reader we have included in the bibliography some reports on the subject which contain ample literature references. The cooling by infrared radiation represents, so to speak, the other face of the ozone problem in so far as it accounts for the disposal by the stra-

tosphere of the energy taken out of the solar spectrum in the ozone bands. This physical condition is frequently referred to as radiative equilibrium; it must be remembered, however, that the equilibrium by no means applies to infrared radiation alone, but to a condition in which the received solar energy is reëmitted by the stratosphere in form of infrared radiation. The equilibrium need not be local, since there is evidence of strong horizontal motion all through the stratosphere.

We might finally mention another problem of meteorological importance, the heat balance of the earth as a whole. In the average, the solar radiation absorbed by the earth equals the infrared flux leaving the outer boundary of the atmosphere. The amount of solar radiation absorbed depends essentially only on the albedo of the clouds, while the outgoing infrared radiation is a rather complex function of the distribution of moisture, temperature and cloudiness in the atmosphere and is computed by the same methods as radiative cooling, etc. We may refer to the extensive investigations of Simpson (91), Abbot (59), and Baur and Philipps (64) without entering into a discussion of their results.

APPENDIX: A MECHANICAL COMPUTING DEVICE

In order to carry out the extensive numerical calculations necessary for the construction of the radiation chart, a mechanical device was developed which might be useful to others and which is therefore described below. The device performs the following two operations: First, it permits the computation of a function of a function, $f[g(x)]$ say, if f and g are given graphically. Secondly, it permits the calculation of the integral over the product of two functions $J = \int f(x)\, \varphi(x)\, dx$, say. It may be shown that the second problem can be reduced to the first combined with a simple integration. Indeed, if we put $u = \int_0^x \varphi\, dx$, we have

$$J = \int f\, du = \int f[x(u)]\, du$$

If u is graphically given as function of x, we immediately solve for x (u) by interchanging the axes.

The diagram, Fig. 34, shows the design of the machine. It consists of four movable carriages numbered I to IV. The top of each of the carriages I, II, and III consists of a small drawing board. Carriages I and III are attached to two synchronous worm gears driven by an electric motor. Carriages II and IV are moved by two operators sitting in front of I and II respectively, each holding a handle attached to the arms A and B respectively. The operators move carriages II and IV so that a pointer provided at the end of the arms A and B follows a curve drawn on the boards I and II, respectively. We see from the figure that each of the coordinates x, y, z indicated appears twice on the three drawing boards and with the signs indicated in each case by the arrows. It is now readily seen that if the curve on board I has the equation $y = g(x)$ and the curve on board II has the equation $z = f(y)$, the point C on carriage IV describes the curve $z = f[g(x)]$ relative to the moving board III. If a pencil is attached to C, it will draw this curve on the board III. In this way the first of our two operations is carried out. For the second operation the pencil is replaced by a planimeter attached to C. The planimeter is read at the start and at the end, after carriage III has been brought back to its initial position; the difference of the readings gives the value of the integral desired.

We shall indicate a few details of the construction. The drawing boards I and II are about 12×11 inches; board III is slightly larger. The carriages I and II are equal in construction and consist of a fairly heavy steel frame and four wheels. The two wheels on one side of each carriage have beveled disks of about $1\frac{1}{2}$ inches diameter which roll in a V-shaped groove cut in a steel rail. The other two wheels

are simply flat rollers. For the bearings of the wheels and for the rollers the cheapest type of commercial ball bearings of 1 inch diameter are used. These bearings have a very considerable play, but it is found that after proper adjustment of all parts the random transverse motion of the carriages caused by this play becomes small

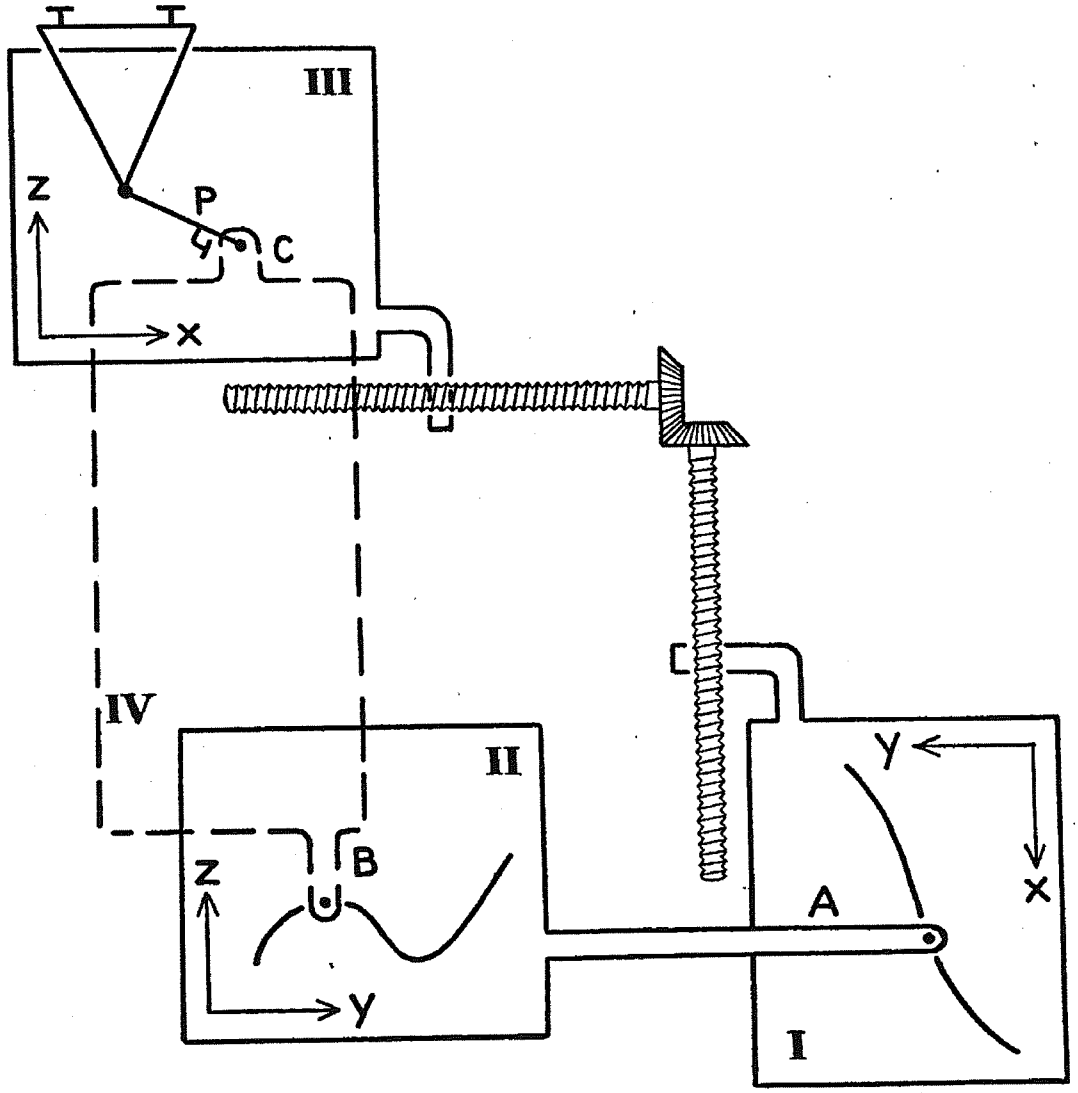

FIG. 34.

enough to be practically negligible. The drawing boards themselves are made of plywood. Carriage IV merely transfers a motion from II to III and consists of a heavy metal frame rolling on two rails elevated above the rest of the machine so as to permit the passage of carriages II and III underneath. Carriage III consists of an ordinary small drawing board reinforced at the sides by L-shaped strips of

brass. In motion it merely slides on the base plate of the machine. A straight motion of this carriage is secured by pairs of rollers (ball bearings) with vertical axes on each side of the board, one pair being pressed to the board with springs. The planimeter used is of the linear type and consists of a triangular frame with an arm pivoting around the point of the triangle. The planimeter wheel is indicated in the figure directly underneath the letter P. The frame of the planimeter rolls on two wheels in the groove of a rail outside the carriage III; the point of the triangle is supported by a roller. Undoubtedly a polar planimeter of sufficiently large size could also be used, although this was not tried since the linear planimeter was the only large planimeter available.

The whole machine is mounted on a large drawing board. The speed of the motor driving the worm gears is regulated by means of a foot rheostat such as those which are used in sewing machines.

It was also necessary to introduce into the calculations functions $f(x + a)$, etc., for various values of the constant a. This can be achieved by developing the drawing boards on I and II so that they can be shifted with respect to the frame of the carriages. They are kept in place by friction, and the displacement is measured by means of a pointer attached to the frame moving over a scale attached to the board.

For our particular work the transmission functions $\tau(lu)$ had to be determined as function of the frequency ν. The coefficient l is given on a logarithmic scale in Fig. 19 and τ is given in Fig. 15. Since the scale of l is logarithmic, various values of u correspond to additive constants which are introduced in the manner just explained. The function $\tau(\nu)$ is drawn on a sheet of paper on carriage III by a pencil inserted in C. The curves thus obtained are put on carriage II and the integral of the Planck function or of its temperature derivative (Table 1, Section 1) is fastened to carriage I. The planimeter is inserted at C and the desired integrals of the form (4.3) or (4.4) are obtained. After some training, an integration could be carried out in about four minutes. With some care in handling the machine an accuracy of about 1% or better was achieved.

BIBLIOGRAPHY

The literature has been divided up under five headings in an effort to facilitate the use of the bibliography, but since this division is entirely arbitrary it may not always do justice to the content of the papers quoted. The divisions are as follows:

1. Books and Reviews (including some reviews on ozone)
2. Infrared spectroscopy
3. Line and band absorption and emission; pressure effect
4. Radiative transfer in the atmosphere
5. Sky radiation (non-spectroscopic).

1. Books and Reviews (including some reviews on ozone)

1. Brunt, D. Physical and Dynamical Meteorology. 2nd ed., Cambridge University Press. 1939.
2. Coblentz, W. W. Investigations of Infra-Red Spectra. Vol. I. Carnegie Foundation of Washington, 1905. (Also Vols. II and III, 1906 and 1908.)
3. Dennison, D. M. The infrared spectra of polyatomic molecules. Rev. Mod. Phys. 3: 280. 1931.
4. Götz, F. W. P. Das atmosphärische Ozon. Ergebnisse der kosmischen Physik I: 180. 1931. The vertical distribution of atmospheric ozone. Ergebnisse der kosmischen Physik. 3: 253. 1938.
5. Haurwitz, B. The Physical State of the Upper Atmosphere. 2nd ed. (reprinted with additions from Jour. Roy. Astron. Soc. Canada, 1936/37). Roy. Astron. Soc. of Canada, Toronto. 1940.
6. Kleinschmidt, E. Handbuch der meteorologischen Instrumente. Springer, Berlin. 1935. See article by Albrecht on radiation instruments.
7. Lecomte, J. Le Spectre Infrarouge. Presses Universitaires de France, Paris. 1928.
8. Linke, F. Meteorologisches Taschenbuch, No. 4 and 5. Akademische Verlagsgesellschaft, Leipzig. 1939.
9. Margenau, H., and W. W. Watson. Pressure effects on spectral lines. Rev. Mod. Phys. 8: 22. 1936.
10. Milne, E. A. Thermodynamics of the Stars. Handbuch der Astrophysik, vol. 3, part 1. Springer, Berlin. 1930. (The article is written in English.)
11. Penndorf, R. Beiträge zum Ozonproblem. Veröff. Geophys. Inst. der Univ. Leipzig. 8: 181. 1931. (Thesis, Leipzig.)
12. Schaefer, C., and F. Matossi. Das Ultrarote Spektrum. Springer, Berlin. 1930.
13. Strong, J. Procedures in Experimental Physics. Prentice Hall, New York. 1938.
14. Weisskopf, V. Die Breite der Spektrallinien in Gasen. Phys. Zeits. 34: 1. 1933.

2. Infrared Spectroscopy

15. Abbot, C. G., and H. B. Freeman. Absorption lines of the infrared solar spectrum. Smithsonian Misc. Coll., vol. 82, no. 1. 1929.
16. Adel, A., and C. O. Lampland. Atmospheric absorption of infrared solar radiation at the Lowell Observatory; 5.5–14μ. Astrophys. J. 91: 1, and 481. 1940. Earlier observations: A. Adel and C. O. Lampland, Astrophys. J. 88: 182 and 186, 1938; A. Adel, Astrophys. J. 89: 1, 1939.
17. Adel, A. The grating infrared solar spectrum: Rotational structure of the nitrous oxide band at 7.8μ. Astrophys. J. 93: 509. 1941. See also A. Adel and C. O. Lampland, Astrophys. J. 87:198, 1938; and A. Adel, Astrophys. J. 90: 627, 1939.
18. —— Origin of the infrared telluric absorption 92. Astrophys. J. 88: 200. 1938.
19. —— The grating infrared solar spectrum: Rotational structure of the heavy water (HDO) band at 7.12μ. Astrophys. J. 93: 506. 1941.
20. Barker, E. F., and A. Adel. Resolution of the two difference bands of CO_2 near 10μ. Phys. Rev. 44: 185. 1935.

21. Deveaux, J. Étude du rayonnenment infrarouge émis par l'atmosphère. Comptes Rendus de l'Acad. Sci., Paris. 193:1207. 1931.

22. Fowle, F. E. Water vapor transparency to low temperature radiation. Smithsonian Misc. Coll. vol. 68, no. 8. 1917. The transparency of aqueous water vapor. Astrophys. J. 42: 394. 1915. See also Astrophys. J. 35: 149, 1912; and 37: 359, 1913.

23. Hettner, G. Ueber das ultrarote Absorptionsspektrum des Wasserdampfes. Ann. der Phys. 55: 476. 1918.

24. Hettner, G., R. Pohlmann, and H. J. Schuhmacher. Die Struktur des Ozonmoleküls und seine Banden im Ultrarot. Zeits. f. Phys. 91:372. 1934.

25. Martin, P. E., and E. F. Barker. The infrared absorption spectrum of carbon dioxide. Phys. Rev. 41:291. 1932.

26. Mecke, R., and H. Baumann. Das Rotationschwingungsspektrum des Wasserdampfes. Phys. Zeits. 33:833. 1932.

27. Plyler, E. K., and W. W. Sleator. Further Studies of the Absorption of infrared radiation by water vapor. Phys. Rev. 37:1493. 1931.

28. Plyler, E. K. The infrared absorption bands of water vapor. Phys. Rev. 40: 835. 1932.

29. Randall, H. M., D. M. Dennison, N. Ginsburg and L. R. Weber. The far infrared spectrum of water vapor. Phys. Rev. 52: 160. 1937.

30. Rubens, H., and E. Aschkinass. Ann. der Phys. 64: 548. 1898.

31. Strong, J. A new radiation pyrometer. J. Opt. Soc. Am. 29: 520. 1939.

32. —— A new method of measuring the height of ozone in the atmosphere. Jour. Franklin Inst. 231: 121. 1941. (See also 57, below.)

33. —— Study of atmospheric absorption and emission in the infrared spectrum. Jour. Franklin Inst. 232: 2. 1941.

33a. Weber, L. R., and H. M. Randall. The absorption spectrum of water vapor beyond 10μ. Phys. Rev. 40: 835. 1932.

3. Line and Band Absorption and Emission. Pressure Effect

34. Albrecht, F. Das quantentheoretische Wasserdampfspektrum und seine Bedeutung für strahlende Luftschichten. Met. Zeits. 48: 476. 1931.

34a. Arrhenius, S. Ueber die Wärmeabsorption der Kohlensäure. Ann. der Phys. 4: 690. 1901.

35. Bahr, E. v. Ueber die Einwirkung des Druckes auf die Absorption ultraroter Strahlung durch Gase. Ann. der Phys. 29: 780, 1909, and 33: 585, 1910; also Verhandl. deutsche phys. Ges. 15: 673. 1913.

36. Becker, G. Ueber die Druckabhängigkeit der Absorption des Chlorwasserstoffs im Ultrarot. Zeits. f. Phys. 34: 255. 1925.

36a. Becker, H. Direkte Messung der Form und Breite ultraroter Spektrallinien. Zeits. f. Phys. 59: 583. 1930.

37. Brooks, F. A. Observations of atmospheric radiation. Mass. Inst. Tech. Papers in Physical Oceanography and Meteorology, vol. 8, no. 2. 1941.

38 Callendar, G. S. Infrared absorption by CO_2 with special reference to atmospheric radiation. Quart. Jour. Roy. Met. Soc. 67: 263. 1941.

39. Cornell, S. D. Pressure effects in bands of several dipole molecules. Phys. Rev. 51: 739. 1937.

39a. Dennison, D. M. The shape and intensity of infrared absorption lines. Phys. Rev. 31: 510. 1928.

40. Elsasser, W. M. Note on atmospheric absorption caused by the rotational water band. Phys. Rev. 53: 768. 1938.

41. —— Far infrared absorption of atmospheric water vapor, Astrophys. J. 87: 497, 1938; also Mo. Wea. Rev. 65: 323, 1937; and Mo. Wea. Rev. 66: 175, 1938.

42. —— Mean absorption and equivalent absorption coefficient of a band spectrum. Phys. Rev. 54: 126. 1938.

43. —— A heat radiation telescope and the measurement of the infrared emission of the atmosphere. Mo. Wea. Rev. 69: 1. 1941.

44. FALCKENBERG, G. Absorptionskoeffizienten einiger meteorologisch wichtiger Körper für infrarote Wellen. Met. Zeits. 45: 334. 1928.

45. —— Experimentelles zur Eigenstrahlung dünner, wasserdampfhaltiger Luftschichten. Met. Zeits. 56: 72 and 415, 1939; also Met. Zeits. 48: 135, 1931; and Met. Zeits. 53: 172, 1936.

46. —— Experimentelles zur Druckabhängigkeit der Absorption des Wasserdampfes und der Kohlensäure. Met. Zeits. 55: 174. 1938.

47. HERTZ, G. Ueber das ultrarote Absorptionsspektrum der Kohlensäure und seine Abhängigkeit vom Druck. Verhandl. deutsche phys. Ges. 13: 617. 1911.

48. HOTTEL, H. C., and H. G. MANGELSDORF. Heat transmission by radiation: Experimental study of carbon dioxide and water vapor. Trans. Am. Inst. Chem. Eng. 31: 517. 1935. (Reviewed in H. C. HOTTEL and R. G. EGBERT, The radiation of furnace gases, Am. Soc. Mechan. Eng. Trans. 1941, p. 297.)

49. KÜHNE, J. Messungen im Rotationsspektrum des Wasserdampfes. Zeits. f. Phys. 84: 722. 1933.

50. KUSSMANN, H. W. Ueber die Verbreiterung der H-Cl Rotationsbande durch Fremdgase. Zeits. f. Phys. 48: 831. 1928.

51. LADENBURG, R. and F. REICHE. Ueber selektive Absorption. Ann. der Phys. 42: 181. 1911.

52. MATHESON, L. A. The intensity of infrared absorption bands. Phys. Rev. 40: 813. 1932.

53. MENZEL, D. H. The theoretical interpretation of equivalent breadth of absorption lines. Astrophys. J. 84: 462. 1936.

54. RUBENS, H., and R. LADENBURG. Ueber das langwellige Absorptionsspektrum der Kohlensäure. Verhandl. deutsche phys. Ges. 3: 170. 1905.

55. SCHNAIDT, F. Ueber die Absorption von Wasserdampf und Kohlendioxyd und ihre Druck- und Temperaturabhängigkeit. Gerl. Beitr. z. Geophys. 54: 203. 1939.

56. SIMPSON, G. C. Further studies in terrestrial radiation. Mem. Roy. Met. Soc. vol. 3, no. 21, p. 1. 1928.

57. STRONG, J., and K. WATANABE. Pressure effect on infrared absorption. Phys. Rev. 57: 1049. 1940.

58. WIMMER, M. Ueber die Beeinflussung der ultraroten Kohlensäurebande bei 4.3μ durch fremde Gase. Ann. der Phys. 81: 1091. 1926.

4. RADIATIVE TRANSFER IN THE ATMOSPHERE

59. ABBOT, C. G. The radiation of the planet Earth to space. Smithsonian Misc. Coll., vol. 82, no. 3, 1929.

60. ALBRECHT, F. Der Wärmeumsatz durch die Strahlung des Wasserdampfes in der Atmosphäre. Zeits. f. Geophys. 6: 421, 1930; Met. Zeits. 48: 57, 1931 (see also 34, above).

61. —— Ein Strahlungsbilanzmesser zur Messung des Strahlungshaushaltes von Oberflächen. Met. Zeits. 50: 62. 1933.

62. —— Theoretische Untersuchungen über den Strahlungsumsatz in Wolken. Met. Zeits. 50: 478. 1933.

63. ASHBURN, E. V. Radiative transfer in atmospheric temperature inversions. Bull. Am. Met. Soc. 21: 205. 1940.

64. BAUR, F., and H. PHILIPPS. Der Wärmehaushalt der Lufthülle der Nordhalbkugel. Gerl. Beitr. z. Geophys. 42: 160, 1934; 45: 82, 1935; 47: 218, 1936.

65. BRUNT, D. The transfer of heat by radiation and turbulence in the lower atmosphere. Proc. Roy. Soc. 124: 201, 1929; and Proc. Roy. Soc. 130: 98, 1930.

66. —— Notes on radiation in the atmosphere. Quart. Jour. Roy. Met. Soc. 58: 389. 1932.

67. —— Radiation in the atmosphere. Quart. J. Roy. Met. Soc. 66 supplt.: 34. 1940.

68. DINES, L. H. G. Greenhouse effect in the upper atmosphere. Met. Mag. 71: 44. 1936.

69. ELSASSER, W. M. An atmospheric radiation chart and its use. Quart. J. Roy. Met. Soc. 66 supplt.: 41. 1940.

70. —— Radiative cooling in the lower atmosphere. Mo. Wea. Rev. 68: 185. 1940.

71. EMDEN, R. Sitzber. Bayr. Akad. der Wiss. München, 1913, p. 55.

72. FALCKENBERG, G. Ueber die Abhängigkeit der Gegenstrahlung der Atmosphäre vom Temperaturgradienten und vom Wetter. Met. Zeits. 57: 241. 1940.

73. GODFREY, G. H. and W. L. PRICE. Thermal absorption and radiation in the upper atmosphere. Proc. Roy. Soc. 163: 228. 1937.

74. GOLD, E. The isothermal layer of the atmosphere and atmospheric radiation. Proc. Roy. Soc. 82: 43. 1909.

75. HOELPER, O. Ueber die Bestimmung der atmosphärischen Trübung und des Wasserdampfgehaltes aus Strahlungsmessungen. Met. Zeits. 54: 458, 1937; also Zeits. f. Geophys. 1: 251, 1925.

75a. HUMPHREYS, W. J. A suggested explanation of the isothermal layer. Astrophys. Journ. 29: 14. 1909.

76. KIMBALL, H. H. Measurements of solar radiation and its depletion by the atmosphere. Mo. Wea. Rev. 58: 43. 1930.

77. KORTÜM, F. Untersuchungen über die strahlungsbedingten Temperaturänderungen in Antizyklonen. Gerl. Beitr. z. Geophys. 54: 148. 1939.

78. MAL, S., S. BASU and B. N. DESAI. Structure and development of temperature inversions in the atmosphere. Beitr. z. Phys. d. freien Atm. 20: 56. 1932.

78a. MALURKAR, S. L. Effect of radiation on surfaces of humidity discontinuity. Gerl. Beitr. z. Geophys. 37: 410. 1932.

79. MOLODETZKI, A. G. Balance of long wave radiation on different levels in the atmosphere. (In Russian.) Meteorologia I Hydrologia 1939, no. 10–11, p. 23.

80. MÖLLER, F. Die Wärmequellen in der freien Atmosphäre. Met. Zeits. 52: 408. 1935.

81. —— Bemerkungen zur Wärmebilanz der Atmosphäre und der Erdoberfläche. Gerl. Beitr. z. Geophys. 47: 215. 1936.

82. MÜGGE, R. Ueber die Stratosphärentemperatur und die Strahlungsbedingungen der oberen Atmosphäre. Zeits. f. Geophys. 5: 194. 1929.

83. MÜGGE, R., and F. MÖLLER. Zur Berechnung von Strahlungsströmen und Temperaturänderungen in Atmosphären von beliebigem Aufbau. Zeits. f. Geophys. 8: 53, 1932; F. MÖLLER and R. MÜGGE, Temperaturänderungen in der Atmosphäre infolge der langwelligen Strahlung des Wasserdampfes, Met. Zeits. 48: 475, 1931.

84. —— Ueber Abkühlung der freien Atmosphäre infolge der langwelligen Strahlung des Wasserdampfes, Met. Zeits. 49: 95, 1932; F. MÖLLER and R. MÜGGE, Gesamte und zonale Gegenstrahlung als Mittel zur Gewinnung aerologischer Aufschlüsse, Beitr. z. Phys. d. freien Atm. 20: 220, 1933.

85. OOTA, M. Long wave radiation in the upper atmosphere. (In Japanese.) Jour. Met. Soc. Japan. 13: 231. 1935.

86. PEKERIS, C. L. The development and present state of the theory of the heat balance in the atmosphere. Mass. Inst. Tech. Meteor. Course, Prof. Notes No. 5. 1932.

87. PHILIPPS, H. Zur Theorie der Wärmestrahlung in Bodennähe. Gerl. Beitr. z. Geophys. 56: 229. 1940.

88. RAMANATHAN, K. R. Effect of radiation on the equilibrium of the higher layers of the troposphere and the nature of the transition from troposphere to stratosphere. Beitr. z. Phys. d. freien Atm. 18: 196. 1932.

89. ROBERTS, O. F. T. On radiative diffusion in the atmosphere. Proc. Roy. Soc. Edinburgh. 50: 225, 1929/30. No. 3.

90. SAUBERER, F. Messungen des Strahlungshaushaltes horizontaler Flächen. Met. Zeits. 54: 213 and 273. 1937.

91. SIMPSON, G. C. Some studies in terrestrial radiation. Mem. Roy. Met. Soc., vol. 2, no. 16, p. 69. 1928. (See also 56, above.)

92. —— The distribution of terrestrial radiation. Mem. Roy. Met. Soc., vol. 3, no. 23, p. 53. 1929.

93. TANCK, H. J. Die tägliche Erwärmung der Atmosphäre infolge Absorption der Sonnenstrahlung durch Wasserdampf. Ann. der Hydrogr. 6: 47. 1940.

94. WEXLER, H. Cooling in the lower atmosphere and the structure of polar continental air. Mo. Wea. Rev. 64: 122. 1936. See also H. WEXLER, Mo. Wea. Rev. 65: 102. 1937.

5. Sky Radiation (Non-Spectroscopic)

95. Albrecht, F. Versuche zur Messung der Effektivstrahlung. Met. Zeits. 43: 493. 1926.

95a. —— Die Messung und Registrierung der Strahlungsdifferenz Ausstrahlung-Einstrahlung mit einem Effektivpyranometer. Met. Zeits. 45: 465. 1928.

96. Aldrich, L. B. The Melikeron, an approximately black body pyrometer. Smithsonian Misc. Coll., vol. 72, no. 13. 1922.

97. Ångström, A. A study of the radiation of the atmosphere. Smithsonian Misc. Coll., vol. 65, no. 3. 1915.

98. —— Messung der nächtlichen Ausstrahlung im Ballon. Beitr. z. Phys. d. freien Atm. 14: 8. 1928.

99. —— Recording nocturnal radiation. Meddel. Meteor. Hydrogr. Anst. Stockholm, vol. 3, no. 12, 1927; also Ark. f. Mat. Astr. och Fys., vol. 22, no. 1, 1929.

100. —— On the variation of atmospheric radiation, Gerl. Beitr. z. Geophys. 21: 145, 1929; The effective radiation during the second international polar year, Meddel. Stat. Meteor. Hydrogr. Anst. Stockholm, vol. 6, no. 8, 1936.

101. Asklöf. Geogr. Ann. 2: 253. 1920.

102. Boutaric, A. Le rayonnement nocturne, La Meteorologie, 4: 289, 1928; and Le rayonnement nocturne au Mont Blanc, Comptes Rendus, Paris, 19: 1392, 1921.

103. Brooks, F. A., A. C. Lorenzen, and L. M. K. Boelter. Observations of nocturnal winter radiation in California. Bull. Am. Met. Soc. 20: 433. 1939.

104. Dines, W. H., and L. H. G. Dines. Monthly mean values of radiation from various points of the sky at Benson, Oxfordshire. Mem. Roy. Met. Soc., vol. 2, no. 11, p. 1. 1927. See also W. H. Dines, Met. Mag. 55: 191. 1920.

105. Dubois, P. Nächtliche effektive Strahlung. Gerl. Beitr. z. Geophys. 22: 41. 1929.

106. Eckel, O. Messung der Ausstrahlung auf der Kanzelhöhe. Met. Zeits. 51: 234. 1934.

107. Hasché, E. Zur Messung der langwelligen Himmels- und Erdstrahlung. Gerl. Beitr. z. Geophys. 42: 228. 1934.

108. —— Messung und Registrierung der langwelligen Strahlung mit dem Effektivpyranometer von F. Albrecht. Met. Zeits. 51: 64. 1934.

109. Kimball, H. H. Nocturnal radiation measurements. Mo. Wea. Rev. 46: 57. 1918.

110. Linke, F. Die nächtliche effektive Ausstrahlung unter verschiedenen Zenitdistanzen. Met. Zeits. 48: 25. 1931.

111. Malurkar, S. L. A note on measurements of atmospheric radiation with restricted apertures. Gerl. Beitr. z. Geophys. 44: 127. 1935.

112. —— Derivation of a formula for nocturnal radiation and its relation to Ångström's formula. Gerl. Beitr. z. Geophys. 47: 357. 1936.

113. Meinander, R. Nächtliche Wärmestrahlung in Helsingfors. Mitt. Meteor. Inst. Helsingfors, No. 6. 1928.

114. Mosby, H. Sunshine and Radiation. Norwegian North Polar Expedition with the "Maud," Scient. Res. vol. 1, no. 7. 1932.

115. Pekeris, C. L. Note on Brunt's formula for nocturnal radiation of the atmosphere. Astrophys. Journ. 79: 441. 1934.

116. Raman, P. K. Heat radiation from the clear atmosphere at night. Proc. Ind. Acad. Sci. 1: 815. 1935. See also P. K. Raman, Proc. Ind. Acad. Sci. 4: 243. 1936.

117. Ramanathan, K. R., and B. N. Desai. Nocturnal atmospheric radiation at Poona 1930–31. Gerl. Beitr. z. Geophys. 35: 68. 1932.

118. Ramanathan, K. R., and L. A. Ramdas. Derivation of Ångström's formula for atmospheric radiation. Proc. Ind. Acad. Sci. 1: 822. 1935.

119. Ramdas, L. A., B. N. Sreenivasiah, and P. K. Raman. Variation in the nocturnal radiation with zenith distance and with time of the night. Proc. Ind. Acad. Sci. 5: 45. 1937.

120. Robitzsch, M. Strahlungsstudien. Arb. Obs. Lindenberg. 15: 194. 1926.

121. SÜSSENBERGER, E. Die nächtliche effektive Ausstrahlung unter verschiedenen Zenitdistanzen. Met. Zeits. 52: 129. 1935.

122. —— Neue Untersuchungen über die nächtliche effektive Ausstrahlung. Gerl. Beitr. z. Geophys. 45: 63. 1935.

123 WEXLER, H. Observations of nocturnal radiation at Fairbanks, Alaska, and Fargo, N. Dak. Mo. Wea. Rev. supplt. 46. 1941.

ATMOSPHERIC RADIATION CHART

SECOND REVISED EDITION

Developed in cooperation with the U.S. Weather Bureau at the California Institute of Technology and the Blue Hill Observatory of Harvard University.

Published by
THE AMERICAN METEOROLOGICAL SOCIETY
Milton, Mass.

Price 10¢ each; wholesale (25 or more) 5¢ each; 20% discount to members of the Society.

WATER	+40°	+30°	+20°	+10°	0°	-10°	-20°	-30°	-40°	-50°	-60°	-70°	-80°	WATER
BLACK	141.4	124.2	108.6	94.5	81.9	70.5	60.4	51.4	43.5	36.5	30.4	25.0	20.5	BLACK
CO_2	117.4	102.6	89.3	77.4	66.8	57.4	49.1	41.8	35.4	29.8	24.9	20.7	17.1	CO_2
0.00025	111.0	96.7	83.8	72.4	62.2	53.1	45.1	38.1	32.0	26.7	22.1	18.1	14.8	0.00025
0.0006	106.8	92.9	80.4	69.2	59.3	50.5	42.7	36.0	30.0	24.9	20.5	16.7	13.5	0.0006
0.001	103.5	89.9	77.7	66.9	57.2	48.6	41.1	34.5	28.7	23.7	19.4	15.8	12.7	0.001
0.0025	96.6	83.7	72.2	61.9	52.8	44.7	37.6	31.4	26.0	21.3	17.3	13.9	11.1	0.0025
0.004	92.4	80.0	68.9	59.1	50.3	42.5	35.7	29.7	24.5	20.0	16.2	13.0	10.2	0.004
0.006	88.6	76.7	66.0	56.4	48.0	40.5	33.9	28.1	23.1	18.8	15.2	12.1	9.5	0.006
0.01	83.4	72.1	62.0	53.0	44.9	37.8	31.6	26.1	21.4	17.3	13.9	11.0	8.6	0.01
0.015	79.5	68.7	59.0	50.3	42.6	35.8	29.9	24.6	20.1	16.2	12.9	10.2	7.9	0.015
0.025	74.2	64.1	54.9	46.8	39.6	33.2	27.5	22.6	18.4	14.8	11.7	9.1	7.0	0.025
0.04	69.4	59.8	51.3	43.6	36.8	30.8	25.5	20.9	17.0	13.6	10.7	8.3	6.3	0.04
0.06	65.2	56.2	48.1	40.8	34.4	28.7	23.7	19.4	15.6	12.4	9.7	7.5	5.7	0.06
0.1	59.7	51.4	43.9	37.2	31.3	26.0	21.4	17.4	14.0	11.1	8.6	6.6	4.9	0.1
0.15	55.1	47.4	40.5	34.3	28.7	23.9	19.6	15.9	12.7	10.0	7.8	5.9	4.4	0.15
0.25	49.2	42.2	36.0	30.4	25.5	21.1	17.3	14.0	11.2	8.8	6.7	5.1	3.7	0.25
0.4	43.9	37.6	32.0	27.0	22.5	18.6	15.2	12.3	9.8	7.6	5.8	4.4	3.2	0.4
0.6	39.5	33.8	28.7	24.1	20.1	16.6	13.5	10.9	8.6	6.7	5.1	3.8	2.8	0.6
1.0	34.0	29.1	24.7	20.8	17.3	14.3	11.6	9.4	7.4	5.7	4.4	3.2	2.3	1.0
1.5	30.0	25.7	21.8	18.3	15.2	12.5	10.2	8.2	6.5	5.0	3.8	2.8	2.0	1.5
2.5	25.0	21.3	18.1	15.2	12.6	10.4	8.4	6.8	5.3	4.1	3.1	2.3	1.6	2.5
4	20.5	17.5	14.8	12.4	10.3	8.5	6.9	5.5	4.4	3.4	2.5	1.9	1.3	4
6	16.5	14.0	11.9	9.9	8.3	6.8	5.5	4.4	3.5	2.7	2.1	1.5	1.1	6
10	11.4	9.6	8.1	6.7	5.6	4.6	3.8	3.0	2.4	1.9	1.4	1.0	0.7	10
15	7.9	6.6	5.5	4.5	3.7	3.1	2.5	2.0	1.6	1.2	0.9	0.7	0.5	15
25	4.6	3.8	3.1	2.5	2.0	1.6	1.3	1.0	0.8	0.7	0.5	0.4	0.3	25
WATER	+40°	+30°	+20°	+10°	0°	-10°	-20°	-30°	-40°	-50°	-60°	-70°	-80°	WATER

USE FRAME OF THIS TABLE FOR PLANIMETER CALIBRATION
DIMENSIONS 3.50 x 3.50 = 12.25 UNITS

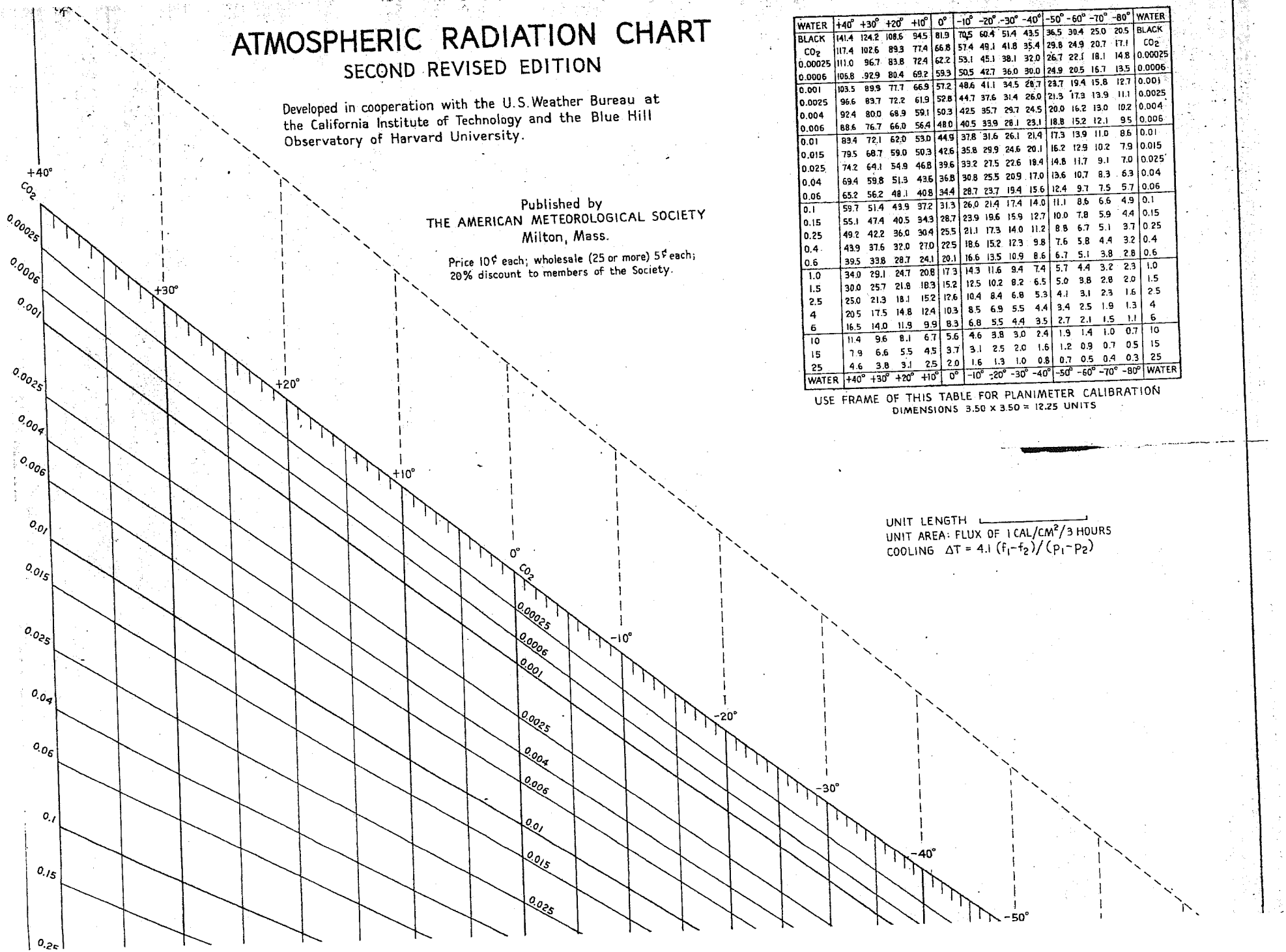

UNIT LENGTH
UNIT AREA: FLUX OF 1 CAL/CM²/3 HOURS
COOLING $\Delta T = 4.1 (f_1 - f_2)/(p_1 - p_2)$

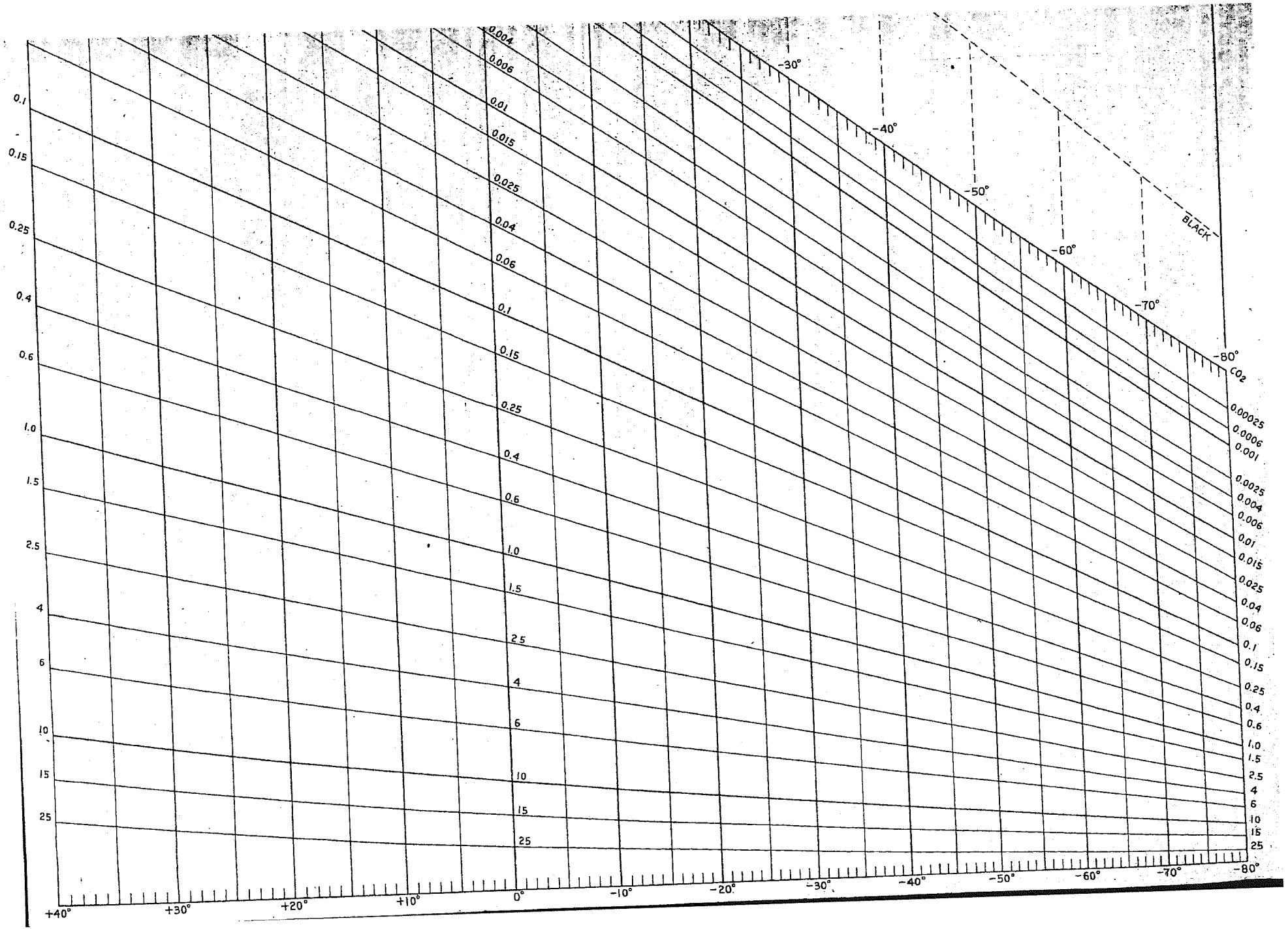
0.1
0.15
0.25
0.4
0.6
1.0
1.5
2.5
4
6
10
15
25
0.004
0.006
0.01
0.015
0.025
0.04
0.06
0.1
0.15
0.25
0.4
0.6
1.0
1.5
2.5
4
6
10
15
25
-30°
-40°
-50°
-60°
-70°
-80°
BLACK
CO_2
0.00025
0.0006
0.001
0.0025
0.004
0.006
0.01
0.015
0.025
0.04
0.06
0.1
0.15
0.25
0.4
0.6
1.0
1.5
2.5
4
6
10
15
25
-80°
+40°
+30°
+20°
+10°
0°
-10°
-20°
-30°
-40°
-50°
-60°
-70°
-80°